INTERNATIONAL TABLES FOR CRYSTALLOGRAPHY

Volume C

MATHEMATICAL, PHYSICAL AND CHEMICAL TABLES

Edited by

E. PRINCE

Contributing Authors

A. ALBINATI: Istituto Chimica Farmaceutica, Università di Milano, Viale Abruzzi 42, Milano 20131, Italy. [8.6]

N. G. ALEXANDROPOULOS: Department of Physics, University of Ioannina, PO Box 1186, Gr-45110 Ioannina, Greece. [7.4.3]

F. H. ALLEN: Cambridge Crystallographic Data Centre, 12 Union Road, Cambridge CB2 1EZ, England. [9.5, 9.6]

Y. AMEMIYA: Engineering Research Institute, Department of Applied Physics, Faculty of Engineering, University of Tokyo, 2-11-16 Yayoi, Bunkyo, Tokyo 113, Japan. [7.1.8]

I. S. ANDERSON: Institut Laue–Langevin, Avenue des Martyrs, BP 156X, F-38042 Grenoble CEDEX, France. [4.4.2]

U. W. ARNDT: MRC Laboratory of Molecular Biology, Hills Road, Cambridge CB2 2QH, England. [4.2.1, 7.1.6]

J. BARUCHEL: Experiment Division, ESRF, BP 220, F-38043 Grenoble CEDEX, France. [2.8]

P. J. BECKER: Ecole Centrale Paris, Centre de Recherche, Grand Voie des Vignes, F-92295 Châtenay Malabry CEDEX, France. [8.7]

G. BERGERHOFF: Institut für Anorganische Chemie der Universität Bonn, Gerhard-Domagkstrasse 1, D-53121 Bonn, Germany. [9.4]

P. T. BOGGS: Scientific Computing Division, National Institute of Standards and Technology, Gaithersburg, MD 20899, USA. [8.1]

L. BRAMMER: Department of Chemistry, University of Missouri–St Louis, 8001 Natural Bridge Road, St Louis, MO 63121-4499, USA. [9.5, 9.6]

K. BRANDENBURG: Institut für Anorganische Chemie der Universität Bonn, Gerhard-Domagkstrasse 1, D-53121 Bonn, Germany. [9.4]

P. J. BROWN: Institut Laue–Langevin, Avenue des Martyrs, BP 156X, F-38042 Grenoble CEDEX, France. [4.4.5, 6.1.2]

†B. BURAS [2.5.1, 7.1.5]

J. M. CARPENTER: Intense Pulsed Neutron Source, Building 360, Argonne National Laboratory, Argonne, IL 60439, USA. [4.4.1]

J. N. CHAPMAN: Department of Physics and Astronomy, University of Glasgow, Glasgow G12 8QQ, Scotland. [7.2]

P. CHIEUX: Institut Laue–Langevin, Avenue des Martyrs, BP 156X, F-38042 Grenoble CEDEX, France. [7.3]

J. CHIKAWA: Center for Advanced Science and Technology, Harima Science Park City, Kamigori-cho, Hyogo 678-12, Japan. [7.1.7, 7.1.8]

C. COLLIEX, Laboratoire Aimé Cotton, CNRS, Campus d'Orsay, Bâtiment 505, F-91405 Orsay CEDEX, France. [4.3.4]

D. M. COLLINS: Laboratory for the Structure of Matter, Code 6030, Naval Research Laboratory, Washington, DC 20375-5341, USA. [8.2]

P. CONVERT: Institut Laue–Langevin, Avenue des Martyrs, BP 156X, F-38042 Grenoble CEDEX, France. [7.3]

M. J. COOPER: Department of Physics, University of Warwick, Coventry CV4 7AL, England. [7.4.3]

P. COPPENS: 732 NSM Building, Department of Chemistry, State University of New York at Buffalo, Buffalo, NY 14260-3000, USA. [8.7]

J. M. COWLEY: Department of Physics and Astronomy, Arizona State University, Tempe, AZ 85287-1504, USA. [2.4.1, 4.3.1, 4.3.2, 4.3.8]

† Deceased.

D. C. CREAGH: Division of Health, Design, and Science, University of Canberra, Canberra, ACT 2601, Australia. [4.2.3, 4.2.4, 4.2.5, 4.2.6, 10]

J. L. C. DAAMS: Materials Analysis Department, Philips Research Laboratories, Prof. Holstaan 4, 5656 AA Eindhoven, The Netherlands. [9.3]

W. I. F. DAVID: ISIS Science Division, Rutherford Appleton Laboratory, Chilton, Didcot, Oxfordshire OX11 0QX, England. [2.5.2]

†R. D. DESLATTES [4.2.2]

S. L. DUDAREV: Department of Materials, University of Oxford, Parks Road, Oxford OX1 3PH, England. [4.3.2]

S. ĎUROVIČ: Department of Theoretical Chemistry, Slovak Academy of Sciences, Dúbravská cesta, 842 36 Bratislava, Slovakia. [9.2.2]

L. W. FINGER: Geophysical Laboratory, Carnegie Institution of Washington, 5251 Broad Branch Road NW, Washington, DC 20015-1305, USA. [8.3]

M. FINK: Department of Physics, University of Texas at Austin, Austin, TX 78712, USA. [4.3.3]

W. FISCHER: Institut für Mineralogie, Petrologie und Kristallographie, Universität Marburg, Hans-Meerwein-Strasse, D-35032 Marburg, Germany. [9.1]

H. M. FLOWER: Department of Metallurgy, Imperial College, London SW7, England. [3.5]

A. G. FOX: Center for Materials Science and Engineering, Naval Postgraduate School, Monterey, CA 93943-5000, USA. [6.1.1]

J. R. FRYER: Department of Chemistry, University of Glasgow, Glasgow G12 8QQ, Scotland. [3.5]

E. GAŁDECKA: Institute of Low Temperature and Structure Research, Polish Academy of Sciences, PO Box 937, 50-950 Wrocław 2, Poland. [5.3]

L. GERWARD: Physics Department, Technical University of Denmark, DK-2800 Lyngby, Denmark. [2.5.1, 7.1.5]

J. GJØNNES: Department of Physics, University of Oslo, PO Box 1048, Blindern, N-0316 Oslo, Norway. [4.3.7, 8.8]

O. GLATTER: Institut für Physikalische Chemie, Universität Graz, Heinrichstrasse 28, A-8010 Graz, Austria. [2.6.1]

J. R. HELLIWELL: Department of Chemistry, University of Manchester, Manchester M13 9PL, England. [2.1, 2.2]

A. W. HEWAT: Institut Laue–Langevin, Avenue des Martyrs, BP 156X, F-38042 Grenoble CEDEX, France. [2.4.2]

R. L. HILDERBRANDT: Chemistry Division, Room 1055, The National Science Foundation, 4201 Wilson Blvd, Arlington, VA 22230, USA. [4.3.3]

A. HOWIE: Cavendish Laboratory, Madingley Road, Cambridge CB3 0HE, England [4.3.6.2]

H.-C. HU: China Institute of Atomic Energy, PO Box 275 (18), Beijing 102413, People's Republic of China [6.2]

J. H. HUBBELL: Room C314, Radiation Physics Building, National Institute of Standards and Technology, Gaithersburg, MD 20899, USA. [4.2.4]

P. INDELICATO: Laboratoire Kastler-Brossel, Case 74, Université Pierre et Marie Curie, 4 Place Jussieu, F-75252 Paris CEDEX 05, France. [4.2.2]

A. JANNER: Institute for Theoretical Physics, University of Nijmegen, Toernooiveld, NL-6525 ED Nijmegen, The Netherlands. [9.8]

T. JANSSEN: Institute for Theoretical Physics, University of Nijmegen, Toernooiveld, NL-6525 ED Nijmegen, The Netherlands. [9.8]

† Deceased.

CONTRIBUTING AUTHORS

A. W. S. JOHNSON: Centre for Microscopy and Microanalysis, University of Western Australia, Nedlands, WA 6009, Australia. [5.4.1]

J. D. JORGENSEN: Materials Science Division, Building 223, Argonne National Laboratory, Argonne, IL 60439, USA. [2.5.2]

V. L. KAREN: NIST Center for Neutron Research, National Institute of Standards and Technology, Gaithersburg, MD 20899, USA. [9.7]

E. G. KESSLER JR: Atomic Physics Division, National Institute of Standards and Technology, Gaithersburg, MD 20899, USA. [4.2.2]

E. KOCH: Institut für Mineralogie, Petrologie und Kristallographie, Universität Marburg, Hans-Meerwein-Strasse, D-35032 Marburg, Germany. [1.1, 1.2, 1.3, 9.1]

J. H. KONNERT: Laboratory for the Structure of Matter, Code 6030, Naval Research Laboratory, Washington, DC 20375-5000, USA. [8.3]

P. KRISHNA: Rajghat Education Center, Krishnamurti Foundation India, Rajghat Fort, Varanasi 221001, India. [9.2.1]

G. LANDER: ITU, European Commission, Postfach 2340, D-76125 Karlsruhe, Germany. [4.4.1]

A. R. LANG: H. H. Wills Physics Laboratory, University of Bristol, Tyndall Avenue, Bristol BS8 1TL, England. [2.7]

J. I. LANGFORD: School of Physics & Astronomy, University of Birmingham, Birmingham B15 2TT, England. [2.3, 5.2, 6.2, 7.1.2]

†E. S. LARSEN JR. [3.3]

P. F. LINDLEY: ESRF, Avenue des Martyrs, BP 220, F-38043 Grenoble CEDEX, France. [3.1, 3.2.1, 3.2.3, 3.4]

E. LINDROTH, Department of Atomic Physics, Stockholm University, S-104 05 Stockholm, Sweden. [4.2.2]

† H. LIPSON. [6.2]

A. LOOIJENGA-VOS: Roland Holstlaan 908, NL-2624 JK Delft, The Netherlands. [9.8]

D. F. LYNCH: CSIRO Division of Materials Science & Technology, Private Bag 33, Rosebank MDC, Clayton, Victoria 3169, Australia. [4.3.6.1]

C. F. MAJKRZAK: NIST Center for Neutron Research, National Institute of Standards and Technology, Gaithersburg, MD 20899, USA. [2.9]

S. MARTINEZ-CARRERA: San Ernesto, 6-Esc. 3, 28002 Madrid, Spain. [10]

†E. N. MASLEN. [6.1.1, 6.3]

R. P. MAY: Institut Laue–Langevin, Avenue des Martyrs, BP 156X, F-38042 Grenoble CEDEX, France. [2.6.2]

†R. MEYROWITZ. [3.3]

A. MIGHELL: NIST Center for Neutron Research, National Institute of Standards and Technology, Gaithersburg, MD 20899, USA. [9.7]

M. A. O'KEEFE: National Center for Electron Microscopy, Lawrence Berkeley National Laboratory MS-72, University of California, Berkeley, CA 94720, USA. [6.1.1]

A. OLSEN: Department of Physics, University of Oslo, PO Box 1048, N-0316 Blindern, Norway. [5.4.2]

A. G. ORPEN: School of Chemistry, University of Bristol, Bristol BS8 1TS, England. [9.5, 9.6]

D. PANDEY: Physics Department, Banaras Hindu University, Varanasi 221005, India. [9.2.1]

†W. PARRISH. [2.3, 5.2, 7.1.2, 7.1.3, 7.1.4]

L. M. PENG: Department of Electronics, Peking University, Beijing 100817, People's Republic of China. [4.3.2]

E. PRINCE: NIST Center for Neutron Research, National Institute of Standards and Technology, Gaithersburg, MD 20899, USA. [8.1, 8.2, 8.3, 8.4, 8.5]

† Deceased.

R. PYNN: LANSCE, MS H805, Los Alamos National Laboratory, PO Box 1663, Los Alamos, NM 87545, USA. [4.4.3]

G. REN: Beijing Laboratory of Electron Microscopy, Chinese Academy of Sciences, PO Box 2724, Beijing 100080, People's Republic of China. [4.3.2]

F. M. RICHARDS: Department of Molecular Biophysics and Biochemistry, Yale University, 260 Whitney Ave, New Haven, CT 06520-8114, USA. [3.2.2]

J. R. RODGERS: National Research Council of Canada, Canada Institute for Scientific and Technical Information, Ottawa, Canada K1A 0S2. [9.3]

A. W. ROSS: Physics Department, The University of Texas at Austin, Austin, TX 78712, USA. [4.3.3]

J. M. ROWE: NIST Center for Neutron Research, National Institute of Standards and Technology, Gaithersburg, MD 20899, USA. [4.4.3]

T. M. SABINE: ANSTO, Private Mail Bag 1, Menai, NSW 2234, Australia. [6.4]

O. SCHÄRPF: Physik-Department E13, TU München, James-Franck-Strasse 1, D-85748 Garching, Germany. [4.4.2]

M. SCHLENKER: l'Institut National Polytechnique de Grenoble, Laboratoire Louis Néel du CNRS, BP 166, F-38042 Grenoble CEDEX 9, France. [2.8]

V. F. SEARS: Atomic Energy of Canada Limited, Chalk River Laboratories, Chalk River, Ontario, Canada K0J 1J0. [4.4.4]

G. S. SMITH: Manuel Lujan Jr Neutron Scattering Center, Los Alamos National Laboratory, Los Alamos, NM 87545, USA. [2.9]

V. H. SMITH JR: Department of Chemistry, Queen's University, Kingston, Ontario, Canada K7L 3N6. [4.3.3]

J. C. H. SPENCE: Department of Physics, Arizona State University, Tempe, AZ 85287, USA. [4.3.8]

C. H. SPIEGELMAN: Department of Statistics, Texas A&M University, College Station, TX 77843, USA. [8.4, 8.5]

J. W. STEEDS: H. H. Wills Physics Laboratory, University of Bristol, Tyndall Avenue, Bristol BS8 1TL, England. [4.3.7]

Z. SU: Digital Equipment Co., 129 Parker Street, PKO1/C22, Maynard, MA 01754-2122, USA. [8.7]

P. SUORTTI: Department of Physics, PO Box 9, University of Helsinki, FIN-00014 Helsinki, Finland. [7.4.4]

R. TAYLOR: Cambridge Crystallographic Data Centre, 12 Union Road, Cambridge CB2 1EZ, England. [9.5, 9.6]

N. J. TIGHE: 42 Lema Lane, Palm Coast, FL 32137-2417, USA. [3.5]

V. VALVODA: Department of Physics of Semiconductors, Faculty of Mathematics and Physics, Charles University, Ke Karlovu 5, 121 16 Praha 2, Czech Republic. [4.1]

P. VILLARS: Intermetallic Phases Databank, Postal Box 1, CH-6354 Vitznau, Switzerland. [9.3]

J. WANG: Department of Chemistry, Queen's University, Kingston, Ontario, Canada K7L 3N6. [4.3.3]

D. G. WATSON: Cambridge Crystallographic Data Centre, 12 Union Road, Cambridge CB2 1EZ, England. [9.5, 9.6]

M. J. WHELAN: Department of Materials, University of Oxford, Parks Road, Oxford OX1 3PH, England. [4.3.2]

B. T. M. WILLIS: Chemical Crystallography Laboratory, University of Oxford, 9 Parks Road, Oxford OX1 3PD, England. [2.5.2, 3.6, 4.4.6, 5.5, 6.1.3, 7.4.2, 8.6]

†A. J. C. WILSON. [1.4, 3.3, 5.1, 5.2, 7.5, 9.7]

†P. M. DE WOLFF. [7.1.1, 9.8]

†B. B. ZVYAGIN. [4.3.5]

† Deceased.

Contents

PAGE

PREFACE (A. J. C. Wilson) xxxi

PREFACE TO THE THIRD EDITION (E. Prince) xxxi

PART 1: CRYSTAL GEOMETRY AND SYMMETRY 1

1.1. SUMMARY OF GENERAL FORMULAE (E. Koch) 2

1.1.1. General relations between direct and reciprocal lattices 2

1.1.1.1. Primitive crystallographic bases 2
1.1.1.2. Non-primitive crystallographic bases 3

Table 1.1.1.1. *Direct and reciprocal lattices described with respect to conventional basis systems* 3

1.1.2. Lattice vectors, point rows, and net planes 3

1.1.3. Angles in direct and reciprocal space 4

1.1.4. The Miller formulae 5

1.2. APPLICATION TO THE CRYSTAL SYSTEMS (E. Koch) 6

1.2.1. Triclinic crystal system 6

1.2.2. Monoclinic crystal system 6

1.2.2.1. Setting with 'unique axis ***b***' 6
1.2.2.2. Setting with 'unique axis ***c***' 6

1.2.3. Orthorhombic crystal system 6

1.2.4. Tetragonal crystal system 7

Table 1.2.4.1. *Assignment of integers $s \leq 100$ to pairs h, k with $s = h^2 + k^2$* 7

1.2.5. Trigonal and hexagonal crystal system 7

1.2.5.1. Description referred to hexagonal axes 7
1.2.5.2. Description referred to rhombohedral axes 8

Table 1.2.5.1. *Assignment of integers $s \leq 100$ to pairs h, k with $s = h^2 + k^2 + hk$* 8
Table 1.2.5.2. *Assignment of integers $s_1 \leq 50$ to triplets h, k, l with $s_1 = h^2 + k^2 + l^2$ and to integers $s_2 = hk + hl + kl$* 8

1.2.6. Cubic crystal system 9

Table 1.2.6.1. *Assignment of integers $s \leq 100$ to triplets h, k, l with $s = h^2 + k^2 + l^2$* 9

1.3. TWINNING (E. Koch) 10

1.3.1. General remarks 10

1.3.2. Twin lattices 10

1.3.2.1. Examples 11

Table 1.3.2.1. *Lattice planes and rows that are perpendicular to each other independently of the metrical parameters* 11

1.3.3. Implication of twinning in reciprocal space 12

1.3.4. Twinning by merohedry 12

Table 1.3.4.1. *Possible twin operations for twins by merohedry* 13
Table 1.3.4.2. *Simulated Laue classes, extinction symbols, simulated 'possible space groups', and possible true space groups for crystals twinned by merohedry (type 2)* 13

1.3.5. Calculation of the twin element 14

1.4. ARITHMETIC CRYSTAL CLASSES AND SYMMORPHIC SPACE GROUPS (A. J. C. Wilson) 15

1.4.1. Arithmetic crystal classes 15

1.4.1.1. Arithmetic crystal classes in three dimensions.. 15
1.4.1.2. Arithmetic crystal classes in one, two and higher dimensions 16

Table 1.4.1.1. *The two-dimensional arithmetic crystal classes* 15

1.4.2. Classification of space groups 20

1.4.2.1. Symmorphic space groups 21
Table 1.4.2.1. *The three-dimensional space groups, arranged by arithmetic crystal class* 16

1.4.3. Effect of dispersion on diffraction symmetry .. 21
1.4.3.1. Symmetry of the Patterson function .. 21
1.4.3.2. 'Laue' symmetry .. 21
Table 1.4.3.1. *Arithmetic crystal classes classified by the number of space groups that they contain* .. 20
References .. 21

PART 2: DIFFRACTION GEOMETRY AND ITS PRACTICAL REALIZATION .. 23

2.1. Classification of Experimental Techniques (J. R. Helliwell) .. 24
Table 2.1.1. *Summary of main experimental techniques for structure analysis* .. 25

2.2. Single-Crystal X-ray Techniques (J. R. Helliwell) .. 26
2.2.1. Laue geometry .. 26
2.2.1.1. General .. 26
2.2.1.2. Crystal setting .. 27
2.2.1.3. Single-order and multiple-order reflections .. 27
2.2.1.4. Angular distribution of reflections in Laue diffraction .. 29
2.2.1.5. Gnomonic and stereographic transformations .. 29
2.2.2. Monochromatic methods .. 29
2.2.2.1. Monochromatic still exposure .. 30
2.2.2.2. Crystal setting .. 30
2.2.3. Rotation/oscillation geometry .. 31
2.2.3.1. General .. 31
2.2.3.2. Diffraction coordinates .. 31
2.2.3.3. Relationship of reciprocal-lattice coordinates to crystal system parameters .. 33
2.2.3.4. Maximum oscillation angle without spot overlap .. 33
2.2.3.5. Blind region .. 34
Table 2.2.3.1. *Glossary of symbols used to specify quantitites on diffraction patterns and in reciprocal space* 32
2.2.4. Weissenberg geometry .. 34
2.2.4.1. General .. 34
2.2.4.2. Recording of zero layer .. 34
2.2.4.3. Recording of upper layers .. 34
2.2.5. Precession geometry .. 35
2.2.5.1. General .. 35
2.2.5.2. Crystal setting .. 35
2.2.5.3. Recording of zero-layer photograph .. 35
2.2.5.4. Recording of upper-layer photographs .. 35
2.2.5.5. Recording of cone-axis photograph .. 36
Table 2.2.5.1. *The distance displacement (in mm) measured on the film versus angular setting error of the crystal for a screenless precession ($\bar{\mu} = 5^\circ$) setting photograph* .. 35
2.2.6. Diffractometry .. 36
2.2.6.1. General .. 36
2.2.6.2. Normal-beam equatorial geometry .. 36
2.2.6.3. Fixed $\chi = 45^\circ$ geometry with area detector .. 37
2.2.7. Practical realization of diffraction geometry: sources, optics, and detectors .. 37
2.2.7.1. General .. 37
2.2.7.2. Conventional X-ray sources: spectral character, crystal rocking curve, and spot size .. 37
2.2.7.3. Synchrotron X-ray sources .. 38
2.2.7.4. Geometric effects and distortions associated with area detectors .. 41

2.3. Powder and Related Techniques: X-ray Techniques (W. Parrish and J. I. Langford) .. 42
2.3.1. Focusing diffractometer geometries .. 43
2.3.1.1. Conventional reflection specimen, θ–2θ scan .. 44
2.3.1.1.1. Geometrical instrument parameters .. 44
2.3.1.1.2. Use of monochromators .. 46
2.3.1.1.3. Alignment and angular calibration .. 46
2.3.1.1.4. Instrument broadening and aberrations .. 47
2.3.1.1.5. Focal line and receiving-slit widths .. 48
2.3.1.1.6. Aberrations related to the specimen .. 48

2.3.1.1.7. Axial divergence .. 50
2.3.1.1.8. Combined aberrations .. 50
2.3.1.2. Transmission specimen, θ–2θ scan .. 50
2.3.1.3. Seemann–Bohlin method .. 52
2.3.1.4. Reflection specimen, θ–θ scan .. 53
2.3.1.5. Microdiffractometry .. 53

2.3.2. Parallel-beam geometries, synchrotron radiation .. 54
2.3.2.1. Monochromatic radiation, θ–2θ scan .. 55
2.3.2.2. Cylindrical specimen, 2θ scan .. 57
2.3.2.3. Grazing-incidence diffraction .. 58
2.3.2.4. High-resolution energy-dispersive diffraction .. 58

2.3.3. Specimen factors, angle, intensity, and profile-shape measurement .. 60
2.3.3.1. Specimen factors .. 60
2.3.3.1.1. Preferred orientation .. 60
2.3.3.1.2. Crystallite-size effects .. 62
2.3.3.2. Problems arising from the $K\alpha$ doublet .. 62
2.3.3.3. Use of peak or centroid for angle definition .. 63
2.3.3.4. Rate-meter/strip-chart recording .. 63
2.3.3.5. Computer-controlled automation .. 63
2.3.3.6. Counting statistics .. 64
2.3.3.7. Peak search .. 65
2.3.3.8. Profile fitting .. 66
2.3.3.9. Computer graphics for powder patterns .. 69
Table 2.3.3.1. *Preferred-orientation data for silicon* .. 61
Table 2.3.3.2. *R(Bragg) values obtained with different preferred-orientation formulae* .. 61

2.3.4. Powder cameras .. 70
2.3.4.1. Cylindrical cameras (Debye–Scherrer) .. 70
2.3.4.2. Focusing cameras (Guinier) .. 70
2.3.4.3. Miscellaneous camera types .. 71

2.3.5. Generation, modifications, and measurement of X-ray spectra .. 71
2.3.5.1. X-ray tubes .. 71
2.3.5.1.1. Stability .. 72
2.3.5.1.2. Spectral purity .. 72
2.3.5.1.3. Source intensity distribution and size .. 73
2.3.5.1.4. Air and window transmission .. 73
2.3.5.1.5. Intensity variation with take-off angle .. 74
2.3.5.2. X-ray spectra .. 74
2.3.5.2.1. Wavelength selection .. 75
2.3.5.3. Other X-ray sources .. 75
2.3.5.4. Methods for modifying the spectrum .. 75
2.3.5.4.1. Crystal monochromators .. 76
2.3.5.4.2. Single and balanced filters .. 78
Table 2.3.5.1. *X-ray tube maximum ratings* .. 72
Table 2.3.5.2. *β filters for common target elements* .. 78
Table 2.3.5.3. *Calculated thickness of balanced filters for common target elements* .. 79

2.4. Powder and Related Techniques: Electron and Neutron Techniques .. 80

2.4.1. Electron techniques (J. M. Cowley) .. 80
2.4.1.1. Powder-pattern geometry .. 80
2.4.1.2. Diffraction patterns in electron microscopes .. 80
2.4.1.3. Preferred orientations .. 80
2.4.1.4. Powder-pattern intensities .. 80
2.4.1.5. Crystal-size analysis .. 81
2.4.1.6. Unknown-phase identification: databases .. 81

2.4.2. Neutron techniques (A. W. Hewat) .. 82

2.5. Energy-Dispersive Techniques .. 84

2.5.1. Techniques for X-rays (B. Buras and L. Gerward) .. 84
2.5.1.1. Recording powder diffraction spectra .. 84

2.5.1.2. Incident X-ray beam .. 84
2.5.1.3. Resolution .. 85
2.5.1.4. Integrated intensity for powder sample .. 85
2.5.1.5. Corrections .. 86
2.5.1.6. The Rietveld method .. 86
2.5.1.7. Single-crystal diffraction .. 86
2.5.1.8. Applications .. 86

2.5.2. White-beam and time-of-flight neutron diffraction (J. D. Jorgensen, W. I. F. David, and B. T. M. Willis) .. 87
2.5.2.1. Neutron single-crystal Laue diffraction .. 87
2.5.2.2. Neutron time-of-flight powder diffraction .. 87

2.6. SMALL-ANGLE TECHNIQUES .. 89

2.6.1. X-ray techniques (O. Glatter) .. 89
2.6.1.1. Introduction .. 89
2.6.1.2. General principles .. 90
2.6.1.3. Monodisperse systems .. 91
2.6.1.3.1. Parameters of a particle .. 91
2.6.1.3.2. Shape and structure of particles .. 93
2.6.1.3.2.1. Homogeneous particles .. 93
2.6.1.3.2.2. Hollow and inhomogeneous particles .. 96
2.6.1.3.3. Interparticle interference, concentration effects .. 97
2.6.1.4. Polydisperse systems .. 99
2.6.1.5. Instrumentation .. 99
2.6.1.5.1. Small-angle cameras .. 99
2.6.1.5.2. Detectors .. 100
2.6.1.6. Data evaluation and interpretation .. 100
2.6.1.6.1. Primary data handling .. 100
2.6.1.6.2. Instrumental broadening – smearing .. 101
2.6.1.6.3. Smoothing, desmearing, and Fourier transformation .. 101
2.6.1.6.4. Direct structure analysis .. 103
2.6.1.6.5. Interpretation of results .. 103
2.6.1.7. Simulations and model calculations .. 103
2.6.1.7.1. Simulations .. 103
2.6.1.7.2. Model calculation .. 104
2.6.1.7.3. Calculation of scattering intensities .. 104
2.6.1.7.4. Method of finite elements .. 104
2.6.1.7.5. Calculation of distance-distribution functions .. 104
2.6.1.8. Suggestions for further reading .. 104
Table 2.6.1.1. *Formulae for the various parameters for h and m scales* .. 92

2.6.2. Neutron techniques (R. May) .. 105
2.6.2.1. Relation of X-ray and neutron small-angle scattering .. 105
2.6.2.1.1. Wavelength .. 105
2.6.2.1.2. Geometry .. 106
2.6.2.1.3. Correction of wavelength, slit, and detector-element effects .. 106
2.6.2.2. Isotopic composition of the sample .. 106
2.6.2.2.1. Contrast variation .. 107
2.6.2.2.2. Specific isotopic labelling .. 107
2.6.2.3. Magnetic properties of the neutron .. 107
2.6.2.3.1. Spin-contrast variation .. 108
2.6.2.4. Long wavelengths .. 108
2.6.2.5. Sample environment .. 108
2.6.2.6. Incoherent scattering .. 108
2.6.2.6.1. Absolute scaling .. 108
2.6.2.6.2. Detector-response correction .. 109
2.6.2.6.3. Estimation of the incoherent scattering level .. 109
2.6.2.6.4. Inner surface area .. 109
2.6.2.7. Single-particle scattering .. 110
2.6.2.7.1. Particle shape .. 110
2.6.2.7.2. Particle mass .. 110

2.6.2.7.3. Real-space considerations .. 110
2.6.2.7.4. Particle-size distribution .. 111
2.6.2.7.5. Model fitting .. 111
2.6.2.7.6. Label triangulation .. 111
2.6.2.7.7. Triplet isotropic replacement .. 111

2.6.2.8. Dense systems .. 112

2.7. Topography (A. R. Lang) .. 113

2.7.1. Principles .. 113

2.7.2. Single-crystal techniques .. 114
2.7.2.1. Reflection topographs .. 114
2.7.2.2. Transmission topographs .. 115

2.7.3. Double-crystal topography .. 117

2.7.4. Developments with synchrotron radiation .. 119
2.7.4.1. White-radiation topography .. 119
2.7.4.2. Incident-beam monochromatization .. 120

Table 2.7.4.1. *Monolithic monochromator for plane-wave synchrotron-radiation topography* .. 121

2.7.5. Some special techniques .. 121
2.7.5.1. Moiré topography .. 121
2.7.5.2. Real-time viewing of topograph images .. 122

2.8. Neutron Diffraction Topography (M. Schlenker and J. Baruchel) .. 124

2.8.1. Introduction .. 124

2.8.2. Implementation .. 124

2.8.3. Application to investigations of heavy crystals .. 124

2.8.4. Investigation of magnetic domains and magnetic phase transitions .. 124

2.9. Neutron Reflectometry (G. S. Smith and C. F. Majkrzak) .. 126

2.9.1. Introduction .. 126

2.9.2. Theory of elastic specular neutron reflection .. 126

2.9.3. Polarized neutron reflectivity .. 127

2.9.4. Surface roughness .. 128

2.9.5. Experimental methodology .. 128

2.9.6. Resolution in real space .. 129

2.9.7. Applications of neutron reflectometry .. 129
2.9.7.1. Self-diffusion .. 129
2.9.7.2. Magnetic multilayers .. 130
2.9.7.3. Hydrogenous materials .. 130

References .. 130

PART 3: PREPARATION AND EXAMINATION OF SPECIMENS .. 147

3.1. Preparation, Selection, and Investigation of Specimens (P. F. Lindley) .. 148

3.1.1. Crystallization .. 148
3.1.1.1. Introduction .. 148
3.1.1.2. Crystal growth .. 148
3.1.1.3. Methods of growing crystals .. 148
3.1.1.4. Factors affecting the solubility of biological macromolecules .. 148
3.1.1.5. Screening procedures for the crystallization of biological macromolecules .. 150
3.1.1.6. Automated protein crystallization .. 150
3.1.1.7. Membrane proteins .. 150

Table 3.1.1.1. *Survey of crystallization techniques suitable for the crystallization of low-molecular-weight organic compounds for X-ray crystallography* .. 149
Table 3.1.1.2. *Commonly used ionic and organic precipitants* .. 150
Table 3.1.1.3. *Crystallization matrix parameters for sparse-matrix sampling* .. 151
Table 3.1.1.4. *Reservoir solutions for sparse-matrix sampling* .. 152

3.1.2. Selection of single crystals .. 151
3.1.2.1. Introduction .. 151
3.1.2.2. Size, shape, and quality .. 151
3.1.2.3. Optical examination .. 154
3.1.2.4. Twinning .. 155
Table 3.1.2.1. *Use of crystal properties for selection and preliminary study of crystals; morphological, optical, and mechanical properties* .. 153

3.2. Determination of the Density of Solids .. 156

3.2.1. Introduction (P. F. Lindley) .. 156
3.2.1.1. General precautions .. 156
3.2.2. Description and discussion of techniques (F. M. Richards) .. 156
3.2.2.1. Gradient tube.. .. 156
3.2.2.1.1. Technique .. 156
3.2.2.1.2. Suitable substances for columns .. 157
3.2.2.1.3. Sensitivity .. 158
3.2.2.2. Flotation method .. 158
3.2.2.3. Pycnometry .. 158
3.2.2.4. Method of Archimedes .. 158
3.2.2.5. Immersion microbalance .. 158
3.2.2.6. Volumenometry .. 158
3.2.2.7. Other procedures .. 158
Table 3.2.2.1. *Possible substances for use as gradient-column components* .. 157
3.2.3. Biological macromolecules (P. F. Lindley) .. 159
Table 3.2.3.1. *Typical calculations of the values of V_M and V_{solv} for proteins* .. 159

3.3. Measurement of Refractive Index (E. S. Larsen Jr, R. Meyrowitz, and A. J. C. Wilson) .. 160

3.3.1. Introduction .. 160
3.3.2. Media for general use .. 160
Table 3.3.2.1. *Immersion media for general use in the measurement of index of refraction* .. 160
3.3.3. High-index media .. 160
3.3.4. Media for organic substances .. 161
Table 3.3.4.1. *Aqueous solutions for use as immersion media for organic crystals* .. 160
Table 3.3.4.2. *Organic immersion media for use with organic crystals of low solubility* .. 160

3.4. Mounting and Setting of Specimens for X-ray Crystallographic Studies (P. F. Lindley) .. 162

3.4.1. Mounting of specimens .. 162
3.4.1.1. Introduction .. 162
3.4.1.2. Polycrystalline specimens .. 162
3.4.1.2.1. General.. .. 162
3.4.1.2.2. Non-ambient conditions .. 162
3.4.1.3. Single crystals (small molecules) .. 163
3.4.1.3.1. General.. .. 163
3.4.1.3.2. Non-ambient conditions .. 164
3.4.1.4. Single crystals of biological macromolecules at ambient temperatures .. 165
3.4.1.5. Cryogenic studies of biological macromolecules .. 166
3.4.1.5.1. Radiation damage .. 166
3.4.1.5.2. Cryoprotectants .. 166
3.4.1.5.3. Crystal mounting and cooling .. 166
3.4.1.5.4. Cooling devices .. 167
3.4.1.5.5. General.. .. 167
Table 3.4.1.1. *Single-crystal and powder mounting, capillary tubes and other containers* .. 163
Table 3.4.1.2. *Single-crystal mounting – adhesives* .. 164
Table 3.4.1.3. *Cryoprotectants commonly used for biological macromolecules* .. 166
3.4.2. Setting of single crystals by X-rays .. 167
3.4.2.1. Introduction .. 167
3.4.2.2. Preliminary considerations .. 168
3.4.2.3. Equatorial setting using a rotation camera .. 168

3.4.2.4. Precession geometry setting with moving-crystal methods .. 168
3.4.2.5. Setting and orientation with stationary-crystal methods .. 169
3.4.2.5.1. Laue images – white radiation .. 169
3.4.2.5.2. 'Still' images – monochromatic radiation .. 169
3.4.2.6. Setting and orientation for crystals with large unit cells using oscillation geometry .. 169
3.4.2.7. Diffractometer-setting considerations .. 170
3.4.2.8. Crystal setting and data-collection efficiency .. 170

3.5. Preparation of Specimens for Electron Diffraction and Electron Microscopy (N. J. Tighe, J. R. Fryer, and H. M. Flower) .. 171

3.5.1. Ceramics and rock minerals .. 171
3.5.1.1. Thin fragments, particles, and flakes .. 171
3.5.1.2. Thin-section preparation .. 171
3.5.1.3. Final thinning by argon-ion etching .. 172
3.5.1.4. Final thinning by chemical etching .. 173
3.5.1.5. Evaporated and sputtered thin films .. 173
Table 3.5.1.1. *Chemical etchants used for preparing thin foils from single-crystal ceramic materials* .. 173

3.5.2. Metals .. 173
3.5.2.1. Thin sections .. 174
3.5.2.2. Final thinning methods .. 174
3.5.2.3. Chemical and electrochemical thinning solutions .. 175

3.5.3. Polymers and organic specimens .. 176
3.5.3.1. Cast films .. 176
3.5.3.2. Sublimed films .. 176
3.5.3.3. Oriented solidification .. 176

3.6. Specimens for Neutron Diffraction (B. T. M. Willis) .. 177

References .. 177

PART 4: PRODUCTION AND PROPERTIES OF RADIATIONS .. 185

4.1. Radiations used in Crystallography (V. Valvoda) .. 186

4.1.1. Introduction .. 186

4.1.2. Electromagnetic waves and particles .. 186

4.1.3. Most frequently used radiations .. 187
Table 4.1.3.1. *Average diffraction properties of X-rays, electrons, and neutrons* .. 187

4.1.4. Special applications of X-rays, electrons, and neutrons .. 189
4.1.4.1. X-rays, synchrotron radiation, and γ-rays .. 189
4.1.4.2. Electrons .. 189
4.1.4.3. Neutrons .. 189

4.1.5. Other radiations .. 189
4.1.5.1. Atomic and molecular beams .. 189
4.1.5.2. Positrons and muons .. 189
4.1.5.3. Infrared, visible, and ultraviolet light .. 189
4.1.5.4. Radiofrequency and microwaves .. 190

4.2. X-rays .. 191

4.2.1. Generation of X-rays (U. W. Arndt) .. 191
4.2.1.1. The characteristic line spectrum .. 191
4.2.1.1.1. The intensity of characteristic lines .. 191
4.2.1.2. The continuous spectrum .. 192
4.2.1.3. X-ray tubes .. 193
4.2.1.3.1. Power dissipation in the anode .. 195
4.2.1.4. Radioactive X-ray sources .. 195
4.2.1.5. Synchrotron-radiation sources .. 196
4.2.1.6. Plasma X-ray sources .. 198
4.2.1.7. Other sources of X-rays .. 199
Table 4.2.1.1. *Correspondence between X-ray diagram levels and electron configurations* .. 191
Table 4.2.1.2. *Correspondence between IUPAC and Siegbahn notations for X-ray diagram lines* .. 191

Table 4.2.1.3. *Copper-target X-ray tubes and their loading* .. 194
Table 4.2.1.4. *Relative permissible loading for different target materials* .. 196
Table 4.2.1.5. *Radionuclides decaying wholly by electron capture, and yielding little or no* γ*-radiation* .. 196
Table 4.2.1.6. *Comparison of storage-ring synchrotron-radiation sources* .. 199
Table 4.2.1.7. *Intensity gain with storage rings over conventional sources* .. 200

4.2.2. X-ray wavelengths (R. D. Deslattes, E. G. Kessler Jr, P. Indelicato, and E. Lindroth) .. 200
4.2.2.1. Historical introduction .. 200
4.2.2.2. Known problems .. 201
4.2.2.3. Alternative strategies .. 201
4.2.2.4. The X-ray wavelength scales, old and new .. 201
4.2.2.5. *K*-series reference wavelengths .. 202
4.2.2.6. *L*-series reference wavelengths .. 202
4.2.2.7. Absorption-edge locations .. 202
4.2.2.8. Outline of the theoretical procedures .. 204
4.2.2.9. Evaluation of the uncorrelated energy with Dirac–Fock method .. 205
4.2.2.10. Correlation and Auger shifts .. 205
4.2.2.11. QED corrections .. 205
4.2.2.12. Structure and format of the summary tables .. 211
4.2.2.13. Availability of a more complete X-ray wavelength table .. 212
4.2.2.14. Connection with scales used in previous literature .. 212
Table 4.2.2.1. *K-series reference wavelengths* .. 203
Table 4.2.2.2. *Directly measured L-series reference wavelengths* .. 204
Table 4.2.2.3. *Directly measured and emission + binding energies K-absorption edges* .. 205
Table 4.2.2.4. *Wavelengths of K-emission lines and K-absorption edges* .. 206
Table 4.2.2.5. *Wavelengths of L-emission lines and L-absorption edges* .. 209
Table 4.2.2.6. *Wavelength conversion factors* .. 212

4.2.3. X-ray absorption spectra (D. C. Creagh) .. 213
4.2.3.1. Introduction .. 213
4.2.3.1.1. Definitions .. 213
4.2.3.1.2. Variation of X-ray attenuation coefficients with photon energy .. 213
4.2.3.1.3. Normal attenuation, XAFS, and XANES .. 213
4.2.3.2. Techniques for the measurement of X-ray attenuation coefficients .. 214
4.2.3.2.1. Experimental configurations .. 214
4.2.3.2.2. Specimen selection .. 215
4.2.3.2.3. Requirements for the absolute measurement of μ_l or (μ/ρ) .. 215
4.2.3.3. Normal attenuation coefficients .. 215
4.2.3.4. Attenuation coefficients in the neighbourhood of an absorption edge .. 216
4.2.3.4.1. XAFS .. 216
4.2.3.4.1.1. Theory .. 216
4.2.3.4.1.2. Techniques of data analysis .. 217
4.2.3.4.1.3. XAFS experiments .. 218
4.2.3.4.2. X-ray absorption near edge structure (XANES) .. 219
4.2.3.5. Comments .. 220
Table 4.2.3.1. *Some synchrotron-radiation facilities providing XAFS databases and analysis utilities* .. 219

4.2.4. X-ray absorption (or attenuation) coefficients (D. C. Creagh and J. H. Hubbell) .. 220
4.2.4.1. Introduction .. 220
4.2.4.2. Sources of information .. 221
4.2.4.2.1. Theoretical photo-effect data: $\sigma_{\rm pe}$ .. 221
4.2.4.2.2. Theoretical Rayleigh scattering data: σ_R .. 221
4.2.4.2.3. Theoretical Compton scattering data: σ_C .. 229
4.2.4.3. Comparison between theoretical and experimental data sets .. 229
4.2.4.4. Uncertainty in the data tables .. 229
Table 4.2.4.1. *Table of wavelengths and energies for the characteristic radiations used in Tables 4.2.4.2 and 4.2.4.3* .. 221
Table 4.2.4.2. *Total photon interaction cross section* .. 223
Table 4.2.4.3. *Mass attenuation coefficients* .. 230

4.2.5. Filters and monochromators (D. C. Creagh) .. 229
4.2.5.1. Introduction .. 229
4.2.5.2. Mirrors and capillaries .. 236

4.2.5.2.1. Mirrors .. 236
4.2.5.2.2. Capillaries .. 237
4.2.5.2.3. Quasi-Bragg reflectors .. 237
4.2.5.3. Filters .. 238
4.2.5.4. Monochromators .. 238
4.2.5.4.1. Crystal monochromators .. 238
4.2.5.4.2. Laboratory monochromator systems .. 239
4.2.5.4.3. Multiple-reflection monochromators for use with laboratory and synchrotron-radiation sources .. 239
4.2.5.4.4. Polarization .. 240

4.2.6. X-ray dispersion corrections (D. C. Creagh) .. 241

4.2.6.1. Definitions .. 242
4.2.6.1.1. Rayleigh scattering .. 242
4.2.6.1.2. Thomson scattering by a free electron .. 242
4.2.6.1.3. Elastic scattering from electrons bound to atoms: the atomic scattering factor, the atomic form factor, and the dispersion corrections .. 242
4.2.6.2. Theoretical approaches for the calculation of the dispersion corrections .. 243
4.2.6.2.1. The classical approach .. 243
4.2.6.2.2. Non-relativistic theories .. 244
4.2.6.2.3. Relativistic theories .. 245
4.2.6.2.3.1. Cromer and Liberman: relativistic dipole approach .. 245
4.2.6.2.3.2. The scattering matrix formalism .. 246
4.2.6.2.4. Intercomparison of theories .. 248
4.2.6.3. Modern experimental techniques .. 248
4.2.6.3.1. Determination of the real part of the dispersion correction: $f'(\omega, 0)$ .. 248
4.2.6.3.2. Determination of the real part of the dispersion correction: $f'(\omega, \boldsymbol{\Delta})$ .. 250
4.2.6.3.2.1. Measurements using the dynamical theory of X-ray diffraction .. 250
4.2.6.3.2.2. Friedel- and Bijvoet-pair techniques .. 251
4.2.6.3.3. Comparison of theory with experiment .. 251
4.2.6.3.3.1. Measurements in the high-energy limit ($\omega/\omega_\kappa \to 0$) .. 251
4.2.6.3.3.2. Measurements in the vicinity of an absorption edge .. 252
4.2.6.3.3.3. Accuracy in the tables of dispersion corrections .. 253
4.2.6.3.3.4. Towards a tensor formalism .. 253
4.2.6.3.3.5. Summary .. 258
4.2.6.4. Table of wavelengths, energies, and linewidths used in compiling the tables of the dispersion corrections .. 258
4.2.6.5. Tables of the dispersion corrections for forward scattering, averaged polarization using the relativistic multipole approach .. 258
Table 4.2.6.1. *Values of E_{tot}/mc^2 listed as a function of atomic number Z* .. 246
Table 4.2.6.2(*a*). *Comparison between the S-matrix calculations of Kissel (1977) and the form-factor calculations of Cromer & Liberman (1970, 1981, 1983) and Creagh & McAuley for the noble gases and several common metals* .. 249
Table 4.2.6.2(*b*). *A comparison of the real part of the forward-scattering amplitudes computed using different theoretical approaches* .. 249
Table 4.2.6.3. *A comparison of the imaginary part of the forward-scattering amplitudes $f''(\omega, 0)$ computed using different theoretical approaches* .. 250
Table 4.2.6.4. *Comparison of measurements of the real part of the dispersion correction for LiF, Si, Al and Ge for characteristic wavelengths Ag $K\alpha_1$, Mo $K\alpha_1$ and Cu $K\alpha_1$ with theoretical predictions* .. 252
Table 4.2.6.5. *Comparison of measurements of $f'(\omega, 0)$ for C, Si and Cu for characteristic wavelengths Ag $K\alpha_1$, Mo $K\alpha_1$ and Cu $K\alpha_1$ with theoretical predictions* .. 253
Table 4.2.6.6. *Comparison of $f'(\omega_A, 0)$ for copper, nickel, zirconium, and niobium for theoretical and experimental data sets* .. 254
Table 4.2.6.7. *List of wavelengths, energies, and linewidths used in compiling the table of dispersion corrections* .. 254
Table 4.2.6.8. *Dispersion corrections for forward scattering* .. 255

4.3. Electron Diffraction .. 259

4.3.1. Scattering factors for the diffraction of electrons by crystalline solids (J. M. Cowley) .. 259

4.3.1.1. Elastic scattering from a perfect crystal .. 259
4.3.1.2. Atomic scattering factors .. 259
4.3.1.3. Approximations of restricted validity .. 260
4.3.1.4. Relativistic effects .. 260
4.3.1.5. Absorption effects .. 261
4.3.1.6. Tables of atomic scattering amplitudes for electrons .. 261
4.3.1.7. Use of Tables 4.3.1.1 and 4.3.1.2 .. 261

Table 4.3.1.1. *Atomic scattering amplitudes for electrons for neutral atoms* .. 263
Table 4.3.1.2. *Atomic scattering amplitudes for electrons for ionized atoms* .. 272

4.3.2. Parameterizations of electron atomic scattering factors (J. M. Cowley, L. M. Peng, G. Ren, S. L. Dudarev, and M. J. Whelan) .. 262

Table 4.3.2.1. *Parameters useful in electron diffraction as a function of accelerating voltage* .. 281
Table 4.3.2.2. *Elastic atomic scattering factors of electrons for neutral atoms and s up to 2.0 Å^{-1}* .. 282
Table 4.3.2.3. *Elastic atomic scattering factors of electrons for neutral atoms and s up to 6.0 Å^{-1}* .. 284

4.3.3. Complex scattering factors for the diffraction of electrons by gases (A. W. Ross, M. Fink, R. Hilderbrandt, J. Wang, and V. H. Smith Jr) .. 262

4.3.3.1. Introduction .. 262
4.3.3.2. Complex atomic scattering factors for electrons .. 262

4.3.3.2.1. Elastic scattering factors for atoms .. 262
4.3.3.2.2. Total inelastic scattering factors .. 389
4.3.3.2.3. Corrections for defects in the theory of atomic scattering .. 390

4.3.3.3. Molecular scattering factors for electrons .. 390

Table 4.3.3.1. *Partial wave elastic scattering factors for neutral atoms* .. 286
Table 4.3.3.2. *Inelastic scattering factors* .. 378

4.3.4. Electron energy-loss spectroscopy on solids (C. Colliex) .. 391

4.3.4.1. Definitions .. 391

4.3.4.1.1. Use of electron beams .. 391
4.3.4.1.2. Parameters involved in the description of a single inelastic scattering event .. 392
4.3.4.1.3. Problems associated with multiple scattering .. 392
4.3.4.1.4. Classification of the different types of excitations contained in an electron energy-loss spectrum .. 393

4.3.4.2. Instrumentation .. 394

4.3.4.2.1. General instrumental considerations .. 394
4.3.4.2.2. Spectrometers .. 395
4.3.4.2.3. Detection systems .. 397

4.3.4.3. Excitation spectrum of valence electrons .. 397

4.3.4.3.1. Volume plasmons .. 397
4.3.4.3.2. Dielectric description .. 399
4.3.4.3.3. Real solids .. 401
4.3.4.3.4. Surface plasmons .. 403

4.3.4.4. Excitation spectrum of core electrons .. 404

4.3.4.4.1. Definition and classification of core edges .. 404
4.3.4.4.2. Bethe theory for inelastic scattering by an isolated atom .. 406
4.3.4.4.3. Solid-state effects .. 408
4.3.4.4.4. Applications of core-loss spectroscopy .. 410

4.3.4.5. Conclusions .. 411

Table 4.3.4.1. *Different possibilities for using EELS information as a function of the different accessible parameters* ($\mathbf{r}$, θ, ΔE) .. 394
Table 4.3.4.2. *Plasmon energies measured (and calculated) for a few simple metals* .. 397
Table 4.3.4.3. *Experimental and theoretical values for the coefficient* α *in the plasmon dispersion curve together with estimates of the cut-off wavevector* .. 398
Table 4.3.4.4. *Comparison of measured and calculated values for the halfwidth* $\Delta E_{1/2}(0)$ *of the plasmon line* .. 398

4.3.5. Oriented texture patterns (B. B. Zvyagin) .. 412

4.3.5.1. Texture patterns .. 412
4.3.5.2. Lattice plane oriented perpendicular to a direction (lamellar texture) .. 412
4.3.5.3. Lattice direction oriented parallel to a direction (fibre texture) .. 413
4.3.5.4. Applications to metals and organic materials .. 414

4.3.6. Computation of dynamical wave amplitudes .. 414

4.3.6.1. The multislice method (D. F. Lynch) .. 414
4.3.6.2. The Bloch-wave method (A. Howie) .. 415

4.3.7. Measurement of structure factors and determination of crystal thickness by electron diffraction (J. Gjønnes and J. W. Steeds) .. 416

4.3.8. Crystal structure determination by high-resolution electron microscopy (J. C. H. Spence and J. M. Cowley) 419
4.3.8.1. Introduction .. 419
4.3.8.2. Lattice-fringe images .. 421
4.3.8.3. Crystal structure images .. 422
4.3.8.4. Parameters affecting HREM images .. 424
4.3.8.5. Computing methods .. 425
4.3.8.6. Resolution and hyper-resolution .. 427
4.3.8.7. Alternative methods .. 427
4.3.8.8. Combined use of HREM and electron diffraction .. 428

4.4. Neutron Techniques .. 430

4.4.1. Production of neutrons (J. M. Carpenter and G. Lander) .. 430

4.4.2. Beam-definition devices (I. S. Anderson and O. Schärpf) .. 431
4.4.2.1. Introduction .. 431
4.4.2.2. Collimators .. 431
4.4.2.3. Crystal monochromators .. 432
4.4.2.4. Mirror reflection devices .. 435
4.4.2.4.1. Neutron guides .. 435
4.4.2.4.2. Focusing mirrors .. 436
4.4.2.4.3. Multilayers .. 436
4.4.2.4.4. Capillary optics .. 437
4.4.2.5. Filters .. 438
4.4.2.6. Polarizers .. 438
4.4.2.6.1. Single-crystal polarizers .. 438
4.4.2.6.2. Polarizing mirrors .. 440
4.4.2.6.3. Polarizing filters .. 440
4.4.2.6.4. Zeeman polarizer .. 442
4.4.2.7. Spin-orientation devices .. 442
4.4.2.7.1. Maintaining the direction of polarization .. 442
4.4.2.7.2. Rotation of the polarization direction .. 442
4.4.2.7.3. Flipping of the polarization direction .. 442
4.4.2.8. Mechanical choppers and selectors .. 443
Table 4.4.2.1. *Some important properties of materials used for neutron monochromator crystals* .. 433
Table 4.4.2.2. *Neutron scattering-length densities, Nb_{coh}, for some commonly used materials* .. 435
Table 4.4.2.3. *Characteristics of some typical elements and isotopes used as neutron filters* .. 439
Table 4.4.2.4. *Properties of polarizing crystal monochromators* .. 440
Table 4.4.2.5. *Scattering-length densities for some typical materials used for polarizing multilayers* .. 441

4.4.3. Resolution functions (R. Pynn and J. M. Rowe) .. 443

4.4.4. Scattering lengths for neutrons (V. F. Sears) .. 444
4.4.4.1. Scattering lengths .. 444
4.4.4.2. Scattering and absorption cross sections .. 452
4.4.4.3. Isotope effects .. 452
4.4.4.4. Correction for electromagnetic interactions .. 453
4.4.4.5. Measurement of scattering lengths .. 453
4.4.4.6. Compilation of scattering lengths and cross sections .. 453
Table 4.4.4.1. *Bound scattering lengths, b, and cross sections, σ, of the elements and their isotopes* .. 445

4.4.5. Magnetic form factors (P. J. Brown) .. 454
Table 4.4.5.1. $\langle j_0 \rangle$ *form factors for 3d transition elements and their ions* .. 454
Table 4.4.5.2. $\langle j_0 \rangle$ *form factors for 4d atoms and their ions* .. 455
Table 4.4.5.3. $\langle j_0 \rangle$ *form factors for rare-earth ions* .. 455
Table 4.4.5.4. $\langle j_0 \rangle$ *form factors for actinide ions* .. 455
Table 4.4.5.5. $\langle j_2 \rangle$ *form factors for 3d transition elements and their ions* .. 456
Table 4.4.5.6. $\langle j_2 \rangle$ *form factors for 4d atoms and their ions* .. 457
Table 4.4.5.7. $\langle j_2 \rangle$ *form factors for rare-earth ions* .. 457
Table 4.4.5.8. $\langle j_2 \rangle$ *form factors for actinide ions* .. 457
Table 4.4.5.9. $\langle j_4 \rangle$ *form factors for 3d atoms and their ions* .. 458

Table 4.4.5.10. $\langle j_4 \rangle$ *form factors for 4d atoms and their ions* .. 459
Table 4.4.5.11. $\langle j_4 \rangle$ *form factors for rare-earth ions* .. 459
Table 4.4.5.12. $\langle j_4 \rangle$ *form factors for actinide ions* .. 459
Table 4.4.5.13. $\langle j_6 \rangle$ *form factors for rare-earth ions* .. 460
Table 4.4.5.14. $\langle j_6 \rangle$ *form factors for actinide ions* .. 460

4.4.6. Absorption coefficients for neutrons (B. T. M. Willis) .. 461
Table 4.4.6.1. *Absorption of the elements for neutrons* .. 461

References .. 462

PART 5: DETERMINATION OF LATTICE PARAMETERS .. 489

5.1. Introduction (A. J. C. Wilson) .. 490

5.2. X-ray Diffraction Methods: Polycrystalline (W. Parrish, A. J. C. Wilson, and J. I. Langford) .. 491

5.2.1. Introduction .. 491
5.2.1.1. The techniques available .. 491
5.2.1.2. Errors and aberrations: general discussion .. 491
5.2.1.3. Errors of the Bragg angle .. 491
5.2.1.4. Bragg angle: operational definitions .. 491
Table 5.2.1.1. *Functions of the cell angles in equation (5.2.1.3) for the possible unit cells* .. 492

5.2.2. Wavelength and related problems .. 492
5.2.2.1. Errors and uncertainties in wavelength .. 492
5.2.2.2. Refraction .. 492
5.2.2.3. Statistical fluctuations .. 492

5.2.3. Geometrical and physical aberrations .. 493
5.2.3.1. Aberrations .. 493
5.2.3.2. Extrapolation, graphical and analytical .. 493

5.2.4. Angle-dispersive diffractometer methods: conventional sources .. 495
Table 5.2.4.1. *Centroid displacement $\langle \Delta\theta/\theta \rangle$ and variance W of certain aberrations of an angle-dispersive diffractometer* .. 494

5.2.5. Angle-dispersive diffractometer methods: synchrotron sources .. 495

5.2.6. Whole-pattern methods .. 496

5.2.7. Energy-dispersive techniques .. 496
Table 5.2.7.1. *Centroid displacement $\langle \Delta E/E \rangle$ and variance W of certain aberrations of an energy-dispersive diffractometer* .. 497

5.2.8. Camera methods .. 497
Table 5.2.8.1. *Some geometrical aberrations in the Debye–Scherrer method* .. 498

5.2.9. Testing for remanent systematic error .. 498

5.2.10. Powder-diffraction standards .. 498
Table 5.2.10.1. *NIST values for silicon standards* .. 499
Table 5.2.10.2. *Reflection angles for tungsten, silver, and silicon* .. 499
Table 5.2.10.3. *Silicon standard reflection angles* .. 500
Table 5.2.10.4. *Silicon standard high reflection angles* .. 501
Table 5.2.10.5. *Tungsten reflection angles* .. 502
Table 5.2.10.6. *Fluorophlogopite standard reflection angles* .. 503
Table 5.2.10.7. *Silver behenate standard reflection angles* .. 503

5.2.11. Intensity standards .. 500
Table 5.2.11.1. *NIST intensity standards, SRM 674* .. 503

5.2.12. Instrumental line-profile-shape standards .. 501

5.2.13. Factors determining accuracy .. 501

5.3. X-ray Diffraction Methods: Single Crystal (E. Gałdecka) .. 505

5.3.1. Introduction .. 505
5.3.1.1. General remarks .. 505
5.3.1.2. Introduction to single-crystal methods .. 506

5.3.2. Photographic methods .. 508
5.3.2.1. Introduction .. 508

5.3.2.2. The Laue method .. 508
5.3.2.3. Moving-crystal methods .. 508
5.3.2.3.1. Rotating-crystal method .. 508
5.3.2.3.2. Moving-film methods .. 509
5.3.2.3.3. Combined methods .. 509
5.3.2.3.4. Accurate and precise lattice-parameter determinations .. 509
5.3.2.3.5. Photographic cameras for investigation of small lattice-parameter changes .. 510
5.3.2.4. The Kossel method and divergent-beam techniques .. 510
5.3.2.4.1. The principle .. 510
5.3.2.4.2. Review of methods of accurate lattice-parameter determination .. 512
5.3.2.4.3. Accuracy and precision .. 515
5.3.2.4.4. Applications .. 515
5.3.3. Methods with counter recording .. 516
5.3.3.1. Introduction .. 516
5.3.3.2. Standard diffractometers .. 516
5.3.3.2.1. Four-circle diffractometer .. 516
5.3.3.2.2. Two-circle diffractometer .. 517
5.3.3.3. Data processing and optimization of the experiment .. 517
5.3.3.3.1. Models of the diffraction profile .. 517
5.3.3.3.2. Precision and accuracy of the Bragg-angle determination; optimization of the experiment 519
5.3.3.4. One-crystal spectrometers .. 521
5.3.3.4.1. General characteristics .. 521
5.3.3.4.2. Development of methods based on an asymmetric arrangement and their applications .. 521
5.3.3.4.3. The Bond method .. 522
5.3.3.4.3.1. Description of the method .. 522
5.3.3.4.3.2. Systematic errors .. 523
5.3.3.4.3.3. Development of the Bond method and its applications .. 524
5.3.3.4.3.4. Advantages and disadvantages of the Bond method .. 526
5.3.3.5. Limitations of traditional methods .. 526
5.3.3.6. Multiple-diffraction methods .. 526
5.3.3.7. Multiple-crystal – pseudo-non-dispersive techniques .. 528
5.3.3.7.1. Double-crystal spectrometers .. 528
5.3.3.7.2. Triple-crystal spectrometers .. 530
5.3.3.7.3. Multiple-beam methods .. 531
5.3.3.7.4. Combined methods .. 531
5.3.3.8. Optical and X-ray interferometry – a non-dispersive technique .. 533
5.3.3.9. Lattice-parameter and wavelength standards .. 534
5.3.4. Final remarks .. 534

5.4. Electron-Diffraction Methods .. 537
5.4.1. Determination of cell parameters from single-crystal patterns (A. W. S. Johnson) .. 537
5.4.1.1. Introduction .. 537
5.4.1.2. Zero-zone analysis .. 538
5.4.1.3. Non-zero-zone analysis .. 538
Table 5.4.1.1. *Unit-cell information available for photographic recording* .. 537
5.4.2. Kikuchi and HOLZ techniques (A. Olsen) .. 538

5.5. Neutron Methods (B. T. M. Willis) .. 541
References .. 541

PART 6: INTERPRETATION OF DIFFRACTED INTENSITIES .. 553

6.1. Intensity of Diffracted Intensities .. 554
6.1.1. X-ray scattering (E. N. Maslen, A. G. Fox, and M. A. O'Keefe) .. 554
6.1.1.1. Coherent (Rayleigh) scattering .. 554
6.1.1.2. Incoherent (Compton) scattering .. 554
6.1.1.3. Atomic scattering factor .. 554
6.1.1.3.1. Scattering-factor interpolation .. 565

6.1.1.4. Generalized scattering factors .. 565
6.1.1.5. The temperature factor .. 584
6.1.1.6. The generalized temperature factor .. 585
6.1.1.6.1. Gram–Charlier series .. 586
6.1.1.6.2. Fourier-invariant expansions .. 586
6.1.1.6.3. Cumulant expansion .. 588
6.1.1.6.4. Curvilinear density functions .. 588
6.1.1.6.5. Model-based curvilinear density functions .. 589
6.1.1.6.6. The quasi-Gaussian approximation for curvilinear motion .. 590
6.1.1.7. Structure factor .. 590
6.1.1.8. Reflecting power of a crystal .. 590
Table 6.1.1.1. *Mean atomic scattering factors in electrons for free atoms* .. 555
Table 6.1.1.2. *Spherical bonded hydrogen-atom scattering factors* .. 565
Table 6.1.1.3. *Mean atomic scattering factors in electrons for chemically significant ions* .. 566
Table 6.1.1.4. *Coefficients for analytical approximation to the scattering factors of Tables 6.1.1.1 and 6.1.1.3* 578
Table 6.1.1.5. *Coefficients for analytical approximation to the scattering factors of Table 6.1.1.1 for the range* $2.0 < (\sin\theta)/\lambda < 6.0$ Å^{-1} .. 581
Table 6.1.1.6. *Angle dependence of multipole functions* .. 583
Table 6.1.1.7. *Indices allowed by the site symmetry for the real form of the spherical harmonics* $Y_{lmp(\theta,\varphi)}$ .. 584
Table 6.1.1.8. *Cubic harmonics* $K_{lj}(\theta,\varphi)$ *for cubic site symmetries* .. 585
Table 6.1.1.9. $f_{nl}(\alpha, S) = \int_0^\infty r^n exp(-\alpha r) j_l(Sr) dr$ .. 586
Table 6.1.1.10. *Indices nmp allowed by the site symmetry for the functions* $H_n(z)\Phi_{mp}(\varphi)$ .. 586
Table 6.1.1.11. *Indices* n_x, n_y, n_z *allowed for the basis functions* $H_{n_x}(Ax)H_{n_y}(By)H_{n_z}(Cz)$ .. 587

6.1.2. Magnetic scattering of neutrons (P. J. Brown) .. 590
6.1.2.1. Glossary of symbols .. 590
6.1.2.2. General formulae for the magnetic cross section .. 591
6.1.2.3. Calculation of magnetic structure factors and cross sections .. 591
6.1.2.4. The magnetic form factor .. 592
6.1.2.5. The scattering cross section for polarized neutrons .. 592
6.1.2.6. Rotation of the polarization of the scattered neutrons .. 593

6.1.3. Nuclear scattering of neutrons (B. T. M. Willis) .. 593
6.1.3.1. Glossary of symbols .. 593
6.1.3.2. Scattering by a single nucleus .. 593
6.1.3.3. Scattering by a single atom .. 594
6.1.3.4. Scattering by a single crystal .. 594

6.2. Trigonometric Intensity Factors (H. Lipson, J. I. Langford and H.-C. Hu) .. 596

6.2.1. Expressions for intensity of diffraction .. 596
Table 6.2.1.1. *Summary of formulae for integrated powers of reflection* .. 597

6.2.2. The polarization factor .. 596

6.2.3. The angular-velocity factor .. 596

6.2.4. The Lorentz factor .. 596

6.2.5. Special factors in the powder method .. 596

6.2.6. Some remarks about the integrated reflection power ratio formulae for single-crystal slabs .. 598

6.2.7. Other factors .. 598

6.3. X-ray Absorption (E. N. Maslen) .. 599

6.3.1. Linear absorption coefficient .. 599
6.3.1.1. True or photoelectric absorption .. 599
6.3.1.2. Scattering .. 599
6.3.1.3. Extinction .. 599
6.3.1.4. Attenuation (mass absorption) coefficients .. 600

6.3.2. Dispersion .. 600

6.3.3. Absorption corrections .. 600
6.3.3.1. Special cases .. 600
6.3.3.2. Cylinders and spheres .. 600
6.3.3.3. Analytical method for crystals with regular faces .. 604
6.3.3.4. Gaussian integration .. 606

6.3.3.5. Empirical methods .. 607
6.3.3.6. Measuring crystals for absorption .. 608
Table 6.3.3.1. *Transmission coefficients* .. 601
Table 6.3.3.2. *Values of* A^* *for cylinders* .. 602
Table 6.3.3.3. *Values of* A^* *for spheres* .. 602
Table 6.3.3.4. *Values of* $(1/A^*)(dA^*/d\mu R)$ *for spheres* .. 603
Table 6.3.3.5. *Coefficients for interpolation of* A^* *and* $\bar{T}$ .. 603

6.4. The Flow of Radiation in a Real Crystal (T. M. Sabine) .. 609

6.4.1. Introduction .. 609

6.4.2. The model of a real crystal .. 609

6.4.3. Primary and secondary extinction .. 609

6.4.4. Radiation flow .. 610

6.4.5. Primary extinction .. 610

6.4.6. The finite crystal .. 610

6.4.7. Angular variation of E .. 610

6.4.8. The value of x .. 610

6.4.9. Secondary extinction .. 611

6.4.10. The extinction factor .. 611
6.4.10.1. The correlated block model .. 611
6.4.10.2. The uncorrelated block model .. 611

6.4.11. Polarization .. 611

6.4.12. Anisotropy .. 612

6.4.13. Asymptotic behaviour of the integrated intensity .. 612
6.4.13.1. Non-absorbing crystal, strong primary extinction .. 612
6.4.13.2. Non-absorbing crystal, strong secondary extinction .. 612
6.4.13.3. The absorbing crystal.. .. 612

6.4.14. Relationship with the dynamical theory .. 612

6.4.15. Definitions .. 612

References .. 613

PART 7: MEASUREMENT OF INTENSITIES .. 617

7.1. Detectors for X-rays .. 618

7.1.1. Photographic film (P. M. de Wolff) .. 618
7.1.1.1. Visual estimation .. 618
7.1.1.2. Densitometry .. 618

7.1.2. Geiger counters (W. Parrish and J. I. Langford) .. 618

7.1.3. Proportional counters (W. Parrish) .. 619
7.1.3.1. The detector system .. 619
7.1.3.2. Proportional counters .. 619
7.1.3.3. Position-sensitive detectors .. 619
7.1.3.4. Resolution, discriminination, efficiency .. 619

7.1.4. Scintillation and solid-state detectors (W. Parrish) .. 619
7.1.4.1. Scintillation counters .. 619
7.1.4.2. Solid-state detectors .. 620
7.1.4.3. Energy resolution and pulse-amplitude discrimination .. 620
7.1.4.4. Quantum-counting efficiency and linearity .. 621
7.1.4.5. Escape peaks .. 622

7.1.5. Energy-dispersive detectors (B. Buras and L. Gerward) .. 622

7.1.6. Position-sensitive detectors (U. W. Arndt) .. 623
7.1.6.1. Choice of detector .. 623
7.1.6.1.1. Detection efficiency .. 624
7.1.6.1.2. Linearity of response .. 624
7.1.6.1.3. Dynamic range .. 625

7.1.6.1.4. Spatial resolution .. 625
7.1.6.1.5. Uniformity of response .. 625
7.1.6.1.6. Spatial distortion .. 625
7.1.6.1.7. Energy discrimination .. 625
7.1.6.1.8. Suitability for dynamic measurements .. 626
7.1.6.1.9. Stability .. 626
7.1.6.1.10. Size and weight .. 626

7.1.6.2. Gas-filled counters .. 626

7.1.6.2.1. Localization of the detected photon .. 627
7.1.6.2.2. Parallel-plate counters .. 627
7.1.6.2.3. Current ionization PSD's .. 628

7.1.6.3. Semiconductor detectors .. 629

7.1.6.3.1. X-ray-sensitive semiconductor PSD's .. 629
7.1.6.3.2. Light-sensitive semiconductor PSD's .. 630
7.1.6.3.3. Electron-sensitive PSD's .. 630

7.1.6.4. Devices with an X-ray-sensitive photocathode .. 630
7.1.6.5. Television area detectors with external phosphor .. 630

7.1.6.5.1. X-ray phosphors .. 631
7.1.6.5.2. Light coupling .. 632
7.1.6.5.3. Image intensifiers .. 632
7.1.6.5.4. TV camera tubes .. 632

7.1.6.6. Some applications .. 632

Table 7.1.6.1. *The importance of some detector properties for different X-ray patterns* .. 624
Table 7.1.6.2. *X-ray phosphors* .. 631

7.1.7. X-ray-sensitive TV cameras (J. Chikawa) .. 633

7.1.7.1. Signal-to-noise ratio .. 633
7.1.7.2. Imaging system .. 634
7.1.7.3. Image processing .. 635

7.1.8. Storage phosphors (Y. Amemiya and J. Chikawa) .. 635

7.2. Detectors for Electrons (J. N. Chapman) .. 639

7.2.1. Introduction .. 639

7.2.2. Characterization of detectors .. 639

7.2.3. Parallel detectors .. 640

7.2.3.1. Fluorescent screens .. 640
7.2.3.2. Photographic emulsions .. 640
7.2.3.3. Detector systems based on an electron-tube device .. 641
7.2.3.4. Electronic detection systems based on solid-state devices .. 641
7.2.3.5. Imaging plates .. 641

7.2.4. Serial detectors .. 642

7.2.4.1. Faraday cage .. 642
7.2.4.2. Scintillation detectors .. 642
7.2.4.3. Semiconductor detectors .. 642

7.2.5. Conclusions .. 643

7.3. Thermal Neutron Detection (P. Convert and P. Chieux) .. 644

7.3.1. Introduction .. 644

7.3.2. Neutron capture .. 644

Table 7.3.2.1. *Neutron capture reactions used in neutron detection* .. 645

7.3.3. Neutron detection processes .. 644

7.3.3.1. Detection *via* gas converter and gas ionization: the gas detector .. 644
7.3.3.2. Detection *via* solid converter and gas ionization: the foil detector .. 645
7.3.3.3. Detection *via* scintillation .. 645
7.3.3.4. Films .. 646

Table 7.3.3.1. *Commonly used detection processes* .. 646
Table 7.3.3.2. *A few examples of gas-detector characteristics* .. 646

7.3.4. Electronic aspects of neutron detection .. 648

7.3.4.1. The electronic chain .. 648

7.3.4.2. Controls and adjustments of the electronics .. 648

7.3.5. Typical detection systems .. 649
7.3.5.1. Single detectors .. 649
7.3.5.2. Position-sensitive detectors .. 649
7.3.5.3. Banks of detectors .. 650
Table 7.3.5.1. *Characteristics of some PSDs* .. 651

7.3.6. Characteristics of detection systems .. 651

7.3.7. Corrections to the intensity measurements depending on the detection system .. 652
7.3.7.1. Single detector .. 652
7.3.7.2. Banks of detectors .. 652
7.3.7.3. Position-sensitive detectors .. 652

7.4. Correction of Systematic Errors .. 653

7.4.1. Absorption .. 653

7.4.2. Thermal diffuse scattering (B. T. M. Willis) .. 653
7.4.2.1. Glossary of symbols .. 653
7.4.2.2. TDS correction factor for X-rays (single crystals) .. 654
7.4.2.2.1. Evaluation of $J(\mathbf{q})$ .. 654
7.4.2.2.2. Calculation of α .. 655
7.4.2.3. TDS correction factor for thermal neutrons (single crystals) .. 656
7.4.2.4. Correction factor for powders .. 657

7.4.3. Compton scattering (N. G. Alexandropoulos and M. J. Cooper) .. 657
7.4.3.1. Introduction .. 657
7.4.3.2. Non-relativistic calculations of the incoherent scattering cross section .. 657
7.4.3.2.1. Semi-classical radiation theory .. 657
7.4.3.2.2. Thomas–Fermi model .. 659
7.4.3.2.3. Exact calculations .. 659
7.4.3.3. Relativistic treatment of incoherent scattering .. 659
7.4.3.4. Plasmon, Raman, and resonant Raman scattering .. 660
7.4.3.5. Magnetic scattering .. 661
Table 7.4.3.1. *The energy transfer in the Compton scattering process for selected X-ray energies* .. 657
Table 7.4.3.2. *The incoherent scattering function for elements up to $Z = 55$* .. 658
Table 7.4.3.3. *Compton scattering of Mo $K\alpha$ X-radiation through 170° from 2s electrons* .. 659

7.4.4. White radiation and other sources of backgound (P. Suortti) .. 661
7.4.4.1. Introduction .. 661
7.4.4.2. Incident beam and sample .. 661
7.4.4.3. Detecting system .. 663
7.4.4.4. Powder diffraction .. 664

7.5. Statistical Fluctuations (A. J. C. Wilson) .. 666

7.5.1. Distributions of intensities of diffraction .. 666

7.5.2. Counting modes .. 666

7.5.3. Fixed-time counting .. 666

7.5.4. Fixed-count timing .. 667

7.5.5. Complicating phenomena .. 667
7.5.5.1. Dead time .. 667
7.5.5.2. Voltage fluctuations .. 667

7.5.6. Treatment of measured-as-negative (and other weak) intensities .. 667

7.5.7. Optimization of counting times .. 667

References .. 668

PART 8: REFINEMENT OF STRUCTURAL PARAMETERS .. 677

8.1. Least Squares (E. Prince and P. T. Boggs) .. 678

8.1.1. Definitions .. 678
8.1.1.1. Linear algebra .. 678
8.1.1.2. Statistics .. 679

8.1.2. Principles of least squares .. 680

8.1.3. Implementation of linear least squares .. 681
8.1.3.1. Use of the QR factorization .. 681
8.1.3.2. The normal equations .. 682
8.1.3.3. Conditioning .. 682

8.1.4. Methods for nonlinear least squares .. 682
8.1.4.1. The Gauss–Newton algorithm .. 683
8.1.4.2. Trust-region methods – the Levenberg–Marquardt algorithm .. 683
8.1.4.3. Quasi-Newton, or secant, methods .. 683
8.1.4.4. Stopping rules .. 684
8.1.4.5. Recommendations .. 685

8.1.5. Numerical methods for large-scale problems .. 685
8.1.5.1. Methods for sparse matrices .. 685
8.1.5.2. Conjugate-gradient methods .. 686

8.1.6. Orthogonal distance regression .. 687

8.1.7. Software for least-squares calculations .. 688

8.2. Other Refinement Methods (E. Prince and D. M. Collins) .. 689

8.2.1. Maximum-likelihood methods .. 689

8.2.2. Robust/resistant methods .. 689

8.2.3. Entropy maximization .. 691
8.2.3.1. Introduction .. 691
8.2.3.2. Some examples .. 691

8.3. Constraints and Restraints in Refinement (E. Prince, L. W. Finger, and J. H. Konnert) .. 693

8.3.1. Constrained models .. 693
8.3.1.1. Lagrange undetermined multipliers .. 693
8.3.1.2. Direct application of constraints .. 693
Table 8.3.1.1. *Symmetry conditions for second-cumulant tensors* .. 695

8.3.2. Stereochemically restrained least-squares refinement .. 698
8.3.2.1. Stereochemical constraints as observational equations .. 698
Table 8.3.2.1. *Coordinates of atoms in standard groups appearing in polypeptides and proteins* .. 699
Table 8.3.2.2. *Ideal values for distances, torsion angles, etc. for a glycine–alanine dipeptide with a trans peptide bond* .. 700
Table 8.3.2.3. *Typical values of standard deviations for use in determining weights in restrained refinement of protein structures* .. 701

8.4. Statistical Significance Tests (E. Prince and C. H. Spiegelman) .. 702

8.4.1. The χ^2 distribution .. 702
Table 8.4.1.1. *Values of χ^2/ν for which the c.d.f. $\Psi(\chi_2, \nu)$ has the values given in the column headings, for various values of ν* .. 703

8.4.2. The F distribution .. 703
Table 8.4.2.1. *Values of the F ratio for which the c.d.f. $\Psi(F, \nu_1, \nu_2)$ has the value 0.95, for various choices of ν_1 and ν_2* .. 704

8.4.3. Comparison of different models .. 704
Table 8.4.3.1. *Values of t for which the c.d.f. $\Psi(t, \nu)$ has the values given in the column headings, for various values of ν* .. 704

8.4.4. Influence of individual data points .. 705

8.5. Detection and Treatment of Systematic Error (E. Prince and C. H. Spiegleman) .. 707

8.5.1. Accuracy .. 707

8.5.2. Lack of fit .. 707

8.5.3. Influential data points .. 708

8.5.4. Plausibility of results .. 709

8.6. The Rietveld Method (A. Albinati and B. T. M. Willis) .. 710

8.6.1. Basic theory .. 710

8.6.2. Problems with the Rietveld method .. 711

8.6.2.1. Indexing .. 711
8.6.2.2. Peak-shape function (PSF) .. 711
8.6.2.3. Background .. 711
8.6.2.4. Preferred orientation and texture .. 712
8.6.2.5. Statistical validity .. 712

8.7. Analysis of Charge and Spin Densities (P. Coppens, Z. Su, and P. J. Becker) .. 713

8.7.1. Outline of this chapter .. 713

8.7.2. Electron densities and the *n*-particle wavefunction .. 713

8.7.3. Charge densities .. 714

8.7.3.1. Introduction .. 714
8.7.3.2. Modelling of the charge density .. 714
8.7.3.3. Physical constraints .. 715

8.7.3.3.1. Electroneutrality constraint .. 715
8.7.3.3.2. Cusp constraint .. 715
8.7.3.3.3. Radial constraint .. 715
8.7.3.3.4. Hellmann–Feynman constraint .. 715

8.7.3.4. Electrostatic moments and the potential due to a charge distribution .. 716

8.7.3.4.1. Moments of a charge distribution .. 716

8.7.3.4.1.1. Moments as a function of the atomic multipole expansion .. 716
8.7.3.4.1.2. Molecular moments based on the deformation density .. 717
8.7.3.4.1.3. The effect of an origin shift on the outer moments .. 717
8.7.3.4.1.4. Total moments as a sum over the pseudoatom moments .. 718
8.7.3.4.1.5. Electrostatic moments of a subvolume of space by Fourier summation .. 718

8.7.3.4.2. The electrostatic potential .. 718

8.7.3.4.2.1. The electrostatic potential and its derivatives .. 718
8.7.3.4.2.2. Electrostatic potential outside a charge distribution .. 720
8.7.3.4.2.3. Evaluation of the electrostatic functions in direct space .. 720

8.7.3.4.3. Electrostatic functions of crystals by modified Fourier summation .. 720
8.7.3.4.4. The total energy of a crystal as a function of the electron density .. 721

8.7.3.5. Quantitative comparison with theory .. 721
8.7.3.6. Occupancies of transition-metal valence orbitals from multipole coefficients .. 722
8.7.3.7. Thermal smearing of theoretical densities .. 723

8.7.3.7.1. General considerations .. 723
8.7.3.7.2. Reciprocal-space averaging over external vibrations .. 723

8.7.3.8. Uncertainties in experimental electron densities .. 724
8.7.3.9. Uncertainties in derived functions .. 725

Table 8.7.3.1. *Definition of difference density functions* .. 714
Table 8.7.3.2. *Expressions for the shape factors S for a parallelepiped with edges δ_x, δ_y, and δ_z* .. 719
Table 8.7.3.3. *The matrix M^{-1} relating d-orbital occupancies P_{ij} to multipole populations P_{lm}* .. 722
Table 8.7.3.4. *Orbital–multipole relations for square-planar complexes (point group D_{4h})* .. 723
Table 8.7.3.5. *Orbital–multipole relations for trigonal complexes* .. 723

8.7.4. Spin densities .. 725

8.7.4.1. Introduction .. 725
8.7.4.2. Magnetization densities from neutron magnetic elastic scattering .. 725
8.7.4.3. Magnetization densities and spin densities .. 726

8.7.4.3.1. Spin-only density at zero temperature .. 726
8.7.4.3.2. Thermally averaged spin-only magnetization density .. 726
8.7.4.3.3. Spin density for an assembly of localized systems .. 727
8.7.4.3.4. Orbital magnetization density .. 727

8.7.4.4. Probing spin densities by neutron elastic scattering .. 727

8.7.4.4.1. Introduction .. 727
8.7.4.4.2. Unpolarized neutron scattering .. 728
8.7.4.4.3. Polarized neutron scattering .. 728

8.7.4.4.4. Polarized neutron scattering of centrosymmetric crystals .. 728
8.7.4.4.5. Polarized neutron scattering in the noncentrosymmetric case .. 728
8.7.4.4.6. Effect of extinction .. 728
8.7.4.4.7. Error analysis .. 729

8.7.4.5. Modelling the spin density .. 729

8.7.4.5.1. Atom-centred expansion .. 729

8.7.4.5.1.1. Spherical-atom model .. 729
8.7.4.5.1.2. Crystal-field approximation .. 729
8.7.4.5.1.3. Scaling of the spin density .. 730

8.7.4.5.2. General multipolar expansion .. 730
8.7.4.5.3. Other types of model .. 730

8.7.4.6. Orbital contribution to the magnetic scattering .. 730

8.7.4.6.1. The dipolar approximation .. 731
8.7.4.6.2. Beyond the dipolar approximation .. 731
8.7.4.6.3. Electronic structure of rare-earth elements .. 731

8.7.4.7. Properties derivable from spin densities .. 731

8.7.4.7.1. Vector fields .. 732
8.7.4.7.2. Moments of the magnetization density .. 732

8.7.4.8. Comparison between theory and experiment .. 732
8.7.4.9. Combined charge- and spin-density analysis .. 732
8.7.4.10. Magnetic X-ray scattering separation between spin and orbital magnetism .. 733

8.7.4.10.1. Introduction .. 733
8.7.4.10.2. Magnetic X-ray structure factor as a function of photon polarization .. 733

8.8. Accurate Structure-Factor Determination with Electron Diffraction (J. Gjønnes) .. 735

References .. 738

PART 9: BASIC STRUCTURAL FEATURES .. 745

9.1. Sphere Packings and Packings of Ellipsoids (E. Koch and W. Fischer) .. 746

9.1.1. Sphere packings and packings of circles .. 746

9.1.1.1. Definitions .. 746
9.1.1.2. Homogeneous packings of circles .. 746
9.1.1.3. Homogeneous sphere packings .. 746
9.1.1.4. Applications .. 750
9.1.1.5. Interpenetrating sphere packings .. 751

Table 9.1.1.1. *Types of circle packings in the plane* .. 747
Table 9.1.1.2. *Examples for sphere packings with high contact numbers and high densities and with low contact numbers and low densities* .. 748

9.1.2. Packings of ellipses and ellipsoids .. 751

9.2. Layer Stacking .. 752

9.2.1. Layer stacking in close-packed structures (D. Pandey and P. Krishna) .. 752

9.2.1.1. Close packing of equal spheres .. 752

9.2.1.1.1. Close-packed layer .. 752
9.2.1.1.2. Close-packed structures .. 752
9.2.1.1.3. Notations for close-packed structures .. 752

9.2.1.2. Structure of compounds based on close-packed layer stackings .. 753

9.2.1.2.1. Voids in close packing .. 753
9.2.1.2.2. Structures of SiC and ZnS .. 753
9.2.1.2.3. Structure of CdI_2 .. 754
9.2.1.2.4. Structure of GaSe .. 754

9.2.1.3. Symmetry of close-packed layer stackings of equal spheres .. 755
9.2.1.4. Possible lattice types .. 755
9.2.1.5. Possible space groups .. 755
9.2.1.6. Crystallographic uses of Zhdanov symbols .. 756
9.2.1.7. Structure determination of close-packed layer stackings .. 756

9.2.1.7.1. General considerations .. 756
9.2.1.7.2. Determination of the lattice type .. 757

9.2.1.7.3. Determination of the identity period.. 757
9.2.1.7.4. Determination of the stacking sequence of layers 757
9.2.1.8. Stacking faults in close-packed structures 758
9.2.1.8.1. Structure determination of one-dimensionally disordered crystals 759
Table 9.2.1.1. *Common close-packed metallic structures* 753
Table 9.2.1.2. *List of SiC polytypes with known structures in order of increasing periodicity* 754
Table 9.2.1.3. *Intrinsic fault configurations in the 6H ($A_0B_1C_2A_3C_4B_5$,...) structure* 758
Table 9.2.1.4. *Intrinsic fault configurations in the 9R ($A_0B_1A_2C_0A_1C_2B_0C_1B_2$,...) structure* 759

9.2.2. Layer stacking in general polytypic structures (S. Ďurovič) 760
9.2.2.1. The notion of polytypism 760
9.2.2.2. Symmetry aspects of polytypism 761
9.2.2.2.1. Close packing of spheres 761
9.2.2.2.2. Polytype families and OD groupoid families 761
9.2.2.2.3. MDO polytypes 762
9.2.2.2.4. Some geometrical properties of OD structures 762
9.2.2.2.5. Diffraction pattern – structure analysis 763
9.2.2.2.6. The vicinity condition 763
9.2.2.2.7. Categories of OD structures 764
9.2.2.2.7.1. OD structures of equivalent layers 764
9.2.2.2.7.2. OD structures with more than one kind of layer 765
9.2.2.2.8. Desymmetrization of OD structures 765
9.2.2.2.9. Concluding remarks 766
9.2.2.3. Examples of some polytypic structures 766
9.2.2.3.1. Hydrous phyllosilicates 766
9.2.2.3.1.1. General geometry 767
9.2.2.3.1.2. Diffraction pattern and identification of individual polytypes 769
9.2.2.3.2. Stibivanite Sb_2VO_5 769
9.2.2.3.3. γ-$Hg_3S_2Cl_2$ 771
9.2.2.3.4. Remarks for authors 772
9.2.2.4. List of some polytypic structures 772

9.3. Typical Interatomic Distances: Metals and Alloys (J. L. C. Daams, J. R. Rodgers, and P. Villars) 774

9.3.1. Glossary 777

9.4. Typical Interatomic Distances: Inorganic Compounds (G. Bergerhoff and K. Brandenburg) 778

9.4.1. Introduction 778
Table 9.4.1.1. *Atomic distances between halogens and main-group elements in their preferred oxidation states* 779
Table 9.4.1.2. *Atomic distances between halogens and main-group elements in their special oxidation states* 780
Table 9.4.1.3. *Atomic distances between halogens and transition metals* 781
Table 9.4.1.4. *Atomic distances between halogens and lanthanoids* 784
Table 9.4.1.5. *Atomic distances between halogens and actinoids* 785
Table 9.4.1.6. *Atomic distances between oxygen and main-group elements in their preferred oxidation states* 785
Table 9.4.1.7. *Atomic distances between oxygen and main-group elements in their special oxidation states* 786
Table 9.4.1.8. *Atomic distances between oxygen and transition elements in their preferred and special oxidation states* 786
Table 9.4.1.9. *Atomic distances between oxygen and lanthanoids* 787
Table 9.4.1.10. *Atomic distances between oxygen and actinoids* 788
Table 9.4.1.11. *Atomic distances in sulfides and thiometallates* 788
Table 9.4.1.12. *Contact distances between some negatively charged elements* 789

9.4.2. The retrieval system 778

9.4.3. Interpretation of frequency distributions 778

9.5. Typical Interatomic Distances: Organic Compounds (F. H. Allen, D. G. Watson, L. Brammer, A. G. Orpen, and R. Taylor) 790

9.5.1. Introduction 790
Table 9.5.1.1. *Average lengths for bonds involving the elements H, B, C, N, O, F, Si, P, S, Cl, As, Se, Br, Te and I* 796

9.5.2. Methodology 790

9.5.2.1. Selection of crystallographic data .. 790
9.5.2.2. Program system .. 790
9.5.2.3. Classification of bonds .. 791
9.5.2.4. Statistics .. 791

9.5.3. Content and arrangement of the table .. 791
9.5.3.1. Ordering of entries: the 'Bond' column .. 792
9.5.3.2. Definition of 'Substructure' .. 792
9.5.3.3. Use of the 'Note' column .. 793

9.5.4. Discussion .. 794

9.6. Typical Interatomic Distances: Organometallic Compounds and Coordination Complexes of the *d*- and *f*-Block Metals (A. G. Orpen, L. Brammer, F. H. Allen, D. G. Watson, and R. Taylor) .. 812

9.6.1. Introduction .. 812

9.6.2. Methodology .. 812
9.6.2.1. Selection of crystallographic data .. 812
9.6.2.2. Program system .. 813
9.6.2.3. Classification of bonds .. 813
9.6.2.4. Statistics .. 813

9.6.3. Content and arrangement of table of interatomic distances .. 814
9.6.3.1. The 'Bond' column .. 815
9.6.3.2. Definition of 'Substructure' .. 815
9.6.3.3. Use of the 'Note' column .. 817
9.6.3.4. Locating an entry in Table 9.6.3.3 .. 818
Table 9.6.3.1. *Ligand index* .. 814
Table 9.6.3.2. *Numbers of entries in Table 9.6.3.3* .. 817
Table 9.6.3.3. *Interatomic distances* .. 818

9.6.4. Discussion .. 818

9.7. The Space-Group Distribution of Molecular Organic Structures (A. J. C. Wilson, V. L. Karen, and A. Mighell) .. 897

9.7.1. *A priori* classifications of space groups .. 897
9.7.1.1. Kitajgorodskij's categories .. 897
9.7.1.2. Symmorphism and antimorphism .. 897
9.7.1.3. Comparison of Kitajgorodskij's and Wilson's classifications .. 899
9.7.1.4. Relation to structural classes .. 900
Table 9.7.1.1. *Kitajgorodskij's categorization of the triclinic, monoclinic and orthorhombic space groups* .. 898
Table 9.7.1.2. *Space groups arranged by arithmetic crystal class and degree of symmorphism* .. 899

9.7.2. Special positions of given symmetry .. 900
Table 9.7.2.1. *Statistics of the use of Wyckoff positions of specified symmetry $\mathcal{G}$ in the homomolecular organic crystals* .. 903

9.7.3. Empirical space-group frequencies .. 902

9.7.4. Use of molecular symmetry .. 902
9.7.4.1. Positions with symmetry $\underline{1}$ .. 902
9.7.4.2. Positions with symmetry $\bar{1}$ .. 902
9.7.4.3. Other symmetries .. 903
9.7.4.4. Positions with the full symmetry of the geometric class .. 903
Table 9.7.4.1. *Occurrence of molecules with specified point group in centred symmmorphic and other space groups* .. 905

9.7.5. Structural classes .. 904

9.7.6. A statistical model .. 904

9.7.7. Molecular packing .. 904
9.7.7.1. Relation to sphere packing .. 904
9.7.7.2. The hydrogen bond and the definition of the packing units .. 906

9.7.8. *A priori* predictions of molecular crystal structures .. 906

9.8. Incommensurate and Commensurate Modulated Structures (T. Janssen, A. Janner, A. Looijenga-Vos, and P. M. de Wolff) .. 907

9.8.1. Introduction .. 907

9.8.1.1. Modulated crystal structures.. .. 907
9.8.1.2. The basic ideas of higher-dimensional crystallography .. 908
9.8.1.3. The simple case of a displacively modulated crystal.. .. 909

9.8.1.3.1. The diffraction pattern .. 909
9.8.1.3.2. The symmetry .. 909

9.8.1.4. Basic symmetry considerations .. 910

9.8.1.4.1. Bravais classes of vector modules .. 910
9.8.1.4.2. Description in four dimensions.. .. 911
9.8.1.4.3. Four-dimensional crystallography .. 911
9.8.1.4.4. Generalized nomenclature .. 912
9.8.1.4.5. Four-dimensional space groups.. .. 912

9.8.1.5. Occupation modulation .. 913

9.8.2. Outline for a superspace-group determination .. 913

9.8.3. Introduction to the tables .. 915

9.8.3.1. Tables of Bravais lattices .. 915
9.8.3.2. Table for geometric and arithmetic crystal classes .. 916
9.8.3.3. Tables of superspace groups.. .. 916

9.8.3.3.1. Symmetry elements.. .. 916
9.8.3.3.2. Reflection conditions .. 921

9.8.3.4. Guide to the use of the tables .. 935
9.8.3.5. Examples .. 936
9.8.3.6. Ambiguities in the notation .. 936

Table 9.8.3.1(*a*). (2 + *1*)-*Dimensional Bravais classes for incommensurate structures* .. 915
Table 9.8.3.1(*b*). (2 + *2*)-*Dimensional Bravais classes for incommensurate structures* .. 916
Table 9.8.3.2(*a*). (*3* + *1*)-*Dimensional Bravais classes for incommensurate structures* .. 917
Table 9.8.3.2(*b*). (*3* + *1*)-*Dimensional Bravais classes for commensurate structures* .. 918
Table 9.8.3.3. (*3* + *1*)-*Dimensional point groups and arithmetic crystal classes* .. 919
Table 9.8.3.4(*a*). (*2* + *1*)-*Dimensional superspace groups*.. .. 920
Table 9.8.3.4(*b*). (*2* + *2*)-*Dimensional superspace groups* .. 921
Table 9.8.3.5. (*3* + *1*)-*Dimensional superspace groups* .. 922
Table 9.8.3.6. *Centring reflection conditions for* (*3* + *1*)-*dimensional Bravais classes* .. 935

9.8.4. Theoretical foundation .. 937

9.8.4.1. Lattices and metric .. 937
9.8.4.2. Point groups .. 938

9.8.4.2.1. Laue class .. 938
9.8.4.2.2. Geometric and arithmetic crystal classes .. 939

9.8.4.3. Systems and Bravais classes .. 939

9.8.4.3.1. Holohedry .. 939
9.8.4.3.2. Crystallographic systems .. 940
9.8.4.3.3. Bravais classes .. 940

9.8.4.4. Superspace groups .. 940

9.8.4.4.1. Symmetry elements.. .. 940
9.8.4.4.2. Equivalent positions and modulation relations .. 940
9.8.4.4.3. Structure factor .. 941

9.8.5. Generalizations .. 941

9.8.5.1. Incommensurate composite crystal structures .. 941
9.8.5.2. The incommensurate *versus* the commensurate case .. 942

References .. 945

PART 10: PRECAUTIONS AGAINST RADIATION INJURY (D. C. Creagh and S. Martinez-Carrera) .. 957

10.1. Introduction .. 958

10.1.1. Definitions .. 958

Table 10.1.1. *The relationship between SI and the earlier system of units* .. 958

Table 10.1.2. *Maximum primary-dose limit per quarter* .. 960
Table 10.1.3. *Quality factors (QF)* .. 960

10.1.2. Objectives of radiation protection .. 960

10.1.3. Responsibilities .. 960
10.1.3.1. General .. 960
10.1.3.2. The radiation safety officer .. 960
10.1.3.3. The worker .. 960
10.1.3.4. Primary-dose limits .. 961

10.2. Protection from Ionizing Radiation .. 962

10.2.1. General .. 962

10.2.2. Sealed sources and radiation-producing apparatus .. 962
10.2.2.1. Enclosed installations .. 962
10.2.2.2. Open installations .. 962
10.2.2.3. Sealed sources .. 962
10.2.2.4. X-ray diffraction and X-ray analysis apparatus .. 962
10.2.2.5. Particle accelerators .. 962

10.2.3. Ionizing-radiation protection – unsealed radioactive materials .. 963

10.3. Responsible Bodies .. 964

Table 10.3.1. *Regulatory authorities* .. 964

References .. 967

Author Index .. 968

Subject Index .. 984

Preface

BY A. J. C. WILSON

A new volume of the *International Tables for Crystallography* containing mathematical, physical and chemical tables was discussed by the Executive Committee of the International Union of Crystallography at least as early as August 1979. My own ideas about what has become Volume C began to develop in the course of the Executive Committee meeting held at the Ottawa Congress in August 1981. It was then conceived as an editorial condensation of the old volumes II, III and IV, with obsolete material deleted and tables easily reproduced on a pocket calculator reduced to a skeleton form or omitted altogether. However, it soon became obvious that advances since the old volumes were produced could not be satisfactorily accommodated within such a condensation, and that if Volume C were to be a worthy companion of Volume A (*Space-Group Symmetry*) and Volume B (*Reciprocal Space*) it would have to consist largely of new material.

Work on Volumes B and C began officially on 1 January 1983, and the general outlines of the volumes were circulated to the Executive Committee, the National Committees, and others interested. This circulation generated much constructive criticism and offers of help, particularly from several Commissions of the Union. The Chairmen of certain Commissions were particularly helpful in finding qualified contributors of specialist sections, and from time to time served as members of the Commission on *International Tables for Crystallography*. I often had occasion to lament the lack of a Commission on X-ray Diffraction. The revised outlines of the two volumes were approved by the Executive Committee during the Hamburg Congress in 1984.

For various reasons the publication of Volume C has taken longer than expected. A requirement that prospective contributors should be approved by the Executive Committee produced some delays, and more serious delays were caused by authors who failed to deliver their contributions by the agreed date – or at all. A decision was taken to include in this first edition only what was in the Editor's hands in January 1990, and since that date the timetable has been set by the printers. The present Volume is the result. Readers will find a few sections resulting from the original idea of editorial condensation from Volumes II, III and IV, and some sections from those volumes revised or rewritten by their original authors. Most of Volume C is entirely new.

I am indebted to many crystallographers for advice and encouragement, to the authors of contributions that arrived before the deadline, to the Chairmen of various Commissions for their help, and to the Technical Editor for his skill and good humour in dealing with much difficult material.

Preface to the third edition

BY E. PRINCE

This is the third edition of *International Tables for Crystallography* Volume C. The purpose of this volume is to provide the mathematical, physical and chemical information needed for experimental studies in structural crystallography. It covers all aspects of experimental techniques, using all three principal radiation types, from the selection and mounting of crystals and production of radiation, through data collection and analysis, to the interpretation of results. As such, it is an essential source of information for all workers using crystallographic techniques in physics, chemistry, metallurgy, earth sciences and molecular biology.

Volume C of *International Tables for Crystallography* is one of the many legacies to crystallographers of the late Professor A. J. C. Wilson, whose death on 1 July 1995 left the preparation of a revised and expanded second edition unfinished. When I was appointed as Professor Wilson's successor as Editor, I realised that although most of the material in the first edition was new, some had been carried over from Volumes II, III, and IV of the earlier series *International Tables for X-ray Crystallography* and had become outdated. Moreover, many of the topics covered were changing very rapidly, so needed to be brought up to date. In fact, by the time the second edition was published in 1999, more than half the chapters had been revised or updated and two completely new chapters, on reflectometry and neutron topography, had been included. The second edition of Volume C was also the first volume of *International Tables* to be produced entirely electronically.

The authors of the second edition were asked if they wished to submit revisions to their articles for this third edition in August 2001. All revisions were received within the following year. In total, 11 chapters have been revised, corrected or updated, and all known errors in the second edition have been corrected. I hope few new errors have been introduced. I thank all authors, especially those who have submitted revisions, and I particularly thank the Editorial staff in Chester for their continued dilligence.

SAMPLE PAGES

Table 1.1.1.1. *Direct and reciprocal lattices described with respect to conventional basis systems*

Direct lattice $\mathbf{a}_c, \mathbf{b}_c, \mathbf{c}_c$			Reciprocal lattice $\mathbf{a}_c^*, \mathbf{b}_c^*, \mathbf{c}_c^*$		
Bravais letter	Centring vectors	Unit-cell volume V_c	Conditions for reciprocal-lattice vectors $h\mathbf{a}_c^* + k\mathbf{b}_c^* + l\mathbf{c}_c^*$	Unit-cell volume V_c^*	Bravais letter
A	$\frac{1}{2}\mathbf{b}_c + \frac{1}{2}\mathbf{c}_c$	$2V$	$k + l = 2n$	$\frac{1}{2}V^*$	A
B	$\frac{1}{2}\mathbf{a}_c + \frac{1}{2}\mathbf{c}_c$	$2V$	$h + l = 2n$	$\frac{1}{2}V^*$	B
C	$\frac{1}{2}\mathbf{a}_c + \frac{1}{2}\mathbf{b}_c$	$2V$	$h + k = 2n$	$\frac{1}{2}V^*$	C
I	$\frac{1}{2}\mathbf{a}_c + \frac{1}{2}\mathbf{b}_c + \frac{1}{2}\mathbf{c}_c$	$2V$	$h + k + l = 2n$	$\frac{1}{2}V^*$	F
F	$\frac{1}{2}\mathbf{a}_c + \frac{1}{2}\mathbf{b}_c$, $\frac{1}{2}\mathbf{a}_c + \frac{1}{2}\mathbf{c}_c$, $\frac{1}{2}\mathbf{b}_c + \frac{1}{2}\mathbf{c}_c$	$4V$	$h + k = 2n$, $h + l = 2n$, $k + l = 2n$	$\frac{1}{4}V^*$	I
R	$\frac{1}{3}\mathbf{a}_c + \frac{2}{3}\mathbf{b}_c + \frac{2}{3}\mathbf{c}_c$, $\frac{2}{3}\mathbf{a}_c + \frac{1}{3}\mathbf{b}_c + \frac{1}{3}\mathbf{c}_c$	$3V$	$-h + k + l = 3n$	$\frac{1}{3}V^*$	R

$$\begin{aligned} V^* &= a^*b^*c^* \sin\alpha \sin\beta^* \sin\gamma^* \\ &= a^*b^*c^* \sin\alpha^* \sin\beta \sin\gamma^* \\ &= a^*b^*c^* \sin\alpha^* \sin\beta^* \sin\gamma. \end{aligned} \quad (1.1.1.9)$$

1.1.1.2. *Non-primitive crystallographic bases*

For certain lattice types, it is usual in crystallography to refer to a 'conventional' crystallographic basis $\mathbf{a}_c, \mathbf{b}_c, \mathbf{c}_c$ instead of a primitive basis $\mathbf{a}, \mathbf{b}, \mathbf{c}$. In that case, $\mathbf{a}_c$, $\mathbf{b}_c$, and $\mathbf{c}_c$ with all their integral linear combinations are lattice vectors again, but there exist other lattice vectors $\mathbf{t} \in \mathbf{L}$,

$$\mathbf{t} = t_1\mathbf{a}_c + t_2\mathbf{b}_c + t_3\mathbf{c}_c,$$

with at least two of the coefficients t_1, t_2, t_3 being fractional.

Such a conventional basis defines a conventional or centred unit cell for a corresponding point lattice, the volume V_c of which may be calculated by analogy with V by substituting $\mathbf{a}_c, \mathbf{b}_c, \mathbf{c}_c$ for $\mathbf{a}, \mathbf{b}$, and $\mathbf{c}$ in (1.1.1.1).

If m designates the number of centring lattice vectors $\mathbf{t}$ with $0 \le t_1, t_2, t_3 < 1$, V_c may be expressed as a multiple of the primitive unit-cell volume V:

$$V_c = mV. \quad (1.1.1.10)$$

With the aid of equations (1.1.1.2) and (1.1.1.3), the reciprocal basis $\mathbf{a}_c^*, \mathbf{b}_c^*, \mathbf{c}_c^*$ may be derived from $\mathbf{a}_c, \mathbf{b}_c, \mathbf{c}_c$. Again, each reciprocal-lattice vector

$$\mathbf{r}^* = h\mathbf{a}_c^* + k\mathbf{b}_c^* + l\mathbf{c}_c^* \in \mathbf{L}^*$$

is an integral linear combination of the reciprocal basis vectors, but in contrast to the use of a primitive basis only certain triplets h, k, l refer to reciprocal-lattice vectors.

Equation (1.1.1.5) also relates V_c to V_c^*, the reciprocal cell volume referred to $\mathbf{a}_c^*, \mathbf{b}_c^*, \mathbf{c}_c^*$. From this it follows that

$$V_c^* = \frac{1}{m}V^*. \quad (1.1.1.11)$$

Table 1.1.1.1 contains detailed information on 'centred lattices' described with respect to conventional basis systems.

As a direct lattice and its corresponding reciprocal lattice do not necessarily belong to the same type of Bravais lattices [*IT* A (1987, Section 8.2.4)], the Bravais letter of $\mathbf{L}^*$ is given in the last column of Table 1.1.1.1. Except for P lattices, a conventionally chosen basis for $\mathbf{L}^*$ coincides neither with $\mathbf{a}^*, \mathbf{b}^*, \mathbf{c}^*$ nor with $\mathbf{a}_c^*, \mathbf{b}_c^*, \mathbf{c}_c^*$. This third basis, however, is not used in crystallography. The designation of scattering vectors and the indexing of Bragg reflections usually refers to $\mathbf{a}_c^*, \mathbf{b}_c^*, \mathbf{c}_c^*$.

If the differences with respect to the coefficients of direct- and reciprocal-lattice vectors are disregarded, all other relations discussed in Part 1 are equally true for primitive bases and for conventional bases.

1.1.2. Lattice vectors, point rows, and net planes

The length t of a vector $\mathbf{t} = u\mathbf{a} + v\mathbf{b} + w\mathbf{c}$ is given by

$$\begin{aligned} t^2 &= u^2\mathbf{a}^2 + v^2\mathbf{b}^2 + w^2\mathbf{c}^2 + 2uvab\cos\gamma \\ &\quad + 2uwac\cos\beta + 2vwbc\cos\alpha. \end{aligned} \quad (1.1.2.1)$$

Accordingly, the length r^* of a reciprocal-lattice vector $\mathbf{r}^* = h\mathbf{a}^* + k\mathbf{b}^* + l\mathbf{c}^*$ may be calculated from

$$\begin{aligned} r^{*2} &= h^2a^{*2} + k^2b^{*2} + l^2c^{*2} + 2hka^*b^*\cos\gamma^* \\ &\quad + 2hla^*c^*\cos\beta^* + 2klb^*c^*\cos\gamma^*. \end{aligned} \quad (1.1.2.2)$$

If the coefficients u, v, w of a vector $\mathbf{t} \in \mathbf{L}$ are coprime, [*uvw*] symbolizes the direction parallel to $\mathbf{t}$. In particular, [*uvw*] is used to designate a crystal edge, a zone axis, or a point row with that direction.

The integer coefficients h, k, l of a vector $\mathbf{r}^* \in \mathbf{L}^*$ are also the coordinates of a point of the corresponding reciprocal lattice and designate the Bragg reflection with scattering vector $\mathbf{r}^*$. If h, k, l are coprime, the direction parallel to $\mathbf{r}^*$ is symbolized by $[hkl]^*$.

Each vector $\mathbf{r}^*$ is perpendicular to a family of equidistant parallel nets within a corresponding direct point lattice. If the coefficients h, k, l of $\mathbf{r}^*$ are coprime, the symbol (*hkl*) describes that family of nets. The distance $d(hkl)$ between two neighbouring nets is given by

(2) Orthorhombic lattice with $b = \sqrt{3}a$: [310] is perpendicular to (110).

(i) P lattice (*cf.* Fig. 1.3.2.2):
$j = hu + kv + lw = 4$ even
$i = |j|/2 = 2$.

(ii) C lattice (*cf.* also Fig. 1.3.2.2):
Because of the C centring, [310] has to be replaced by $[\frac{3}{2}\frac{1}{2}0]$.
$j = hu' + kv' + lw' = 2$ even
$i = |j|/2 = 1$.

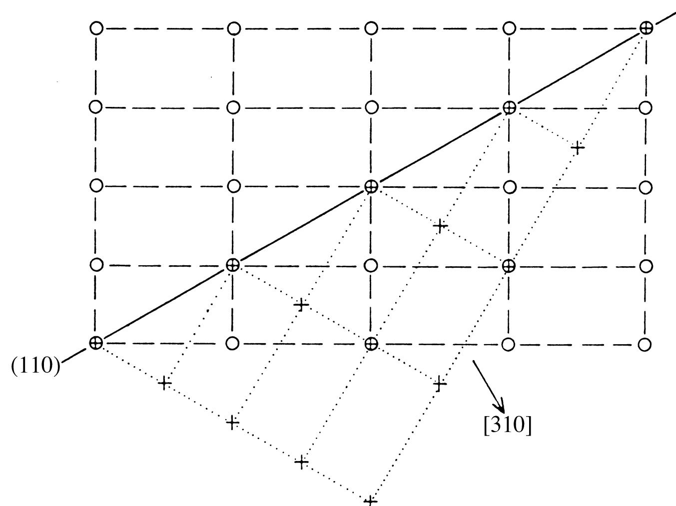

Fig. 1.3.2.2. Projection of the lattices of the twin components of an orthorhombic twinned crystal ($oP, b = \sqrt{3}a$) with twin index 2. The twin may be interpreted either as a rotation twin with twin axis [310] or as a reflection twin with twin plane (110). The figure shows, in addition, that twin index 1 results if the oP lattice is replaced by an oC lattice in this example (twinning by pseudomerohedry).

(3) Orthorhombic C lattice with $b = 2a$: [210] is perpendicular to (120) (*cf.* Fig. 1.3.2.3).
As (120) refers to an 'extinct reflection' of a C lattice, the triplet 240 has to be used in the calculation.
$j = h'u + k'v + l'w = 8$ even
$i = |j|/2 = 4$.

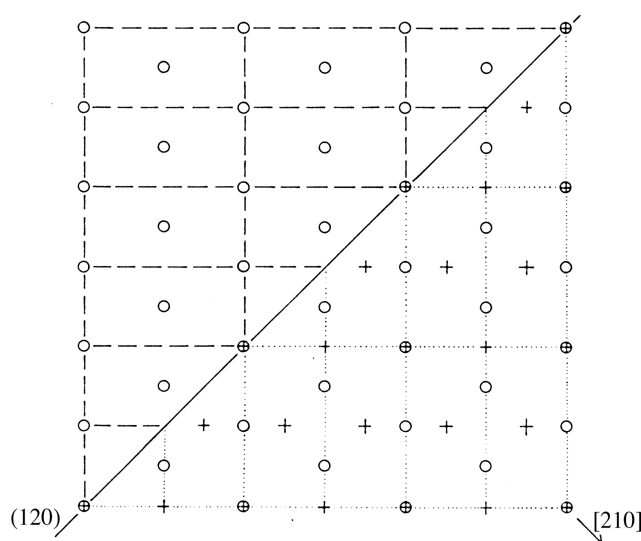

Fig. 1.3.2.3. Projection of the lattices of the twin components of an orthorhombic twinned crystal ($oC, b = 2a$) with twin index 4. The twin may be interpreted either as a rotation twin with twin axis [210] or as a reflection twin with twin plane (120).

(4) Rhombohedral lattice in hexagonal description with $c = \frac{1}{2}\sqrt{3}a$: $[\bar{1}1\bar{2}]$ is perpendicular to $(1\bar{1}1)$.
Because of the R centring, $[\bar{1}1\bar{2}]$ has to be replaced by $[\frac{\bar{1}}{3}\frac{1}{3}\frac{\bar{2}}{3}]$.
As $(1\bar{1}1)$ refers to an 'extinct reflection' of an R lattice, the triplet $1\bar{1}1$ has to be replaced by $3\bar{3}3$.
$j = h'u' + k'v' + l'w' = -4$ even
$i = |j|/2 = 2$.

1.3.3. Implication of twinning in reciprocal space

As shown above, the direct lattices of the components of any twin coincide in at least one row. The same is true for the corresponding reciprocal lattices. They coincide in all rows perpendicular to parallel net planes of the direct lattices.

For a reflection twin with twin plane (hkl), the reciprocal lattices of the twin components have only the lattice points with coefficients nh, nk, nl in common.

For a rotation twin with twofold twin axis [uvw], the reciprocal lattices of the twin components coincide in all points of the plane perpendicular to [uvw], *i.e.* in all points with coefficients h, k, l that fulfil the condition $hu + kv + lw = 0$.

For a rotation twin with irrational twin axis parallel to a net plane (hkl), only reciprocal-lattice points with coefficients nh, nk, nl are common to both twin components.

As the entire direct lattices of the two twin components coincide for an inversion twin, the same must be true for their reciprocal lattices.

For a reflection or rotation twin with a twin lattice of index i, the corresponding reciprocal lattices, too, have a sublattice with index i in common (*cf.* Fig. 1.3.2.1*b*). In analogy to direct space, the twin lattice in reciprocal space consists of each ith lattice plane parallel to the twin plane or perpendicular to the twin axis. If the twin index equals 1, the entire reciprocal lattices of the twin components coincide.

If for a reflection twin there exists only a lattice row [uvw] that is almost (but not exactly) perpendicular to the twin plane (hkl), then the lattices of the two twin components nearly coincide in a three-dimensional subset of lattice points. The corresponding misfit is described by the quantity ω, the *twin obliquity*. It is the angle between the lattice row [uvw] and the direction perpendicular to the twin plane (hkl). In an analogous way, the twin obliquity ω is defined for a rotation twin. If (hkl) is a net plane almost (but not exactly) perpendicular to the twin axis [uvw], then ω is the angle between [uvw] and the direction perpendicular to (hkl).

1.3.4. Twinning by merohedry

A twin is called a *twin by merohedry* if its twin operation belongs to the point group of its vector lattice, *i.e.* to the corresponding holohedry. As each lattice is centrosymmetric, an inversion twin is necessarily a twin by merohedry. Only crystals from merohedral (*i.e.* non-holohedral) point groups may form twins by merohedry; 159 out of the 230 types of space groups belong to merohedral point groups.

For a twin by merohedry, the vector lattices of all twin components coincide in direct *and* in reciprocal space. The twin index is 1. The maximal number of differently oriented twin components equals the subgroup index m of the point group of the crystal with respect to its holohedry.

Table 1.3.4.1 displays all possibilities for twinning by merohedry. For each holohedral point group (column 1), the types of Bravais lattices (column 2) and the corresponding merohedral point groups (column 3) are listed. Column 4 gives the subgroup index m of a merohedral point group in its

Any relp (*hkl*) lying in the region of reciprocal space between the $1/\lambda_{\max}$ and $1/\lambda_{\min}$ Ewald spheres and the resolution sphere $1/d_{\min}$ will diffract (the shaded area in Fig. 2.2.1.1). This region of reciprocal space is referred to as the accessible or stimulated region. Fig. 2.2.1.2 shows a predicted Laue pattern from a well aligned protein crystal. For a description of the indexing of a Laue photograph, see Bragg (1928, pp. 28, 29).

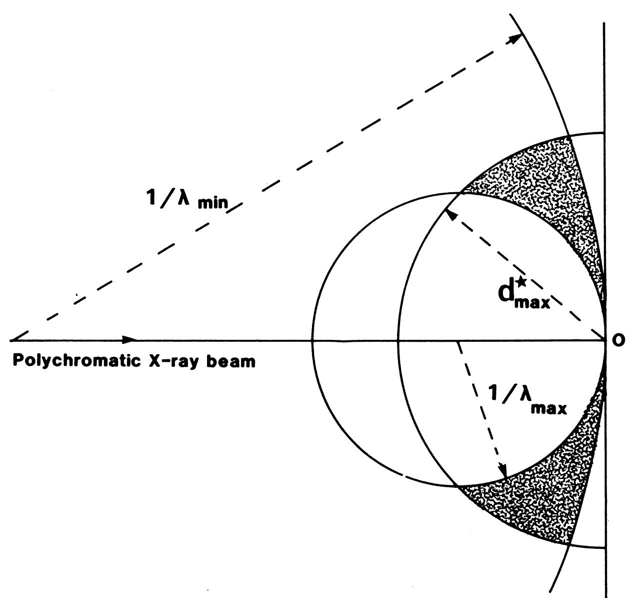

Fig. 2.2.1.1. Laue geometry. A polychromatic beam containing wavelengths $\lambda_{\min}$ to $\lambda_{\max}$ impinges on the crystal sample. The resolution sphere of radius $d^*_{\max} = 1/d_{\min}$ is drawn centred at O, the origin of reciprocal space. Any reciprocal-lattice point falling in the shaded region is stimulated. In this diagram, the radius of each Ewald sphere uses the convention $1/\lambda$.

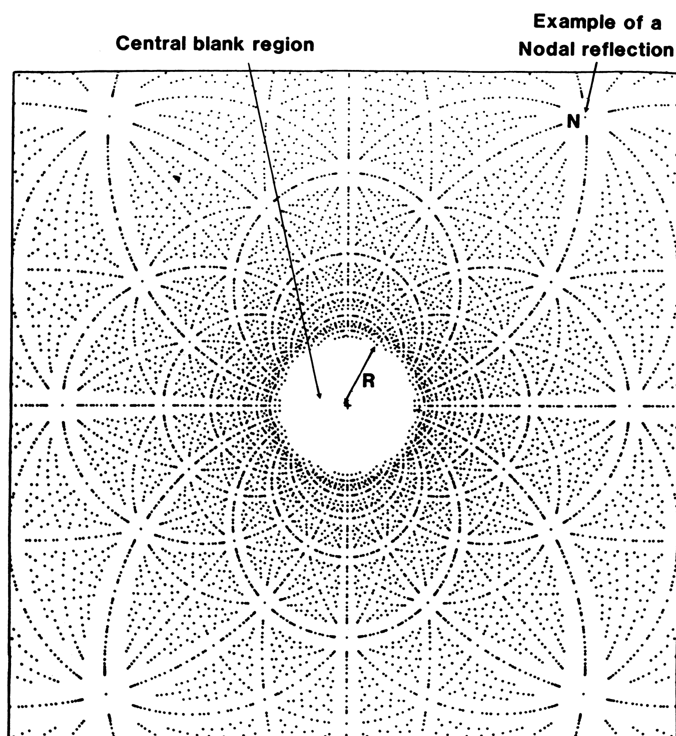

Fig. 2.2.1.2. A predicted Laue pattern of a protein crystal with a zone axis parallel to the incident, polychromatic X-ray beam. There is a pronounced blank region at the centre of the film (see Subsection 2.2.1.2). The spot marked N is one example of a nodal spot (see Subsection 2.2.1.4).

For a Laue spot at a given θ, only the ratio λ/d is determined, whether it is a single or a multiple relp component spot. If the unit-cell parameters are known from a monochromatic experiment, then a Laue spot at a given θ yields λ since d is then known. Conversely, precise unit-cell lengths cannot be determined from a Laue pattern alone; methods are, however, being developed to determine these (see Carr, Cruickshank & Harding, 1992).

The maximum Bragg angle $\theta_{\max}$ is given by the equation

$$\theta_{\max} = \sin^{-1}(\lambda_{\max}/2d_{\min}). \qquad (2.2.1.2)$$

2.2.1.2. *Crystal setting*

The main use of Laue photography has in the past been for adjustment of the crystal to a desired orientation. With small-molecule crystals, the number of diffraction spots on a monochromatic photograph from a stationary crystal is very small. With unfiltered, polychromatic radiation, many more spots are observed and so the Laue photograph serves to give a better idea of the crystal orientation and setting prior to precession photography. With protein crystals, the monochromatic still is used for this purpose before data collection *via* an area detector. This is because the number of diffraction spots is large on a monochromatic still and in a protein-crystal Laue photograph the stimulated spots from the *Bremsstrahlung* continuum are generally very weak. Synchrotron-radiation Laue photographs of protein crystals can be recorded with short exposure times. These patterns consist of a large number of diffraction spots.

Crystal setting *via* Laue photography usually involves trying to direct the X-ray beam along a zone axis. Angular mis-setting angles ε in the spindle and arc are easily calculated from the formula

$$\varepsilon = \tan^{-1}(\Delta/D), \qquad (2.2.1.3)$$

where Δ is the distance (resolved into vertical and horizontal) from the beam centre to the centre of a circle of spots defining a zone axis and D is the crystal-to-film distance.

After suitable angular correction to the sample orientation, the Laue photograph will show a pronounced blank region at the centre of the film (see Fig. 2.2.1.2). The radius of the blank region is determined by the minimum wavelength in the beam and the magnitude of the reciprocal-lattice spacing parallel to the X-ray beam (see Jeffery, 1958). For the case, for example, of the X-ray beam perpendicular to the a^*b^* plane, then

$$\lambda_{\min} = c(1 - \cos 2\theta), \qquad (2.2.1.4a)$$

where

$$2\theta = \tan^{-1}(R/D) \qquad (2.2.1.4b)$$

and R is the radius of the blank region (see Fig. 2.2.1.2), and D is the crystal-to-flat-film distance. If $\lambda_{\min}$ is known then an approximate value of c, for example, can be estimated. The principal zone axes will give the largest radii for the central blank region.

2.2.1.3. *Single-order and multiple-order reflections*

In Laue geometry, several relp's can occur in a Laue spot or ray. The number of relp's in a given spot is called the multiplicity of the spot. The number of spots of a given multiplicity can be plotted as a histogram. This is known as the multiplicity distribution. The form of this distribution is dependent on the ratio $\lambda_{\max}/\lambda_{\min}$. The multiplicity distribution

in all measurements, and errors due to (*b*) and (*c*) vary with each specimen.

Ideally, the specimen should be in the form of a focusing torus because of the beam divergence in the equatorial and axial planes. The curvatures would have to vary continuously and differently during the scan and it is impracticable to make specimens in such forms. An approximation is to make the specimen in a flexible cylindrical form with the radius of curvature increasing with decreasing 2θ (Ogilvie, 1963). This requires a very thin specimen (thus reducing the intensity) to avoid cracking and surface irregularities, and also introduces background from the substrate. A compromise uses rigid curved specimens, which match the SFC (Fig. 2.3.1.3) at the smallest 2θ angle to be scanned, and this eliminates most of the aberration (Parrish, 1968). A major disadvantage of the curvature is that it is not possible to spin the specimen.

In practice, a flat specimen is almost always used. The specimen surface departs from the focusing circle by an amount h at a distance $l/2$ from the specimen centre:

$$h = R_{\rm FC} - [R_{\rm FC}^2 - (l^2/2)]^{1/2}. \qquad (2.3.1.11)$$

This causes a broadening of the low-2θ side of the profile and shifts the centroid $\Delta 2\theta$ to lower 2θ:

$$\Delta 2\theta({\rm rad}) = -\alpha^2/(6\tan\theta). \qquad (2.3.1.12)$$

For $\alpha = 1^\circ$ and $2\theta = 20^\circ$, $\Delta 2\theta = -0.016^\circ$. The peak shift is about one-third as large as the centroid shift in the forward-reflection region. This aberration can be interpreted as a continuous series of specimen-surface displacements, which increase from 0 at the centre of the specimen to a maximum value at the ends. The effect increases with α and decreasing 2θ. The profile distortion is magnified in the small 2θ-angle region where the axial divergence also increases and causes similar effects. Typical flat-specimen profiles are shown in Fig. 2.3.1.10(*c*) and computed centroid shifts in Fig. 2.3.1.10(*d*).

The specimen-transparency aberration is caused by diffraction from below the surface of the specimen which asymmetrically broadens the profile (Langford & Wilson, 1962). The peak and centroid are shifted to smaller 2θ as shown in Fig. 2.3.1.10(*e*). For the case of a thick absorbing specimen, the centroid is shifted

$$\Delta 2\theta({\rm rad}) = \sin 2\theta/2\mu R \qquad (2.3.1.13)$$

and for a thin low-absorbing specimen

$$\Delta 2\theta({\rm rad}) = t\cos\theta/R, \qquad (2.3.1.14)$$

where μ is the effective linear absorption coefficient of the specimen used, t the thickness in cm, and R the diffractometer radius in cm. The intermediate absorption case is described by Wilson (1963). A plot of equation (2.3.1.13) for various values of μ is given in Fig. 2.3.1.10(*f*). The effect varies with $\sin 2\theta$ and is maximum at 90° and zero at 0° and 180°. For example, if $\mu = 50\,{\rm cm}^{-1}$, the centroid shift is -0.033° at 90° and falls to -0.012° at $20^\circ 2\theta$.

The observed intensity is reduced by absorption of the incident and diffracted beams in the specimen. The intensity loss is $\exp(-2\mu/x_s \operatorname{cosec}\theta)$, where μ is the linear absorption coefficient of the powder sample (it is almost always smaller than the solid material) and x_s is the distance below the surface, which may be equal to the thickness in the case of a thin film or low-absorbing material specimen. The thick (1 mm) specimen of LiF in Fig. 2.3.1.10(*e*) had twice the peak intensity of the thin (0.1 mm) specimen.

The aberration can be avoided by making the sample thin. However, the amount of incident-beam intensity contributing to the reflections could then vary with θ because different amounts are transmitted through the sample and this may require corrections of the experimental data. Because the effective reflecting volume of low-absorbing specimens lies below the surface, care must be taken to avoid blocking part of the diffracted beam with the antiscatter slits or the specimen holder, particularly at small 2θ.

There are additional problems related to the specimen such as preferred orientation, particle size, and other factors; these are discussed in Section 2.3.3.

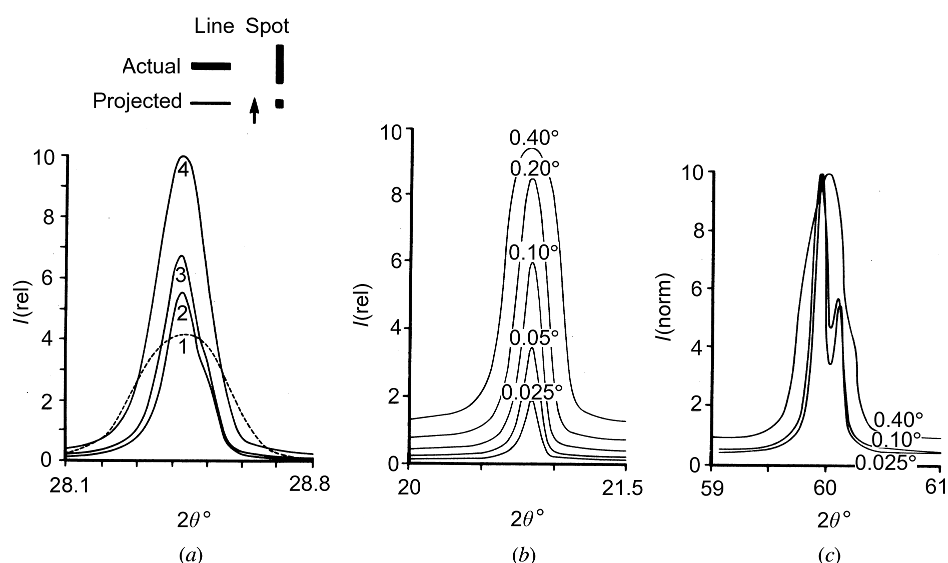

Fig. 2.3.1.9. (*a*) Effect of source size on profile shape, Cu $K\alpha$, $\alpha_{\rm ES}$ 1°, $\alpha_{\rm RS}$ 0.05°, Si(111).

No.	Projected size (mm)	FWHM (°2θ)
1	1.6 × 1.0 (spot)	0.31
2	0.32 × 10 (line)	0.11
3	0.16 × 10 (line)	0.13
4	0.32 × 12 (line)	0.17.

Effect of receiving-slit aperture $\alpha_{\rm RS}$ on profiles of quartz (*b*) (100) and (*c*) (121); peak intensities normalized, Cu $K\alpha$, $\alpha_{\rm ES}$ 1°.

determination, and texture studies. These and other applications can be found in an annotated bibliography covering the period 1968–1978 (Laine & Lähteenmäki, 1980). The short counting time and the simultaneous recording of the diffraction spectrum permit the study of the kinetics of structural transformations in time frames of a few seconds or minutes.

Energy-dispersive powder diffraction has proved to be of great value for high-pressure structural studies in conjunction with synchrotron radiation. The brightness of the radiation source and the efficiency of the detector system permit the recording of a diffraction spectrum with satisfactory counting statistics in a reasonable time (100–1000 s) in spite of the extremely small sample volume (10^{-3}–10^{-5} mm^3). Reviews have been given by Buras & Gerward (1989) and Häusermann (1992). Recently, XED experiments have been performed at pressures above 400 GPa, and pressures near 1 TPa may be attainable in the near future (Ruoff, 1992). At this point, it should be mentioned that XED methods have limited resolution and generally give unreliable peak intensities. The situation has been transformed recently by the introduction of the image-plate area detector, which allows angle-dispersive, monochromatic methods to be used with greatly improved resolution and powder averaging (Nelmes & McMahon, 1994, and references therein).

2.5.2. White-beam and time-of-flight neutron diffraction (By J. D. Jorgensen, W. I. F. David, and B. T. M. Willis)

2.5.2.1. *Neutron single-crystal Laue diffraction*

In traditional neutron-diffraction experiments, using a continuous source of neutrons from a nuclear reactor, a narrow wavelength band is selected from the wide spectrum of neutrons emerging from a moderator within the reactor. This monochromatization process is extremely inefficient in the utilization of the available neutron flux. If the requirement of discriminating between different orders of reflection is relaxed, then the entire white beam can be employed to contribute to the diffraction pattern and the count-rate may increase by several orders of magnitude. Further, by recording the scattered neutrons on photographic film or with a position-sensitive detector, it is possible to probe simultaneously many points in reciprocal space.

If the experiment is performed using a pulsed neutron beam, the different orders of a given reflection may be separated from one another by time-of-flight analysis. Consider a short polychromatic burst of neutrons produced within a moderator. The subsequent times-of-flight, t, of neutrons with differing wavelengths, λ, measured over a total flight path, L, may be discriminated one from another through the de Broglie relationship:

$$m_n(L/t) = h/\lambda, \qquad (2.5.2.1)$$

where m_n is the neutron mass and h is Planck's constant. Expressing t in microseconds, L in metres and λ in Å, equation (2.5.2.1) becomes

$$t = 252.7784\ L\lambda.$$

Inserting Bragg's law, $\lambda = 2(d/n)\sin\theta$, for the nth order of a fundamental reflection with spacing d in Å gives

$$t = (505.5568/n)Ld\sin\theta. \qquad (2.5.2.2)$$

Different orders may be measured simply by recording the time taken, following the release of the initial pulse from the moderator, for the neutron to travel to the sample and then to the detector.

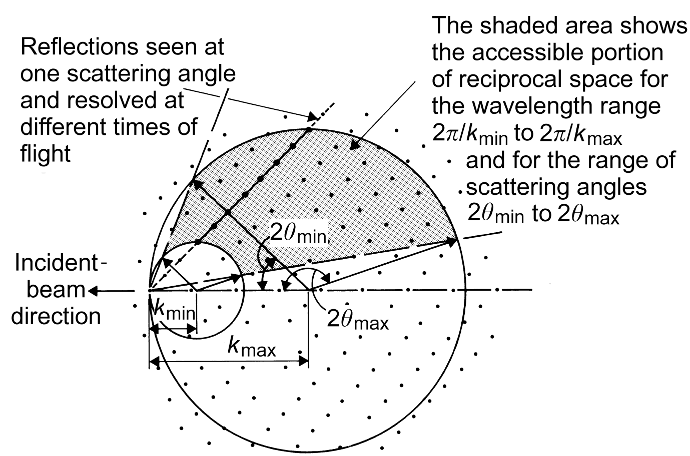

Fig. 2.5.2.1. Construction in reciprocal space to illustrate the use of multi-wavelength radiation in single-crystal diffraction. The circles with radii $k_{max} = 2\pi/\lambda_{min}$ and $k_{min} = 2\pi/\lambda_{max}$ are drawn through the origin. All reciprocal-lattice points within the shaded area may be sampled by a linear position-sensitive detector spanning the scattering angles from $2\theta_{min}$ to $2\theta_{max}$. With a position-sensitive area detector, a three-dimensional portion of reciprocal space may be examined (after Schultz, Srinivasan, Teller, Williams & Lukehart, 1984).

The origins of pulsed neutron diffraction can be traced back to the work of Lowde (1956) and of Buras, Mikke, Lebech & Leciejewicz (1965). Later developments are described by Turberfield (1970) and Windsor (1981). Although a pulsed beam may be produced at a nuclear reactor using a chopper, the major developments in pulsed neutron diffraction have been associated with pulsed sources derived from particle accelerators. Spallation neutron sources, which are based on proton synchrotrons, allow optimal use of the Laue method because the pulse duration and pulse repetition rate can be matched to the experimental requirements. The neutron Laue method is particularly useful for examining crystals in special environments, where the incident and scattered radiations must penetrate heat shields or other window materials. [A good example is the study of the incommensurate structure of α-uranium at low temperature (Marmeggi & Delapalme, 1980).]

A typical time-of-flight single-crystal instrument has a large area detector. For a given setting of detector and sample, a three-dimensional region is viewed in reciprocal space, as shown in Fig. 2.5.2.1. Thus, many Bragg reflections can be measured at the same time. For an ideally imperfect crystal, with volume V_s and unit-cell volume v_c, the number of neutrons of wavelength λ reflected at Bragg angle θ by the planes with structure factor F is given by

$$N = i_0(\lambda)\lambda^4 V_s F^2/(2v_c^2\sin^2\theta), \qquad (2.5.2.3)$$

where $i_0(\lambda)$ is the number of incident neutrons per unit wavelength interval. In practice, the intensity in equation (2.5.2.3) must be corrected for wavelength-dependent factors, such as detector efficiency, sample absorption and extinction, and the contribution of thermal diffuse scattering. Jauch, Schultz & Schneider (1988) have shown that accurate structural data can be obtained using the single-crystal time-of-flight method despite the complexity of these wavelength-dependent corrections.

2.5.2.2. *Neutron time-of-flight powder diffraction*

This technique, first developed by Buras & Leciejewicz (1964), has made a unique impact in the study of powders in confined environments such as high-pressure cells (Jorgensen &

scattering function because that leads to an increasing loss of essential information about the particle (monomer) itself.

2.6.1.4. *Polydisperse systems*

In this subsection, we give a short survey of the problem of polydispersity. It is most important that there is no way to decide from small-angle scattering data whether the sample is mono- or polydisperse. Every data set can be evaluated in terms of monodisperse or polydisperse structures. Independent *a priori* information is necessary to make this decision. It has been shown analytically that a certain size distribution of spheres gives the same scattering function as a monodisperse ellipsoid with axes a, b and c (Mittelbach & Porod, 1962).

The scattering function of a polydisperse system is determined by the shape of the particles and by the size distribution. As mentioned above, we can assume a certain size distribution and can determine the shape, or, more frequently, we assume the shape and determine the size distribution. In order to do this we have to assume that the scattered intensity results from an ensemble of particles of the same shape whose size distribution can be described by $D_n(R)$, where R is a size parameter and $D_n(R)$ denotes the number of particles of size R. Let us further assume that there are no interparticle interferences or multiple scattering effects. Then the scattering function $I(h)$ is given by

$$I(h) = c_n \int\limits_0^\infty D_n(R) R^6 i_0(hR) \,\mathrm{d}R, \qquad (2.6.1.54)$$

where c_n is a constant, the factor R^6 takes into account the fact that the particle volume is proportional to R^3, and $i_0(hR)$ is the normalized form factor of a particle size R. In many cases, one is interested in the mass distribution $D_m(R)$ [sometimes called volume distribution $D_c(R)$]. In this case, we have

$$I(h) = c_m \int\limits_0^\infty D_m(R) R^3 i_0(hR) \,\mathrm{d}R. \qquad (2.6.1.55)$$

The solution of these integral equations, *i.e.* the computation of $D_n(R)$ or $D_m(R)$ from $I(h)$, needs rather sophisticated numerical or analytical methods and will be discussed later.

The problems of interparticle interference and multiple scattering in the case of polydisperse systems cannot be described analytically and have not been investigated in detail up to now. In general, interference effects start to influence data from small-angle scattering experiments much earlier, *i.e.* at lower concentration, than multiple scattering. Multiple scattering becomes more important with increasing size and contrast and is therefore dominant in light-scattering experiments in higher concentrations.

A concentration series and extrapolation to zero concentration as in monodisperse systems should be performed to eliminate these effects.

2.6.1.5. *Instrumentation*

X-ray sources are the same for small-angle scattering as for crystallographic experiments. One can use conventional generators with sealed tubes or rotating anodes for higher power. For the vast majority of applications, an X-ray tube with copper anode is used; the wavelength of its characteristic radiation (Cu $K\alpha$ line) is 0.154 nm. Different anode materials emit X-rays of different characteristic wavelengths.

X-rays from synchrotrons or storage rings have a continuous wavelength distribution and the actual wavelength for the experiment is selected by a monochromator. The intensity is much higher than for any type of conventional source but synchrotron radiation is available only at a few places in the world. Reviews on synchrotron radiation and its application have been published during recent years (Stuhrmann, 1978; Holmes, 1982; Koch, 1988). In these reviews, one can also find some remarks on the general principles of the systems including cameras and special detectors.

2.6.1.5.1. *Small-angle cameras*

General. In any small-angle scattering experiment, it is necessary to illuminate the sample with a well defined flux of X-rays. The ideal condition would be a parallel monochromatic beam of negligible dimension and very high intensity. These theoretical conditions can never be reached in practice (Pessen, Kumosinski & Timasheff, 1973). One of the main reasons is the fact that there are no lenses as in the visible range of electromagnetic radiation. The refractive index of all materials is equal to or very close to unity for X-rays. On the other hand, this fact has some important advantages. It is, for example, possible to use circular capillaries as sample holders without deflecting the beam. There are different ways of constructing a small-angle scattering system. Slit, pinhole, and block systems define a certain area where the X-rays can pass. Any slit or edge will give rise to secondary scattering (parasitic scattering). The special construction of the instrument has to provide at least a subspace in the detector plane (plane of registration) that is free from this parasitic scattering. The crucial point is of course to provide the conditions to measure at very small scattering angles.

The other possibility of building a small-angle scattering system is to use monochromator crystals and/or bent mirrors to select a narrow wavelength band from the radiation (important for synchrotron radiation) and to focus the X-ray beam to a narrow spot. These systems require slits in addition to eliminate stray radiation.

Block collimation – Kratky camera. The Kratky (1982*a*) collimation system consists of an entrance slit (edge) and two blocks – the *U*-shaped centre piece and a block called *bridge*. With this system, the problem of parasitic scattering can be largely removed for the upper half of the plane of registration and the smallest accessible scattering angle is defined by the size of the entrance slit (see Fig. 2.6.1.13). This system can be integrated in an evacuated housing (Kratky compact camera) and fixed on the top of the X-ray tube. It is widely used in many laboratories for different applications. In the Kratky system, the X-ray beam has a rectangular shape, the length being much larger than the width. Instrumental broadening can be corrected by special numerical routines. The advantage is a relatively high primary-beam intensity. The main disadvantage is that it cannot be used in special applications such as oriented systems where

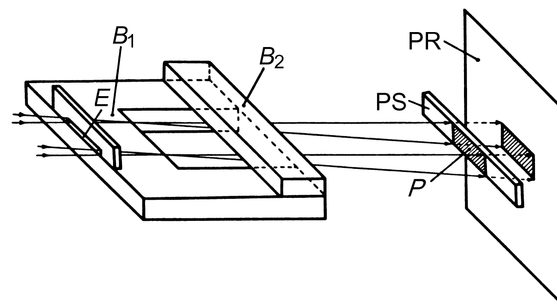

Fig. 2.6.1.13. Schematic drawing of the block collimation (Kratky camera): E edge; B_1 centre piece; B_2 bridge; P primary-beam profile; PS primary-beam stop; PR plane of registration.

diffraction in $CC'D'D$ will take the path shown by the heavy line in Fig. 2.7.2.4, simplifying the picture to the case of extreme confinement of energy flow to parallelism with the Bragg planes. At the X-ray exit surface DD', splitting into $\mathbf{K}_0$ and $\mathbf{K}_h$ beams occurs. A slit-less arrangement, as shown in the figure, may suffice. Then, when S is a point-like source of $K\alpha$ radiation, and distance a is sufficiently large, films F_1 and F_2 will each record a pair of narrow images formed by the α_1 and α_2 wavelengths, respectively. A wider area of specimen can be imaged if a line focus rather than a point focus is placed at S (Barth & Hosemann, 1958), but then the α_1 and α_2 images will overlap. Under conditions of high anomalous transmission, defects in the crystal cause a reduction in transmitted intensity, which appears similarly in the $\mathbf{K}_0$ and $\mathbf{K}_h$ images. Thus, it is possible to gain intensity and improve resolution by recording both images superimposed on a film F_3 placed in close proximity to the X-ray exit face DD' (Gerold & Meier, 1959).

2.7.3. Double-crystal topography

The foregoing description of single-crystal techniques will have indicated that in order to gain greater sensitivity in orientation contrast there are required incident beams with closer collimation, and limitation of dispersion due to wavelength spread of the characteristic X-ray lines used. It suggests turning to prior reflection of the incident beam by a perfect crystal as a means of meeting these needs. Moreover, the application of crystal-reflection-collimated radiation to probe angularly step by step as well as spatially point by point the intensity of Bragg reflection from the vicinity of an individual lattice defect such as a dislocation brings possibilities of new measurements beyond the scope provided by simply recording the local value of the integrated reflection. The X-ray optical principles of double-crystal X-ray topography are basically those of the double-crystal spectrometer (Compton & Allison, 1935). The properties of successive Bragg reflection by two or more crystals can be effectively displayed by a Du Mond diagram (Du Mond 1937), and such will now be applied to show how collimation and monochromatization result from successive reflection by two crystals, U and V, arranged as sketched in Fig. 2.7.3.1. They are in the dispersive, antiparallel, '$++$' setting, and are assumed to be identical perfect crystals set for the same symmetrical Bragg reflection. Only rays making the same glancing angle with both surfaces will be reflected by both U and V. For example, radiation of shorter wavelength reflected at a smaller glancing angle at U (the ray shown by the dashed line) will impinge at a larger glancing angle on V and not satisfy the Bragg condition. In this $++$ setting, with a given angle ω between the Bragg-reflecting planes of each crystal, $\theta_U + \theta_V = \omega$ and $\Delta\theta_U = -\Delta\theta_V$. The Du Mond diagram for the $++$ setting, Fig. 2.7.3.2, shows plots of Bragg's law for each crystal, the V curve being a reflection of the U curve in a vertical mirror line and differing by ω from the U curve in its coordinate of intersection with the axis of abscissa, in accord with the equations given above. The small angular range of reflection of a monochromatic ray by each perfect crystal is represented exaggeratedly by the band between the parallel curves. Where the band for crystal U superimposes on the band for V (the shaded area) defines semiquantitatively the divergence and wavelength spread in the rays successively reflected by U and V. (It is taken for granted that $\frac{1}{2}\omega$ lies between the maximum and minimum incident glancing angles on U, $\theta_{\max}$ and $\theta_{\min}$, afforded by the incident beam, assumed polychromatic.) The reflected beam from U alone contains wavelengths ranging from $\lambda_{\min}$ to $\lambda_{\max}$. Comparison of these θ and λ ranges with the extent of the shaded area illustrates the efficacy of the $++$ arrangement in providing a collimated and monochromatic beam, which can be employed to probe the reflecting properties of a third crystal (Nakayama, Hashizume, Miyoshi, Kikuta & Kohra, 1973). Techniques employing three or more successive Bragg reflections find considerable application when used with synchrotron X-ray sources, and will be considered below, in Section 2.7.4.

The most commonly used arrangement for double-crystal topography is shown in Fig. 2.7.3.3, in which U is the 'reference' crystal, assumed perfect, and V is the specimen crystal under examination. Crystals U and V are in the parallel, '$+-$' setting, which is non-dispersive when the Bragg planes of U and V have the same (or closely similar) spacings. Before considering the Du Mond diagram for this arrangement, note that Bragg reflection at the reference crystal U is asymmetric, from planes inclined at angle α to its surface. Asymmetric reflections have useful properties, discussed, for example, by Renninger (1961), Kohra (1972), Kuriyama & Boettinger (1976), and Boettinger, Burdette & Kuriyama (1979). The asymmetry factor, b, of magnitude $|\mathbf{K}_0 \cdot \mathbf{n}/\mathbf{K}_h \cdot \mathbf{n}|$, $\mathbf{n}$ being the

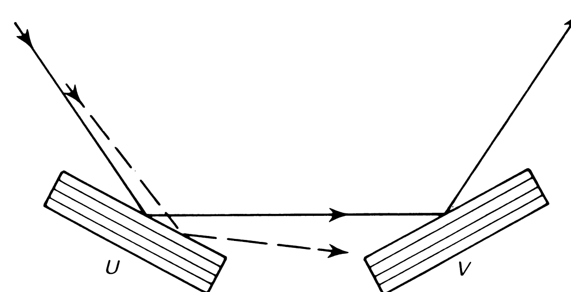

Fig. 2.7.3.1. Double-crystal $++$ setting.

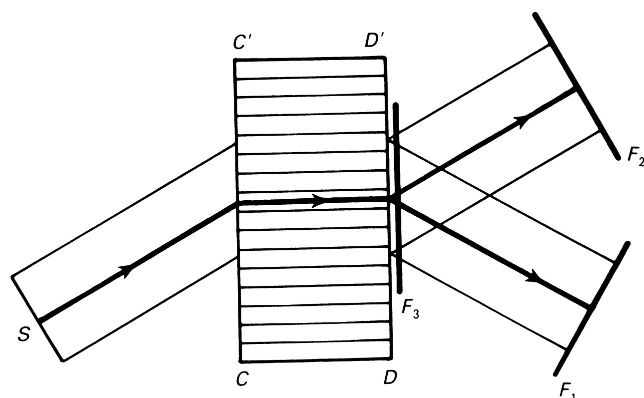

Fig. 2.7.2.4. Topographic techniques using anomalous transmission.

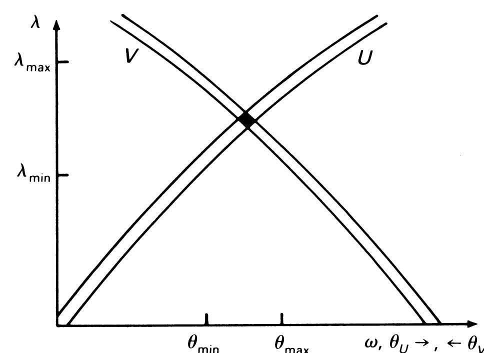

Fig. 2.7.3.2. Du Mond diagram for $++$ setting in Fig. 2.7.3.1.

the wavelength resolution is determined by the monochromator, whereas the timing and moderator characteristics determine the wavelength resolution on a time-of-flight instrument. Although the second term in equation (2.9.5.1) is standard in scattering, it has a unique characteristic, in that the angular divergence of the reflected beam determines the resolution. This is the case because the sample is a δ-function scatterer, so that the angle of the incident beam can be determined precisely by knowing the reflected angle (Hamilton, Hayter & Smith, 1994). For a more complete description of both types of neutron reflectometry instrumentation, see Russell (1990).

2.9.6. Resolution in real space

From Fig. 2.9.2.3, the period δQ of the reflectivity oscillation (in the region where the Born approximation becomes valid, sufficiently far away from the critical angle) is inversely proportional to the thickness t of the film. That is, $2\pi/(\delta Q) = t$. Consequently, in order to be able to resolve reflectivity oscillations for a film of thickness t, the instrumental Q resolution ΔQ [from equation (2.9.5.1)] must be approximately $2\pi/t$ or smaller. With sufficiently good instrumental resolution, even the thickness of a film with non-abrupt interfaces can be accurately determined, as demonstrated by the hypothetical case depicted in Fig. 2.9.6.1 (where the instrumental resolution is taken to be perfect): an overall film-thickness difference of 2 Å (between 42 and 40 Å films) is clearly resolved at a Q of about 0.2 Å^{-1}. In practice, differences even less than this can be distinguished. Note, however, that to 'see' more detailed features in the scattering-density profile (such as the oscillation on top of the plateau shown for the long-dash profile in the inset of Fig. 2.9.6.1), other than the overall film thickness, it can be necessary to make reflectivity measurements at values of Q corresponding to 2π/(characteristic dimension of the feature).

2.9.7. Applications of neutron reflectometry

2.9.7.1. *Self-diffusion*

One of the simplest, yet powerful, examples of the use of neutron reflectivity is in the study of self-diffusion. Most techniques to measure diffusion coefficients rely on chemical and mechanical methods to measure density profiles after a sample

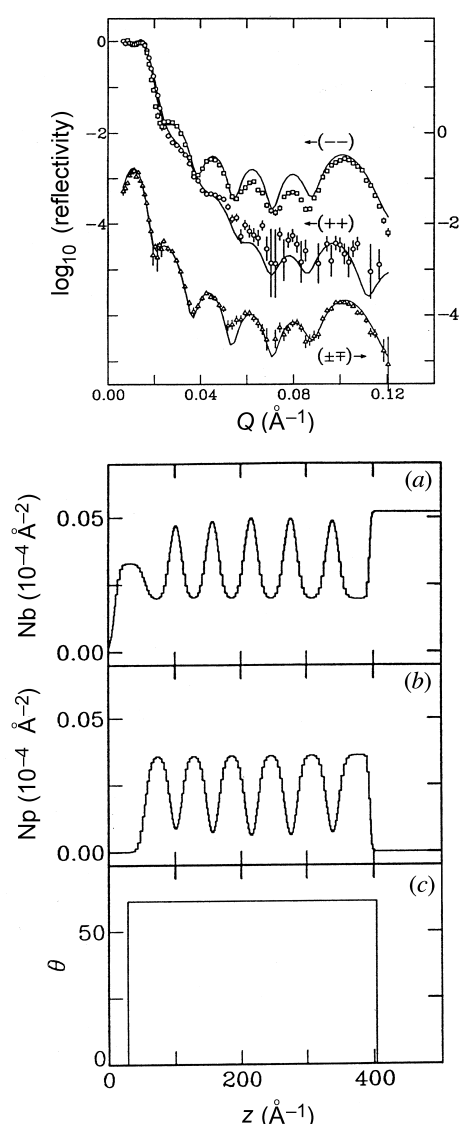

Fig. 2.9.7.3. Co/Cu(111) spin-dependent reflectivities (top). Nuclear (Nb) and magnetic (Np) scattering densities (bottom). Also shown is the (constant) moment direction [after Schreyer *et al.* (1993)].

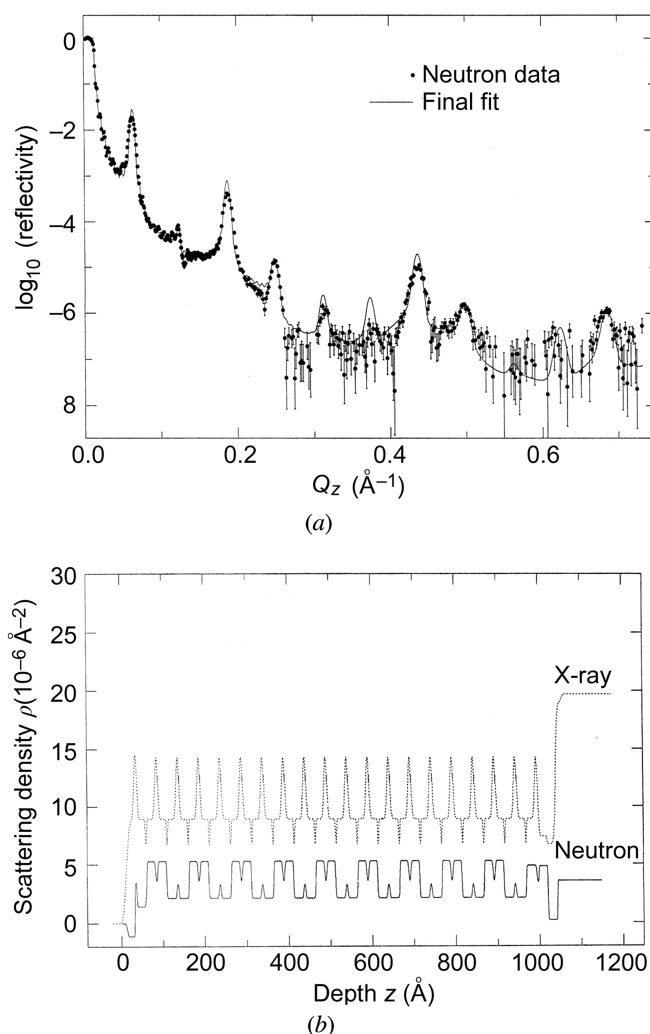

Fig. 2.9.7.4. (*a*) Measured neutron reflectivity for the Langmuir–Blodgett multilayer described in the text along with the fit. (*b*) Both corresponding neutron and X-ray scattering density profiles. The X-ray reflectivity is more sensitive to the high-Z barium in the head groups whereas the neutron reflectivity can distinguish mixing between adjacent hydrogenated and deuterated hydrocarbon tails [after Wiesler *et al.* (1995)].

Table 3.4.1.1. *Single-crystal and powder mounting, capillary tubes and other containers*

Material	Temperature range (K)	Comments
(*A*) Capillary tubes		
Glass Lindemann glass Vitreous silica	< 773 < 773 < 1373	Lindemann glass scatters less, but is moisture sensitive Thinner walled tubes that are less sensitive to atmospheric influences can be obtained using other types of glass
Collodion Polyvinyl methylal resin (*e.g.* Formvar) Cellulose acetate	93 to 343 < 323 < 373	These capillaries can be made by coating a copper wire with a solution of the polymer in an appropriate organic solvent. When dry, the metal core may be removed by stretching, to reduce its diameter
Polyethylene	< 373	Tubes may be drawn from the molten polymer using a glass tube and a slow stream of air. The polymer gives a distinct diffraction pattern
(*B*) Other containers		
Gelatin capsules	< 303	Vessels with very thin, 20 μm, windows can be made
Methyl methacrylate resin (*e.g.* Perspex)	< 338	
Mica	< 1073	Mica windows useful in vessels for small-angle scattering, but the wall size is generally thicker, ~0.3 mm, and there are discrete lines at 10.00, 3.34 and 2.60 Å in the diffraction pattern
Regenerated cellulose film (*e.g.* cellophane)	Ambient	

For optimum results, tube diameters should be between 0.3 and 0.5 mm with wall thicknesses of 0.02 to 0.05 mm. The materials listed above, except where stated, give diffuse diffraction patterns. If necessary, control diffraction patterns, recorded only from the capillary or other container, should be taken.

(1993) have developed a mirror furnace working at up to 2300 K and suitable for polycrystalline or single-crystal samples.

A comprehensive account of cryogenic studies pertinent to both polycrystalline and single-crystal samples is given by Rudman (1976). Nieman, Evans, Heal & Powell (1984) have described a device for the preparation of low-temperature samples of noxious materials. The device is enclosed in a vanadium can and is therefore only suitable for neutron diffraction studies. Ihringer & Küster (1993) have described a cryostat for powder diffraction, temperature range 8–300 K, for use on a synchrotron-radiation beam line at HASYLAB, Germany (Arnold *et al.*, 1989).

3.4.1.3. *Single crystals (small molecules)*

3.4.1.3.1. *General*

Small single crystals of inorganic and organic materials, suitable for intensity data collection, are normally glued to the end of a glass or vitreous silica fibre, or capillary (Denne, 1971*b*; Stout & Jensen, 1968). A simple device that fits onto a conventional microscope stage to facilitate the procedure of cementing a single crystal to a glass fibre has been constructed by Bretherton & Kennard (1976). The support is in turn fixed to a metal pin that fits onto a goniometer head. For preliminary studies, plasticine or wax are useful fixatives, since it is then relatively easy to alter the orientation of the support, and hence the crystal, as required. For data-collection purposes, the support should be firmly fixed or glued to the goniometer head pin. The fibre should be sufficiently thin to minimize absorption effects but thick enough to form a rigid support. The length of the fibre is usually about 10 mm. Kennard (1994) has described a macroscope that allows specimens to be observed remotely during data collection and can also be used for measurement of crystal faces for absorption correction. Large specimens can be directly mounted onto a camera or onto a specially designed goniometer (Denne, 1971*a*; Shaham, 1982). A method using high-temperature diffusion to bond ductile single crystals to a metal backing, for strain-free mounting, has been described by Black, Burdette & Early (1986).

Prior to crystal mounting, it is always prudent to determine the nature of any spatial constraints that are applicable for the proposed experiment. Some diffractometers have relatively little translational flexibility, and the length of the fibre mount or capillary is critical. For some low-temperature devices where the cooling gas stream is coaxial with the specimen mount, the

4.1.4. Special applications of X-rays, electrons, and neutrons

Special sources and/or special properties of these radiations are used in general crystallography.

4.1.4.1. *X-rays, synchrotron radiation, and γ-rays*

X-ray beams from *rotating-anode tubes* are approximately one hundred times more intensive than those from normal X-ray tubes. *Laser plasma X-ray sources* yield intensive nanosecond pulses of the line spectrum of nearly electron-free ions in the X-ray region with a spectral breadth of $\Delta\lambda/\lambda \approx 10^{-3}$. Several such pulses may be repeated per hour (Frankel & Forsyth, 1979). *Synchrotron radiation* is characterized by a continuous spectrum of wavelengths, high spectral flux, high intensity, high brightness, extreme collimation, sharp time structure (pulses with 30–200 ps length emitted in ns intervals), and nearly 100% polarization in the orbital plane (Kuntz, 1979; Bonse, 1980). Some of these properties are utilized in ordinary structure analysis: for example, fine tuning of the wavelength of synchrotron radiation for the solution of the phase problem by resonant scattering on chosen atomic species constituting the material under study. But these radiations also offer new advantages in other fields of crystallography, as, for example, in X-ray topography (Tanner & Bowen, 1980), in time-resolving studies (Bordas, 1980), in X-ray microscopy (Parsons, 1980), in studies of local atomic arrangements by extended X-ray absorption fine structure (XAFS) investigations (Lee, Citrin, Eisenberger & Kincaid, 1981) or studies of surface structures by X-ray photoemission spectroscopy (XPS) (Plummer & Eberhardt, 1982), *etc*. *γ-rays* emitted by radioactive sources such as ^{198}Au ($t_{1/2} = 2.7$ d), ^{153}Sm ($t_{1/2} = 46.8$ h), ^{192}Ir ($t_{1/2} = 74.2$ d) or ^{137}Cs ($t_{1/2} = 29.9$ a) are characterized by short wavelengths (typically hundreds of Å), by narrow spectral breadth ($\Delta E \approx 10^{-8}$ eV, $\Delta\lambda/\lambda \approx 10^{-6}$) and by relatively low beam intensity ($\sim 10^8 - 10^9$ m^{-2} s^{-1}). They are mainly used for studies of the mosaic structure of single crystals (Schneider, 1983) or for the determination of charge density distribution (Hansen & Schneider, 1984). The typical absorption length of $\sim$ 1–4 cm and the increase of the extinction length by a factor of about 50 compared with ordinary X-rays are advantages utilized in these experiments. γ-rays also find applications in magnetic structure studies and in the determination of gradients of electric fields by Mössbauer diffraction and spectroscopy (Kuz'min, Kolpakov & Zhdanov, 1966).

For Compton scattering, see Sections 6.1.1 and 7.4.3.

4.1.4.2. *Electrons*

Low-energy electrons (10–200 eV) have wavelengths near 1 Å and a penetration of a few Å below the surface of a crystal. Low-energy electron diffraction (LEED) is thus used for the study of surface-layer structures (Ertl & Küppers, 1974). High-energy electrons are also currently used in electron microscopy in materials science. Under certain conditions, images of lattice planes with a resolution of 2 Å or better can be obtained. Transmission electron microscopy is also used for reconstruction of the three-dimensional structure of biological objects (such as viruses), alternatively in combination with X-ray diffraction (de Rossier & Klug, 1968).

4.1.4.3. *Neutrons*

The most important application of neutron diffraction is found in studies of magnetic structures (Marshall & Lovesey, 1971). The magnetic moment of neutrons is equal to $1.913\,\mu_N$, where μ_N is the nuclear magneton, and neutrons have spin $I = 1/2$. They can thus interact with the magnetic moments of nuclei or with the magnetic moments of the electron shells with uncompensated spins. Changes in wavelength from 1 to 30 Å enable one to study non-uniformities of different sizes and structures of polymers and biological objects by the small-angle method. Inelastic scattering of neutrons is used for determining phonon-dispersion curves. Neutron topography and neutron texture diffraction can be utilized for the relatively large samples used in technological applications. The *pulsed spallation neutron sources* are used for high-resolution time-of-flight powder diffraction (Windsor, 1981) or for time-resolved Laue diffraction.

4.1.5. Other radiations

4.1.5.1. *Atomic and molecular beams*

Fast charged particles like protons, deuterons or He$^+$ ions show preferential penetration through crystals when the direction of incidence is almost parallel to the prominent planes or axes of the lattice. The reverse effect of this *channelling* is *shadowing* when the centres of emission of the fast charged particles are the atoms of the crystal themselves. These methods are, for example, used in studies of surface structures, lattice defects, orientation, thermal vibrations, atomic displacements, and concentration profiles (Feldman, Mayer & Picraux, 1982). Ion beams are also applied in special analytical methods like Rutherford backscattering (RBS), inelastic scattering, proton-induced X-ray analysis (PIX), *etc*.

4.1.5.2. *Positrons and muons*

These elementary particles are used in crystallography mainly in studies of lattice defects (vacancies, interstitials, and impurity atoms) for the determination of their concentration, location, and diffusion by means of the techniques such as positron annihilation spectroscopy (PAS) and muon spin resonance (μSR) – see, for example, Siegel (1980) and Gyax, Kündig & Meier (1979). The positron implantation range in a solid is $\lesssim 100\,\mu$m from the positron sources usually used (*e.g.* ^{22}Na, ^{64}Cu, ^{58}Co); these sources yield positrons with end-point energies of $\lesssim$1 MeV. The PAS techniques are based on lifetime, Doppler broadening or angular correlation measurements of γ-rays emitted by the decaying nucleus of the radioactive source and those resulting from the positron–electron annihilation process. Muon sources require intense primary medium-energy proton beams. The positive muon μ^+ has charge +e, spin 1/2, mass 105.659 MeV/c^2 and a magnetic moment equal to 1.001 of the muon–magneton units. With a mean lifetime of 2.197 µs, the muon decays into a positron (e$^+$) and two neutrinos (ν_e and $\bar{\nu}_\mu$). The correlation between the direction of the emitted positron and the spin direction of the muon allows one to measure the spin precession frequency and/or the decay of the muon polarization of an ensemble of muons implanted in a solid.

4.1.5.3. *Infrared, visible, and ultraviolet light*

Visible light is one of the oldest tools used by crystallographers for macroscopic symmetry determination, for orientation of crystals, and in metallographic microscopes for phase analysis. Infrared and Raman spectroscopy are highly complementary methods in the infrared and visible range of wavelengths, respectively. The information content available with the two techniques is determined by molecular symmetry and polarity. This information is utilized for the identification of molecules or structural groups [symmetric

Table 4.2.2.1. *K-series reference wavelengths in Å; bold numbers indicate a directly measured line*

Numbers in parentheses are standard uncertainties in the least-significant figures.

Z	Symbol	A	$K\alpha_1$	$K\alpha_2$	$K\beta_1$	$K\beta_3$	References
12	Mg		**9.89153 (10)**	**9.889554 (88)**			(*a*)
13	Al		**8.341831 (58)**	**8.339514 (58)**			(*a*)
14	Si		**7.12801 (14)**	**7.125588 (78)**			(*b*)
16	S		**5.374960 (89)**	**5.372200 (78)**			(*b*)
17	Cl		**4.730693 (71)**	**4.727818 (71)**			(*b*)
18	Ar		**4.194939 (23)**	**4.191938 (23)**			(*c*)
19	K		**3.7443932 (68)**	**3.7412838 (56)**			(*d*)
24	Cr		**2.2936510 (30)**	**2.2897260 (30)**	**2.0848810 (40)**	**2.0848810 (40)**	(*e*)
25	Mn		**2.1058220 (30)**	**2.1018540 (30)**	**1.9102160 (40)**	**1.9102160 (40)**	(*e*)
26	Fe		**1.9399730 (30)**	**1.9360410 (30)**	**1.7566040 (40)**	**1.7566040 (40)**	(*e*)
27	Co		**1.7928350 (10)**	**1.7889960 (10)**	**1.6208260 (30)**	**1.6208260 (30)**	(*e*)
28	Ni		**1.6617560 (10)**	**1.6579300 (10)**	**1.5001520 (30)**	**1.5001520 (30)**	(*e*)
29	Cu		**1.54442740 (50)**	**1.54059290 (50)**	**1.3922340 (60)**	**1.3922340 (60)**	(*e*)
31	Ga		**1.3440260 (40)**	**1.3401270 (96)**	1.208390 (75)	1.207930 (34)	(*b*),(*f*)
33	As		**1.108830 (31)**	**1.104780 (12)**	0.992689 (79)	0.992189 (53)	(*b*),(*f*)
34	Se		1.043836 (30)	**1.039756 (30)**	0.933284 (74)	0.932804 (30)	(*b*),(*f*)
36	Kr		**0.9843590 (44)**	**0.9802670 (40)**	**0.8790110 (70)**	**0.8785220 (50)**	(*b*)
40	Zr		**0.7901790 (25)**	**0.7859579 (27)**	**0.7023554 (30)**	**0.7018008 (30)**	(*b*)
42	Mo		0.713607 (12)	**0.70931715 (41)**	0.632887 (13)	0.632303 (13)	(*d*),(*f*)
44	Ru		0.6474205 (61)	0.6430994 (61)	0.5730816 (42)	0.5724966 (42)	(*d*),(*f*)
45	Rh		0.6176458 (61)	0.6132937 (61)	0.5462139 (42)	0.5456189 (42)	(*d*),(*f*)
46	Pd		0.5898351 (60)	0.5854639 (46)	0.5211363 (41)	0.5205333 (41)	(*d*),(*f*)
47	Ag		**0.5638131 (26)**	**0.55942178 (76)**	0.4976977 (60)	0.4970817 (60)	(*d*),(*f*)
48	Cd		0.5394358 (46)	0.5350147 (46)	0.4757401 (71)	0.4751181 (71)	(*d*),(*f*)
49	In		0.5165572 (60)	0.5121251 (46)	0.4551966 (41)	0.4545616 (41)	(*d*),(*f*)
50	Sn		0.4950646 (46)	0.4906115 (46)	0.4358821 (51)	0.4352421 (51)	(*d*),(*f*)
51	Sb		0.4748391 (45)	0.4703700 (45)	0.4177477 (41)	0.4170966 (31)	(*d*),(*f*)
54	Xe		**0.42088103 (71)**	**0.4163508 (14)**	**0.3694051 (13)**	**0.3687346 (13)**	(*d*)
56	Ba		**0.38968378 (74)**	**0.38512464 (84)**	**0.3415228 (11)**	**0.34082708 (75)**	(*d*)
60	Nd		**0.3248079 (59)**	**0.3201648 (59)**	0.283634 (59)	0.282904 (44)	(*d*),(*f*)
62	Sm		**0.31369830 (79)**	**0.30904506 (46)**	0.273764 (30)	0.273014 (30)	(*d*),(*f*)
67	Ho		0.26549088 (84)	0.2607608 (42)	0.230834 (30)	0.230124 (30)	(*f*),(*g*)
68	Er		**0.2571133 (11)**	**0.25237359 (62)**	**0.2234766 (14)**	**0.22269866 (72)**	(*d*)
69	Tm		0.24910095 (61)	0.24434486 (44)	0.216366 (30)	0.21559182 (57)	(*f*),(*h*)
74	W		0.21383304 (50)	**0.20901314 (18)**	0.18518317 (70)	0.1843768 (30)	(*d*),(*f*)
79	Au		**0.18507664 (61)**	**0.18019780 (47)**	**0.1598249 (13)**	**0.15899527 (77)**	(*d*)
82	Pb		**0.17029527 (56)**	**0.16537816 (38)**	**0.1468129 (10)**	**0.14596836 (58)**	(*d*)
83	Bi		0.1657183 (20)	0.1607903 (46)	0.142780 (11)	0.1419492 (54)	(*f*),(*g*)
90	Th	230	**0.13782600 (31)**	**0.13282021 (36)**	**0.11828686 (78)**	**0.11740759 (59)**	(*d*)
91	Pa	231	0.1343516 (29)	0.1293302 (27)	0.1152427 (21)	0.1143583 (21)	(*i*)
92	U	238	**0.13099111 (78)**	**0.12595977 (36)**	**0.11228858 (66)**	**0.11140132 (65)**	(*d*)
93	Np	237	0.1277287 (39)	0.1226882 (36)	0.1094230 (39)	0.1085265 (28)	(*i*)
94	Pu	239	0.1245782 (15)	0.11952120 (69)			(*h*)
94	Pu	244	0.1245705 (25)	0.1195140 (23)	0.1066611 (18)	0.1057595 (18)	(*i*)
95	Am	243	0.1215158 (24)	0.1164463 (33)	0.1039794 (17)	0.1030803 (17)	(*i*)
96	Cm	248	0.1185427 (23)	0.1134635 (21)	0.1013753 (17)	0.1004708 (16)	(*i*)
97	Bk	249	0.1156630 (54)	0.1105745 (49)	0.0988598 (55)	0.0979514 (54)	(*i*)
98	Cf	250	0.1128799 (82)	0.1077793 (75)			(*i*)

References: (*a*) Schweppe *et al.* (1994); (*b*) Mooney (1996); (*c*) Schweppe (1995); (*d*) Deslattes & Kessler (1985); (*e*) Hölzer *et al.* (1997); (*f*) Bearden (1967); (*g*) Borchert, Hansen, Jonson, Ravn & Desclaux (1980); (*h*) Borchert (1976); (*i*) Barreau, Börner, Egidy & Hoff (1982).

theoretical framework (see below) has been undertaken and will be made available in the longer publication and on the web site.

The feature of absorption spectra customarily designated as 'the absorption edge' has been variously associated with: the first inflection point of the absorption spectrum; the energy needed to produce a single inner vacancy with the photo-electron 'at rest at infinity'; or the energy needed to remove an electron from an inner shell and place it in the lowest unoccupied energy level. A general discussion of this question has been given by Parratt (1959). If we choose the second alternative, then it is easy to see that, with some care for symmetry restrictions, one can estimate the absorption-edge energy by combining the binding energy for any accessible outer shell with the energy of an emission line for which the transition terminus lies in the same outer shell. Of course, this procedure does not focus on the details of absorption thresholds, the locations of which are important for a number of structural applications. On the other hand, our choice gives greater regularity with respect to nuclear charge and facilitates use of electron binding energies, since they are referenced to the Fermi energy or the vacuum.

Electron binding energies have been tabulated for the principal electron shells of all the elements considered in the present table (Fuggle, Burr, Watson, Fabian & Lang, 1974; Cardona & Ley, 1978; Nyholm, Berndtsson & Mårtensson,

Table 4.2.4.3. *Mass attenuation coefficients ($cm^2\ g^{-1}$) (cont.)*

Radiation	Energy (MeV)	49 Indium	50 Tin	51 Antimony	52 Tellurium	53 Iodine	54 Xenon	55 Caesium	56 Barium
Ag $K\beta_1$	2.494E−02	1.13E+01	1.18E+01	1.25E+01	1.29E+01	1.40E+01	1.46E+01	1.56E+01	1.62E+01
Pd $K\beta_1$	2.382E−02	1.27E+01	1.34E+01	1.41E+01	1.46E+01	1.59E+01	1.65E+01	1.76E+01	1.83E+01
Rh $K\beta_1$	2.272E−02	1.45E+01	1.52E+01	1.60E+01	1.66E+01	1.80E+01	1.88E+01	2.00E+01	2.08E+01
Ag $K\bar{\alpha}$	2.210E−02	1.56E+01	1.64E+01	1.73E+01	1.79E+01	1.94E+01	2.02E+01	2.15E+01	2.24E+01
Pd $K\bar{\alpha}$	2.112E−02	1.76E+01	1.85E+01	1.96E+01	2.02E+01	2.19E+01	2.29E+01	2.43E+01	2.54E+01
Rh $K\bar{\alpha}$	2.017E−02	2.00E+01	2.10E+01	2.22E+01	2.29E+01	2.18E+01	2.27E+01	2.42E+01	2.52E+01
Mo $K\beta_1$	1.961E−02	2.16E+01	2.26E+01	2.39E+01	2.47E+01	2.68E+01	2.80E+01	2.98E+01	3.10E+01
Mo $K\bar{\alpha}$	1.744E−02	2.95E+01	3.10E+01	3.27E+01	3.38E+01	3.67E+01	3.82E+01	4.07E+01	4.23E+01
Zn $K\beta_1$	9.572E−03	1.48E+02	1.55E+02	1.64E+02	1.68E+02	1.82E+02	1.90E+02	2.01E+02	2.09E+02
Cu $K\beta_1$	8.905E−03	1.80E+02	1.88E+02	1.98E+02	2.04E+02	2.20E+02	2.29E+02	2.43E+02	2.52E+02
Zn $K\bar{\alpha}$	8.631E−03	1.95E+02	2.04E+02	2.15E+02	2.21E+02	2.39E+02	2.49E+02	2.63E+02	2.73E+02
Ni $K\beta_1$	8.265E−03	2.19E+02	2.29E+02	2.41E+02	2.48E+02	2.68E+02	2.78E+02	2.95E+02	3.06E+02
Cu $K\bar{\alpha}$	8.041E−03	2.36E+02	2.47E+02	2.59E+02	2.67E+02	2.88E+02	2.99E+02	3.17E+02	3.25E+02
Co $K\beta_1$	7.649E−03	2.69E+02	2.81E+02	2.96E+02	3.04E+02	3.30E+02	3.43E+02	3.63E+02	3.76E+02
Ni $K\bar{\alpha}$	7.472E−03	2.86E+02	2.99E+02	3.14E+02	3.23E+02	3.49E+02	3.62E+02	3.83E+02	3.96E+02
Fe $K\beta_1$	7.058E−03	3.32E+02	3.47E+02	3.65E+02	3.74E+02	4.08E+02	4.22E+02	4.46E+02	4.61E+02
Co $K\bar{\alpha}$	6.925E−03	3.49E+02	3.64E+02	3.83E+02	3.94E+02	4.25E+02	4.40E+02	4.65E+02	4.80E+02
Mn $K\beta_1$	6.490E−03	4.13E+02	4.31E+02	4.54E+02	4.66E+02	5.03E+02	5.20E+02	5.49E+02	5.66E+02
Fe $K\bar{\alpha}$	6.400E−03	4.28E+02	4.47E+02	4.71E+02	4.83E+02	5.22E+02	5.40E+02	5.69E+02	5.86E+02
Cr $K\beta_1$	5.947E−03	5.19E+02	5.42E+02	5.70E+02	5.85E+02	6.31E+02	6.52E+02	6.86E+02	6.45E+02
Mn $K\bar{\alpha}$	5.895E−03	5.31E+02	5.54E+02	5.82E+02	5.98E+02	6.45E+02	6.66E+02	7.00E+02	6.60E+02
Cr $K\bar{\alpha}$	5.412E−03	6.63E+02	6.91E+02	7.23E+02	7.40E+02	7.96E+02	7.21E+02	7.60E+02	5.70E+02
Ti $K\beta_1$	4.932E−03	8.41E+02	8.76E+02	9.15E+02	9.32E+02	1.00E+03	1.03E+03	2.60E+02	3.14E+02
Ti $K\bar{\alpha}$	4.509E−03	1.05E+03	1.09E+03	9.91E+02	7.51E+02	2.83E+02	2.65E+02	3.30E+02	3.34E+02

Radiation	Energy (MeV)	57 Lanthanum	58 Cerium	59 Praseodymium	60 Neodymium	61 Promethium	62 Samarium	63 Europium	64 Gadolinium
Ag $K\beta_1$	2.494E−02	1.72E+01	1.83E+01	1.95E+01	2.04E+01	2.17E+01	2.23E+01	2.35E+01	2.42E+01
Pd $K\beta_1$	2.382E−02	1.95E+01	2.07E+01	2.20E+01	2.30E+01	2.45E+01	2.52E+01	2.66E+01	2.74E+01
Rh $K\beta_1$	2.272E−02	2.21E+01	2.35E+01	2.50E+01	2.61E+01	2.78E+01	2.86E+01	3.01E+01	3.10E+01
Ag $K\bar{\alpha}$	2.210E−02	2.38E+01	2.53E+01	2.69E+01	2.81E+01	2.99E+01	3.08E+01	3.24E+01	3.34E+01
Pd $K\bar{\alpha}$	2.112E−02	2.69E+01	2.86E+01	3.04E+01	3.18E+01	3.38E+01	3.48E+01	3.66E+01	3.77E+01
Rh $K\bar{\alpha}$	2.017E−02	3.05E+01	3.24E+01	3.45E+01	3.60E+01	3.83E+01	3.94E+01	4.15E+01	4.27E+01
Mo $K\beta_1$	1.961E−02	3.29E+01	3.49E+01	3.72E+01	3.88E+01	4.13E+01	4.24E+01	4.47E+01	4.60E+01
Mo $K\bar{\alpha}$	1.744E−02	4.49E+01	4.77E+01	5.07E+01	5.30E+01	5.63E+01	5.78E+01	6.09E+01	6.26E+01
Zn $K\beta_1$	9.572E−03	2.21E+02	2.33E+02	2.47E+02	2.57E+02	2.73E+02	2.79E+02	2.93E+02	3.00E+02
Cu $K\beta_1$	8.905E−03	2.66E+02	2.82E+02	2.99E+02	3.10E+02	3.28E+02	3.35E+02	3.52E+02	3.60E+02
Zn $K\bar{\alpha}$	8.631E−03	2.89E+02	3.06E+02	3.24E+02	3.36E+02	3.55E+02	3.63E+02	3.80E+02	3.89E+02
Ni $K\beta_1$	8.265E−03	3.24E+02	3.43E+02	3.63E+02	3.76E+02	3.97E+02	4.05E+02	4.24E+02	4.33E+02
Cu $K\bar{\alpha}$	8.041E−03	3.48E+02	3.68E+02	3.90E+02	4.04E+02	4.26E+02	4.34E+02	4.34E+02	4.03E+02
Co $K\beta_1$	7.649E−03	3.95E+02	4.17E+02	4.41E+02	4.57E+02	4.82E+02	3.54E+02	4.80E+02	3.35E+02
Ni $K\bar{\alpha}$	7.472E−03	4.19E+02	4.42E+02	4.68E+02	4.84E+02	5.11E+02	3.71E+02	3.75E+02	3.56E+02
Fe $K\beta_1$	7.058E−03	4.83E+02	5.10E+02	5.39E+02	4.92E+02	5.88E+02	1.63E+02	4.08E+02	1.53E+02
Co $K\bar{\alpha}$	6.925E−03	5.07E+02	5.35E+02	5.65E+02	5.05E+02	4.00E+02	1.76E+02	4.19E+02	1.61E+02
Mn $K\beta_1$	6.490E−03	5.97E+02	5.47E+02	6.16E+02	4.39E+02	4.68E+02	1.66E+02	1.95E+02	1.89E+02
Fe $K\bar{\alpha}$	6.400E−03	6.18E+02	5.61E+02	4.48E+02	4.55E+02	1.94E+02	2.04E+02	2.03E+02	1.95E+02
Cr $K\beta_1$	5.947E−03	7.44E+02	4.94E+02	1.88E+02	1.98E+02	2.32E+02	2.21E+02	2.44E+02	2.35E+02
Mn $K\bar{\alpha}$	5.895E−03	7.60E+02	5.12E+02	1.93E+02	2.03E+02	2.37E+02	2.25E+02	2.49E+02	2.41E+02
Cr $K\bar{\alpha}$	5.412E−03	2.25E+02	2.38E+02	2.38E+02	2.51E+02	2.94E+02	2.79E+02	3.09E+02	2.98E+02
Ti $K\beta_1$	4.932E−03	2.84E+02	3.00E+02	3.00E+02	3.14E+02	3.69E+02	3.50E+02	3.90E+02	3.74E+02
Ti $K\bar{\alpha}$	4.509E−03	3.55E+02	3.57E+02	3.75E+02	3.97E+02	4.62E+02	4.35E+02	4.88E+02	4.69E+02

Table 4.3.3.1. *Partial wave elastic scattering factors for neutral atoms (cont.)*
Nd; $Z = 60$

s	10 keV		40 keV		60 keV		90 keV	
	$\lvert f(s)\rvert$	$\eta(s)$	$\lvert f(s)\rvert$	$\eta(s)$	$\lvert f(s)\rvert$	$\eta(s)$	$\lvert f(s)\rvert$	$\eta(s)$
0	1.4119E+01	2.8873E−01	1.6423E+01	2.0045E−01	1.7330E+01	1.7798E−01	1.8487E+01	1.5802E−01
1	1.0206E+01	3.8730E−01	1.2180E+01	2.6378E−01	1.2914E+01	2.3333E−01	1.3832E+01	2.0647E−01
2	6.0770E+00	6.0589E−01	7.5938E+00	3.9891E−01	8.1191E+00	3.5059E−01	8.7556E+00	3.0858E−01
3	4.0922E+00	8.2028E−01	5.3104E+00	5.2825E−01	5.7165E+00	4.6231E−01	6.1973E+00	4.0556E−01
4	2.9430E+00	1.0317E+00	3.9433E+00	6.5384E−01	4.2696E+00	5.7046E−01	4.6496E+00	4.9923E−01
5	2.1968E+00	1.2549E+00	3.0173E+00	7.8447E−01	3.2827E+00	6.8261E−01	3.5884E+00	5.9612E−01
6	1.7004E+00	1.4824E+00	2.3737E+00	9.1683E−01	2.5919E+00	7.9603E−01	2.8414E+00	6.9396E−01
7	1.3600E+00	1.7040E+00	1.9174E+00	1.0458E+00	2.0991E+00	9.0649E−01	2.3062E+00	7.8917E−01
8	1.1160E+00	1.9158E+00	1.5834E+00	1.1693E+00	1.7370E+00	1.0122E+00	1.9117E+00	8.8024E−01
9	9.3389E−01	2.1191E+00	1.3307E+00	1.2878E+00	1.4620E+00	1.1136E+00	1.6113E+00	9.6756E−01
10	7.9448E−01	2.3165E+00	1.1340E+00	1.4028E+00	1.2473E+00	1.2120E+00	1.3761E+00	1.0523E+00
11	6.8613E−01	2.5094E+00	9.7772E−01	1.5156E+00	1.0760E+00	1.3085E+00	1.1878E+00	1.1354E+00
12	6.0093E−01	2.6978E+00	8.5185E−01	1.6267E+00	9.3737E−01	1.4036E+00	1.0349E+00	1.2173E+00
13	5.3305E−01	2.8810E+00	7.4934E−01	1.7358E+00	8.2397E−01	1.4972E+00	9.0940E−01	1.2979E+00
14	4.7806E−01	3.0581E+00	6.6503E−01	1.8424E+00	7.3036E−01	1.5887E+00	8.0546E−01	1.3769E+00
15	4.3262E−01	3.2284E+00	5.9499E−01	1.9458E+00	6.5239E−01	1.6777E+00	7.1872E−01	1.4538E+00
16	3.9429E−01	3.3918E+00	5.3618E−01	2.0456E+00	5.8686E−01	1.7637E+00	6.4574E−01	1.5282E+00
17	3.6131E−01	3.5485E+00	4.8624E−01	2.1413E+00	5.3126E−01	1.8462E+00	5.8382E−01	1.5996E+00
18	3.3244E−01	3.6990E+00	4.4336E−01	2.2327E+00	4.8362E−01	1.9251E+00	5.3083E−01	1.6679E+00
19	3.0684E−01	3.8442E+00	4.0614E−01	2.3200E+00	4.4241E−01	2.0003E+00	4.8510E−01	1.7329E+00
20	2.8396E−01	3.9848E+00	3.7353E−01	2.4034E+00	4.0644E−01	2.0719E+00	4.4530E−01	1.7948E+00
21	2.6342E−01	4.1212E+00	3.4475E−01	2.4831E+00	3.7480E−01	2.1403E+00	4.1038E−01	1.8537E+00
22	2.4492E−01	4.2540E+00	3.1918E−01	2.5597E+00	3.4679E−01	2.2058E+00	3.7955E−01	1.9100E+00
23	2.2824E−01	4.3836E+00	2.9636E−01	2.6334E+00	3.2186E−01	2.2687E+00	3.5216E−01	1.9641E+00
24	2.1319E−01	4.5101E+00	2.7590E−01	2.7047E+00	2.9956E−01	2.3294E+00	3.2769E−01	2.0161E+00
25	1.9959E−01	4.6340E+00	2.5749E−01	2.7739E+00	2.7952E−01	2.3882E+00	3.0573E−01	2.0664E+00
26	1.8731E−01	4.7553E+00	2.4088E−01	2.8412E+00	2.6144E−01	2.4452E+00	2.8594E−01	2.1152E+00
27	1.7619E−01	4.8741E+00	2.2584E−01	2.9068E+00	2.4508E−01	2.5008E+00	2.6803E−01	2.1627E+00
28	1.6612E−01	4.9906E+00	2.1222E−01	2.9709E+00	2.3025E−01	2.5551E+00	2.5178E−01	2.2090E+00
29	1.5697E−01	5.1046E+00	1.9985E−01	3.0338E+00	2.1677E−01	2.6084E+00	2.3700E−01	2.2545E+00
30	1.4865E−01	5.2163E+00	1.8859E−01	3.0954E+00	2.0449E−01	2.6606E+00	2.2352E−01	2.2991E+00
31	1.4106E−01	5.3258E+00	1.7832E−01	3.1559E+00	1.9327E−01	2.7119E+00	2.1119E−01	2.3430E+00
32	1.3412E−01	5.4332E+00	1.6892E−01	3.2154E+00	1.8299E−01	2.7624E+00	1.9988E−01	2.3861E+00
33	1.2776E−01	5.5387E+00	1.6031E−01	3.2738E+00	1.7355E−01	2.8120E+00	1.8948E−01	2.4286E+00
34	1.2191E−01	5.6421E+00	1.5239E−01	3.3313E+00	1.6486E−01	2.8609E+00	1.7990E−01	2.4704E+00
35	1.1651E−01	5.7438E+00	1.4510E−01	3.3878E+00	1.5686E−01	2.9090E+00	1.7106E−01	2.5117E+00
36	1.1151E−01	5.8437E+00	1.3837E−01	3.4434E+00	1.4946E−01	2.9563E+00	1.6288E−01	2.5523E+00
37	1.0687E−01	5.9420E+00	1.3215E−01	3.4980E+00	1.4262E−01	3.0029E+00	1.5531E−01	2.5924E+00
38	1.0256E−01	6.0387E+00	1.2637E−01	3.5517E+00	1.3626E−01	3.0488E+00	1.4827E−01	2.6318E+00
39	9.8547E−02	6.1341E+00	1.2099E−01	3.6046E+00	1.3034E−01	3.0939E+00	1.4172E−01	2.6705E+00
40	9.4797E−02	6.2282E+00	1.1598E−01	3.6566E+00	1.2481E−01	3.1383E+00	1.3560E−01	2.7087E+00
41	9.1286E−02	3.7860E−02	1.1129E−01	3.7078E+00	1.1966E−01	3.1819E+00	1.2989E−01	2.7462E+00
42	8.7989E−02	1.2957E−01	1.0691E−01	3.7581E+00	1.1483E−01	3.2248E+00	1.2455E−01	2.7831E+00
43	8.4888E−02	2.2024E−01	1.0280E−01	3.8075E+00	1.1031E−01	3.2670E+00	1.1954E−01	2.8194E+00
44	8.1972E−02	3.0993E−01	9.8933E−02	3.8562E+00	1.0606E−01	3.3085E+00	1.1484E−01	2.8551E+00
45	7.9227E−02	3.9870E−01	9.5290E−02	3.9041E+00	1.0206E−01	3.3493E+00	1.1042E−01	2.8902E+00
46	7.6637E−02	4.8660E−01	9.1852E−02	3.9512E+00	9.8288E−02	3.3894E+00	1.0625E−01	2.9246E+00
47	7.4192E−02	5.7369E−01	8.8603E−02	3.9976E+00	9.4726E−02	3.4289E+00	1.0232E−01	2.9584E+00
48	7.1876E−02	6.6005E−01	8.5532E−02	4.0432E+00	9.1361E−02	3.4676E+00	9.8609E−02	2.9917E+00
49	6.9682E−02	7.4573E−01	8.2624E−02	4.0881E+00	8.8179E−02	3.5057E+00	9.5104E−02	3.0243E+00
50	6.7604E−02	8.3073E−01	7.9865E−02	4.1323E+00	8.5163E−02	3.5432E+00	9.1785E−02	3.0564E+00
51	6.5635E−02	9.1508E−01	7.7243E−02	4.1758E+00	8.2299E−02	3.5801E+00	8.8637E−02	3.0880E+00
52	6.3769E−02	9.9881E−01	7.4750E−02	4.2188E+00	7.9579E−02	3.6164E+00	8.5648E−02	3.1190E+00
53	6.1997E−02	1.0819E+00	7.2378E−02	4.2611E+00	7.6991E−02	3.6521E+00	8.2809E−02	3.1495E+00
54	6.0314E−02	1.1645E+00	7.0119E−02	4.3028E+00	7.4530E−02	3.6873E+00	8.0112E−02	3.1795E+00
55	5.8714E−02	1.2466E+00	6.7967E−02	4.3438E+00	7.2190E−02	3.7219E+00	7.7548E−02	3.2090E+00
56	5.7194E−02	1.3282E+00	6.5914E−02	4.3843E+00	6.9959E−02	3.7559E+00	7.5108E−02	3.2380E+00
57	5.5751E−02	1.4093E+00	6.3954E−02	4.4242E+00	6.7830E−02	3.7895E+00	7.2781E−02	3.2665E+00
58	5.4378E−02	1.4899E+00	6.2081E−02	4.4636E+00	6.5797E−02	3.8225E+00	7.0560E−02	3.2946E+00
59	5.3074E−02	1.5700E+00	6.0291E−02	4.5024E+00	6.3854E−02	3.8551E+00	6.8439E−02	3.3222E+00
60	5.1835E−02	1.6496E+00	5.8579E−02	4.5408E+00	6.1998E−02	3.8872E+00	6.6415E−02	3.3495E+00

particle pulse is short enough, the duration of the moderated neutron pulses is roughly inversely proportional to the neutron speed.

These accelerator-driven pulsed sources are pulsed at frequencies of between 10 and 100 Hz.

There are two fundamental differences between a reactor and a pulsed source.

(1) *All* experiments at a pulsed source must be performed with time-of-flight techniques. The pulsed source produces neutrons in bursts of 1 to 50 μs duration, depending on the energy, spaced about 10 to 100 ms apart, so that the duty cycle is low but there is very high neutron intensity within each pulse. The time-of-flight technique makes it possible to exploit that high intensity. With the de Broglie relationship, for neutrons

$$\lambda\,(\text{Å}) = 0.3966\,t\,(\mu s)/L\,(\text{cm}),$$

where t is the flight time in μs and L is the total flight path in cm.

(2) The spectral characteristics of pulsed sources are somewhat different from reactors in that they have a much larger component of higher-energy (above 100 meV) neutrons than the thermal spectrum at reactors. The exploitation of this new energy regime accompanied by the short pulse duration is one of the great opportunities presented by spallation sources.

Fig. 4.4.1.2 illustrates the essential difference between experiments at a steady-state source (left panel) and a pulsed source (right panel). We confine the discussion here to diffraction. If the time over which useful information is gathered is equivalent to the full period of the source Δt (the case suggested by the lower-right figure), the *peak flux* of the pulsed source is the effective parameter to compare with the flux of the steady-state source. Often this is not the case, so one makes a comparison in terms of *time-averaged flux* (centre panel). For the pulsed source, this is lowered from the peak flux by the duty cycle, but with the time-of-flight method one uses a large interval of the spectrum (shaded area). For the steady-state source, the time-averaged flux is high, but only a small wavelength slice (stippled area) is used in the experiment. It is the *integrals* of the two areas which must be compared; for the pulsed sources now being designed, the integral is generally favourable compared with present-day reactors. Finally, one can see from the central panel that high-energy neutrons (100–1000 meV) are especially plentiful at the pulsed sources. These various features can be exploited in the design of different kinds of experiments at pulsed sources.

4.4.2. Beam-definition devices (By I. S. Anderson and O. Schärpf)

4.4.2.1. *Introduction*

Neutron scattering, when compared with X-ray scattering techniques developed on modern synchrotron sources, is flux limited, but the method remains unique in the resolution and range of energy and momentum space that can be covered. Furthermore, the neutron magnetic moment allows details of microscopic magnetism to be examined, and polarized neutrons can be exploited through their interaction with both nuclear and electron spins.

Owing to the low primary flux of neutrons, the beam definition devices that play the role of defining the beam conditions (direction, divergence, energy, polarization, *etc.*) have to be highly efficient. Progress in the development of such devices not only results in higher-intensity beams but also allows new techniques to be implemented.

The following sections give a (non-exhaustive) review of commonly used beam-definition devices. The reader should keep in mind the fact that neutron scattering experiments are typically carried out with large beams (1 to 50 cm^2) and divergences between 5 and 30 mrad.

4.4.2.2. *Collimators*

A collimator is perhaps the simplest neutron optical device and is used to define the direction and divergence of a neutron beam. The most rudimentary collimator consists of two slits or pinholes

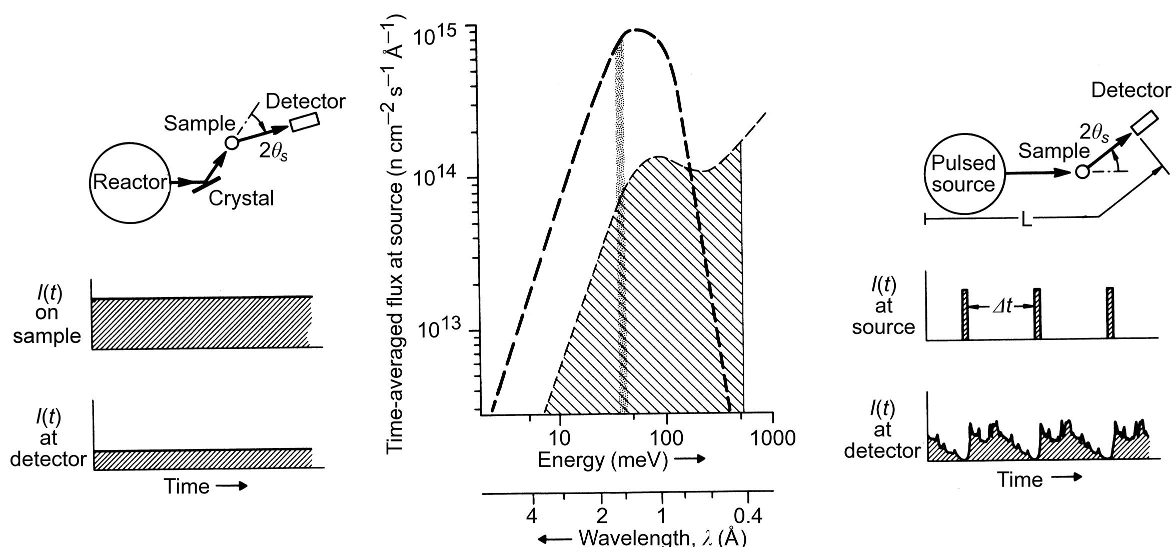

Fig. 4.4.1.2. Schematic diagram for performing diffraction experiments at steady-state and pulsed neutron sources. On the left we see the familiar monochromator crystal allowing a constant (in time) beam to fall on the sample (centre left), which then diffracts the beam through an angle $2\theta_s$ into the detector. The signal in the latter is also constant in time (lower left). On the right, the pulsed source allows a wide spectrum of neutrons to fall on the sample in sharp pulses separated by Δt (centre right). The neutrons are then diffracted by the sample through $2\theta_s$ and their time of arrival in the detector is analysed (lower right). The centre figure shows the time-averaged flux at the source. At a reactor, we make use of a narrow band of neutrons (heavy shading), here chosen with $\lambda = 1.5$ Å. At a pulsed source, we use a wide spectral band, here chosen from 0.4 to 3 Å and each one is identified by its time-of-flight. For the experimentalist, an important parameter is the integrated area of the two-shaded areas. Here they have been made identical.

Table 4.4.5.10. $\langle j_4 \rangle$ *form factors for 4d atoms and their ions*

Atom or ion	A	a	B	b	C	c	D	e
Y	−8.0767	32.201	7.9197	25.156	1.4067	6.827	−0.0001	0.1031
Zr	−5.2697	32.868	4.1930	24.183	1.5202	6.048	−0.0002	0.0855
Zr^+	−5.6384	33.607	4.6729	22.338	1.3258	5.924	−0.0003	0.0674
Nb	−3.1377	25.595	2.3411	16.569	1.2304	4.990	−0.0005	0.0615
Nb^+	−3.3598	25.820	2.8297	16.427	1.1203	4.982	−0.0005	0.0724
Mo	−2.8860	20.572	1.8130	14.628	1.1899	4.264	−0.0008	0.0410
Mo^+	−3.2618	25.486	2.3596	16.462	1.1164	4.491	−0.0007	0.0592
Tc	−2.7975	20.159	1.6520	16.261	1.1726	3.943	−0.0008	0.0657
Tc^+	−2.0470	19.683	1.6306	11.592	0.8698	3.769	−0.0010	0.0723
Ru	−1.5042	17.949	0.6027	9.961	0.9700	3.393	−0.0010	0.0338
Ru^+	1.6278	18.506	1.1828	10.189	0.8138	3.418	−0.0009	0.0673
Rh	−1.3492	17.577	0.4527	10.507	0.9285	3.155	−0.0009	0.0483
Rh^+	−1.4673	17.957	0.7381	9.944	0.8485	3.126	−0.0012	0.0487
Pd	−1.1955	17.628	0.3183	11.309	0.8696	2.909	−0.0006	0.0555
Pd^+	−1.4098	17.765	0.7927	9.999	0.7710	2.930	−0.0006	0.0530

Table 4.4.5.11. $\langle j_4 \rangle$ *form factors for rare-earth ions*

Ion	A	a	B	b	C	c	D	e
Ce^{2+}	−0.6468	10.533	0.4052	5.624	0.3412	1.535	0.0080	0.0522
Nd^{2+}	−0.5416	12.204	0.3571	6.169	0.3154	1.485	0.0098	0.0519
Nd^{3+}	−0.4053	14.014	0.0329	7.005	0.3759	1.707	0.0209	0.0372
Sm^{2+}	−0.4150	14.057	0.1368	7.032	0.3272	1.582	0.0192	0.0319
Sm^{3+}	−0.4288	10.052	0.1782	5.019	0.2833	1.236	0.0088	0.0328
Eu^{2+}	−0.4145	10.193	0.2447	5.164	0.2661	1.205	0.0065	0.0516
Eu^{3+}	−0.4095	10.211	0.1485	5.175	0.2720	1.237	0.0131	0.0494
Gd^{2+}	−0.3824	10.344	0.1955	5.306	0.2622	1.203	0.0097	0.0363
Gd^{3+}	−0.3621	10.353	0.1016	5.310	0.2649	1.219	0.0147	0.0494
Tb^{2+}	−0.3443	10.469	0.1481	5.416	0.2575	1.182	0.0104	0.0280
Tb^{3+}	−0.3228	10.476	0.0638	5.419	0.2566	1.196	0.0159	0.0439
Dy^{2+}	−0.3206	12.071	0.0904	8.026	0.2616	1.230	0.0143	0.0767
Dy^{3+}	−0.2829	9.525	0.0565	4.429	0.2437	1.066	0.0092	0.0181
Ho^{2+}	−0.2976	9.719	0.1224	4.635	0.2279	1.005	0.0063	0.0452
Ho^{3+}	−0.2717	9.731	0.0474	4.638	0.2292	1.047	0.0124	0.0310
Er^{2+}	−0.2975	9.829	0.1189	4.741	0.2116	1.004	0.0117	0.0524
Er^{3+}	−0.2568	9.834	0.0356	4.741	0.2172	1.028	0.0148	0.0434
Tm^{2+}	−0.2677	9.888	0.0925	4.784	0.2056	0.990	0.0124	0.0396
Tm^{3+}	−0.2292	9.895	0.0124	4.785	0.2108	1.007	0.0151	0.0334
Yb^{2+}	−0.2393	9.947	0.0663	4.823	0.2009	0.965	0.0122	0.0311
Yb^{3+}	−0.2121	8.197	0.0325	3.153	0.1975	0.884	0.0093	0.0435

Table 4.4.5.12. $\langle j_4 \rangle$ *form factors for actinide ions*

Ion	A	a	B	b	C	c	D	e
U^{3+}	−0.9859	16.601	0.6116	6.515	0.6020	2.597	−0.0010	0.0599
U^{4+}	−1.0540	16.605	0.4339	6.512	0.6746	2.599	−0.0011	0.0471
U^{5+}	−0.9588	16.485	0.1576	6.440	0.7785	2.640	−0.0010	0.0493
Np^{3+}	0.9029	16.586	0.4006	6.470	0.6545	2.563	−0.0004	0.0470
Np^{4+}	−0.9887	12.441	0.5918	5.294	0.5306	2.263	−0.0021	0.0583
Np^{5+}	−0.8146	16.581	−0.0055	6.475	0.7956	2.562	−0.0004	0.0600
Np^{6+}	0.6738	16.553	−0.2297	6.505	0.8513	2.553	−0.0003	0.0623
Pu^{3+}	−0.7014	16.369	−0.1162	6.697	0.7778	2.450	0.0000	0.0546
Pu^{4+}	−0.9160	12.203	0.4891	5.127	0.5290	2.149	−0.0022	0.0520
Pu^{5+}	−0.7035	16.360	−0.0979	6.706	0.7726	2.447	0.0000	0.0610
Pu^{6+}	−0.5560	16.322	−0.3046	6.768	0.8146	2.426	0.0001	0.0596
Am^{2+}	−0.7433	16.416	0.3481	6.788	0.6014	2.346	0.0000	0.0566
Am^{3+}	0.8092	12.854	0.4161	5.459	0.5476	2.172	−0.0011	0.0530
Am^{4+}	−0.8548	12.226	0.3037	5.909	0.6173	2.188	−0.0016	0.0456
Am^{5+}	−0.6538	15.462	−0.0948	5.997	0.7295	2.297	0.0000	0.0594
Am^{6+}	−0.5390	15.449	−0.2689	6.017	0.7711	2.297	0.0002	0.0729
Am^{7+}	−0.4688	12.019	−0.2692	7.042	0.7297	2.164	−0.0011	0.0262

Table 5.2.4.1. *Centroid displacement $\langle \Delta\theta/\theta \rangle$ and variance W of certain aberrations of an angle-dispersive diffractometer; for references see Wilson (1963, 1965c, 1974) and Gillham (1971)*

For the Seemann–Bohlin arrangement, S and R are given by equations (5.2.4.1) and (5.2.4.2); for the symmetrical arrangement, they are equal to R_0. Other notation is explained at the end of the table.

Aberration	$\langle \Delta(2\theta) \rangle$	W
Zero-angle calibration	Constant	0
Specimen displacement	$-s\{R^{-1}\cos(2\theta-\varphi)+S^{-1}\cos\varphi\}$	0
Specimen transparency Thick specimen	$-\sin 2\varphi/\mu(R+S)$	$\sin^2 2\varphi/\mu^2(R+S)^2$
Thin specimen	See Wilson (1974, p. 547)	
2:1 mis-setting	Zero if centroid of illuminated area is centred	$\beta^2 A^2[R^{-1}\cos(2\theta-\varphi)+S^{-1}\cos\varphi]^2/3$
Inclination of plane of specimen to axis of rotation	Zero if centroid of illuminated area on equator of specimen	$\gamma^2 h^2[R^{-1}\cos(2\theta-\varphi)+S^{-1}\cos\varphi]^2/3$ for uniform illumination
Flat specimen	$-A^2\sin 2\theta/3RS$	$4A^4\sin^2 2\theta/45R^2S^2$
Focal-line width	Small	$\sim f_1^2/12S^2$
Receiving-slit width	Small	$\sim r_1^2/12R^2$
Interaction terms	Small if adjustment reasonably good	See Wilson (1963, 1974)
Axial divergence No Soller slits, source, specimen and receiver equal	$-h^2[(S^{-2}+R^{-2})\cot 2\theta+(RS)^{-1}\operatorname{cosec} 2\theta]/3$	$h^4[\{7S^{-4}+2(RS)^{-2}+7R^{-4}\}\cot^2 2\theta$ $+14(RS)^{-1}(S^{-2}+R^{-2})\cot 2\theta\operatorname{cosec} 2\theta$ $+19(RS)^{-2}\operatorname{cosec}^2 2\theta]/45$
Narrow Soller slits One set in incident beam	$-[\Delta^2/12+h^2/3R^2]\cot 2\theta$	$7[\Delta^4/720+h^4/45R^2]\cot^2 2\theta$ $+h^2\operatorname{cosec}^2 2\theta/9R^2$
One set in diffracted beam	Replace R by S in the above	
Two sets	$-(\Delta^2\cot 2\theta)/6$	$\Delta^4(10+17\cot^2 2\theta)/360$
Wide Soller slits	Complex. See Pike (1957), Langford & Wilson (1962), Wilson (1963, 1974), and Gillham (1971)	
Refraction	$\sim -2\delta\tan\theta$	$\sim \delta^2[-6\ln(\Delta/2)+25]/4\mu p$
Physical aberrations	See Wilson (1963, 1965*c*, 1970*a*, 1974) and Gillham & King (1972)	

Notation: $2A$ = illuminated length of specimen; β = angle of equatorial mis-setting of specimen; γ = angle of inclination of plane of specimen to axis of rotation; Δ = angular aperture of Soller slits; μ = linear absorption coefficient of specimen; r_1 = width of receiving slit (varies with θ in some designs of diffractometer); s = specimen-surface displacement; f_1 = projected width of focal line; h = half height of focal line, specimen, and receiving slit, taken as equal; $1-\delta$ = index of refraction; p = effective particle size.

extrapolation is quick and easy for cubic substances, and by the use of successive approximations it can be applied to hexagonal (Wilson & Lipson, 1941), tetragonal, and even orthorhombic materials. It is, however, very cumbersome for non-cubic substances, and impracticable if the symmetry is less than orthorhombic.

Analytic extrapolation seems to have been first used by Cohen (1936*a,b*). It is now usual even in the cubic case: programs are often included in the software accompanying powder diffractometers, and many others are available separately. Some programs that are frequently referred to are described by Appleman & Evans (1973), Mighell, Hubbard & Stalick (1981), and Ferguson, Rogerson, Wolstenholme, Hughes & Huyton (1987); for a comparison, see Kelly (1988). If the precision warrants it, the single function $KF(\theta)$ may be replaced by a sum of functions $K_iF_i(\theta)$, one for each of the larger aberrations listed in Tables 5.2.4.1, 5.2.7.1, and 5.2.8.1. Two – the zero error and a function corresponding to specimen-surface displacement and transparency – must be used routinely; one or two more may be added if the precision warrants it.

Table 5.2.10.6. *Fluorophlogopite 00l standard reflection angles [NIST SRM 675, d(001) = 9.98104 (7) Å, T = 298 K, λ = 1.5405929 Å]*

l	2θ (°)
1	8.853
2	17.759
3	26.774
4	35.962
5	45.397
6	55.169
7	65.399
8	76.255
10	101.025
11	116.193
12	135.674

Table 5.2.10.7. *Silver behenate 00l standard reflection angles [d(001) = 58.380 (3) Å, λ = 1.5405929 Å (Huang, Toraya, Blanton & Wu, 1993)]*

l	2θ (°)
1	1.512
2	3.024
3	4.537
4	6.051
5	7.565
6	9.081
7	10.599
8	12.118
9	13.640
10	15.164
11	16.691
12	18.221
13	19.754

The forward reflections have been used in parallel-beam synchrotron-radiation lattice-parameter studies (Parrish *et al.*, 1987).

(3) The profile shape has a strong influence on the accuracy of the angle measurement. The geometrical aberrations produce asymmetries that reduce the accuracy; the effects can be minimized by a proper selection of slit sizes. In most cases, it is inadvisable to use $K\beta$ radiation to avoid $K\alpha$-doublet splitting, as the intensity is reduced by a factor of seven. Symmetrical profiles are obtained with parallel-beam optics, but it is usually necessary to use synchrotron radiation to achieve sufficient intensity.

(4) The largest and commonest source of systematic error in focusing geometry is the specimen-surface displacement. Several remountings of the specimen in the diffractometer and measurement of some low-angle reflections may be helpful in determining and minimizing the error. This aberration does not occur in parallel-beam geometry unless a receiving slit is used.

(5) The precision of the diffractometer gears (or the equivalent) may be the limiting factor in high-precision measurements. The use of an electromagnetic encoder mounted on the 2θ-output shaft can increase the precision considerably. It is not normally included in commercial diffractometers because of its cost, but it is essential for adequate accuracy when the 2θ angles must be determined to better than 0.001°. The various types of mechanical error have been described by Jenkins & Schreiner (1986).

The diffractometer must be carefully adjusted to avoid mechanical problems. The effect of backlash can be minimized by slewing beyond and then returning to the starting angle, and by always scanning in the same direction. It is essential to avoid over-tight worm-and-gear meshing, as it causes jerky rather than smooth movement.

(6) The beam must be precisely centred, the slits and monochromator (if used) must be parallel to the line focus of the X-ray tube, and the scanning plane must be perpendicular to the line focus.

(7) The use of standard specimens with accurately known lattice parameters (Section 5.2.10) and ideally free of line broadening is strongly recommended as a test of the overall precision of the instrumentation and method.

(8) For a given total time available for an experiment, it is necessary to strike a balance between numerous short steps with short counting times and fewer longer steps with longer counting times. The former alternative may give a better definition of the line shape; the latter may give lower calculated standard uncertainties (formerly called estimated standard deviations) in any derived parameters. Obviously, the step length must be considerably shorter than the width of any feature of the profile that is considered to be of importance.

(9) Least-squares refinement is discussed in Subsection 5.2.3.2. The programs and the methods of handling the data should be carefully checked, as various programs have been found to give slightly different values from the same experimental data (see, for example, JCPDS – International Centre for Diffraction Data, 1986; Kelly, 1988).

(10) Specimen preparation is very important; the particle size should preferably be less than 10 μm, and a flat smooth surface normal to the diffraction vector is essential. The linearity of the detector and the temperature of the

Table 5.2.11.1. *NIST intensity standards, SRM 674*

Standard	Crystal system	a_0 (Å)	c_0 (Å)	I_{rel} hkl 2	I_{rel} hkl 3	$I_1/I_c(113)$
Al_2O_3 (corundum)	Trigonal	4.75893 (10)	12.9917 (7)	92.5 (26) 116	87.4 (19) 104	—
ZnO	Hexagonal	3.24981 (12)	5.20653 (13)	57.6 (11) 100	40.2 (14) 002	5.17 (13) 101
TiO_2 (rutile)	Tetragonal	4.59365 (10)	2.95874 (8)	56.9 (28) 211	44.0 (17) 101	3.39 (12) 110
Cr_2O_3	Trigonal	4.95916 (12)	13.5972 (6)	94.5 (22) 116	87.1 (23) 110	2.10 (5) 104
CeO_2	Cubic	5.41129 (8)	—	53.5 (20) 220	43.4 (23) 311	7.5 (2) 111

5.4. Electron-diffraction methods

By A. W. S. Johnson and A. Olsen

5.4.1. Determination of cell parameters from single-crystal patterns (By A. W. S. Johnson)

5.4.1.1. *Introduction*

This article treats the recovery of cell axes and angles from (*a*) a single pattern with suitable Laue zones and (*b*) two patterns with different zone axes. It is assumed that instrument distortions, if significant, are corrected and that the patterns are free of artefacts such as twinning, double diffraction *etc.* (Edington, 1975). The treatment is valid for convergent-beam, micro and selected-area electron-diffraction patterns and accelerating voltages above approximately 30 kV. Relevant papers are by LePage (1992) and Zuo (1993), and background reading is contained in Edington (1975), Gard (1976), and Hirsch, Howie, Nicholson, Pashley & Whelan (1965).

The basic requirement in the determination of the unit cell of a crystal is to find, from one or more diffraction patterns, the basis vector set, $\mathbf{a}^*$, $\mathbf{b}^*$, $\mathbf{c}^*$, of a primitive reciprocal unit cell. The Cartesian components of these vectors form an orientation matrix

$$\boldsymbol{UB} = (\mathbf{a}^*, \mathbf{b}^*, \mathbf{c}^*),$$

which, when inverted, gives the vector components of the corresponding real-space cell. The elements of $\boldsymbol{UB}$ can be measured directly from the diffraction pattern in millimetres. Define axes x and y to be in the recording plane and z in the beam direction. A point in the diffraction pattern x, y, z is then related to the indices h, k, l by

$$\begin{pmatrix} x \\ y \\ z \end{pmatrix} = \boldsymbol{UB} \begin{pmatrix} h \\ k \\ l \end{pmatrix}.$$

Note that points with non-zero z are observed on the plane $z = 0$, see Fig. 5.4.1.1.

The metric $\boldsymbol{M}$ of $\boldsymbol{UB}^{-1}$ is used to find the unit-cell edges and angles as

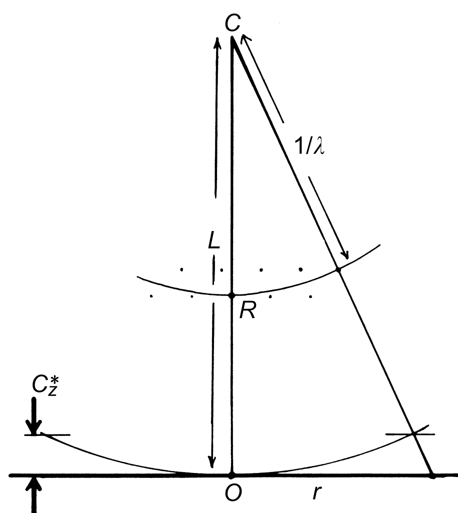

Fig. 5.4.1.1. Diffraction geometry. Crystal at C with the direct transmitted beam, CRO, intersecting the reciprocal-lattice origin at R and the recording plane at normal incidence at O. The camera length L is CO and the reciprocal of the wavelength λ is CR.

Table 5.4.1.1. *Unit-cell information available for photographic recording*

	Pattern type	Constants known	Information available
(1)	Zero zone	None or λ or L	d ratios and interplane angles
(2)		$L\lambda$ or L and λ	d values and interplane angles
(3)	Multiple zone	None or L	As for (1)
(4)		$L\lambda$	As for (2)
(5)		λ	Unit-cell axial ratios and angles
(6)		L and λ	Unit-cell axes and angles
(7)	Two or more zero-zone patterns*	None or L	As for (5)
(8)		$L\lambda$	As for (6)

* See text, Subsection 5.4.1.2.

$$\boldsymbol{M} = \boldsymbol{UB}^{-1} \cdot (\boldsymbol{UB}^{-1})^T,$$

where T means the transpose. Then,

$$\boldsymbol{M} = \begin{pmatrix} \mathbf{a}\cdot\mathbf{a} & \mathbf{a}\cdot\mathbf{b} & \mathbf{a}\cdot\mathbf{c} \\ \mathbf{a}\cdot\mathbf{b} & \mathbf{b}\cdot\mathbf{b} & \mathbf{b}\cdot\mathbf{c} \\ \mathbf{a}\cdot\mathbf{c} & \mathbf{b}\cdot\mathbf{c} & \mathbf{c}\cdot\mathbf{c} \end{pmatrix}$$

gives

$$a = L\lambda(\mathbf{a}\cdot\mathbf{a})^{1/2},$$
$$b = L\lambda(\mathbf{b}\cdot\mathbf{b})^{1/2},$$
$$c = L\lambda(\mathbf{c}\cdot\mathbf{c})^{1/2},$$
$$\cos\gamma = \mathbf{a}\cdot\mathbf{b}/(\mathbf{a}\cdot\mathbf{a}\,\mathbf{b}\cdot\mathbf{b})^{1/2},$$
$$\cos\beta = \mathbf{a}\cdot\mathbf{c}/(\mathbf{a}\cdot\mathbf{a}\,\mathbf{c}\cdot\mathbf{c})^{1/2},$$

and

$$\cos\alpha = \mathbf{b}\cdot\mathbf{c}/(\mathbf{b}\cdot\mathbf{b}\,\mathbf{c}\cdot\mathbf{c})^{1/2},$$

where L is the effective distance between the diffracting crystal and the recording plane and λ is the wavelength. These quantities are defined in Fig. 5.4.1.1 together with the nomenclature and geometrical relationships required in this article.

If necessary, the cell is reduced to the Bravais cell according to the procedures given in *IT* A (1983, Chapter 9.3), before calculating the metric.

In practice, there may be a difficulty in choosing a vector set that describes a *primitive* reciprocal cell. Although a record of any reasonably dense plane of reciprocal space immediately exposes two basis vectors of a cell, the third vector lies out of the plane of the diffraction pattern containing the first two vectors and may not be directly measurable. Hence, some care must be taken to ensure that the third vector chosen makes the cell

Table 6.1.1.1. *Mean atomic scattering factors in electrons for free atoms*

Methods: E: exact; RHF, *RHF (see text): relativistic Hartree–Fock.

Element	H	He	Li	Be	B	C	N	O	F	Ne
Z	1	2	3	4	5	6	7	8	9	10
Method	E	RHF	RHF	RHF	RHF	RHF	RHF	RHF	RHF	RHF
$(\sin\theta)/\lambda$ (Å^{-1})										
0.00	1.000	2.000	3.000	4.000	5.000	6.000	7.000	8.000	9.000	10.000
0.01	0.998	1.998	2.986	3.987	4.988	5.990	6.991	7.992	8.993	9.993
0.02	0.991	1.993	2.947	3.950	4.954	5.958	6.963	7.967	8.970	9.973
0.03	0.980	1.984	2.884	3.889	4.897	5.907	6.918	7.926	8.933	9.938
0.04	0.966	1.972	2.802	3.807	4.820	5.837	6.855	7.869	8.881	9.891
0.05	0.947	1.957	2.708	3.707	4.724	5.749	6.776	7.798	8.815	9.830
0.06	0.925	1.939	2.606	3.592	4.613	5.645	6.682	7.712	8.736	9.757
0.07	0.900	1.917	2.502	3.468	4.488	5.526	6.574	7.612	8.645	9.672
0.08	0.872	1.893	2.400	3.336	4.352	5.396	6.453	7.501	8.541	9.576
0.09	0.842	1.866	2.304	3.201	4.209	5.255	6.321	7.378	8.427	9.469
0.10	0.811	1.837	2.215	3.065	4.060	5.107	6.180	7.245	8.302	9.351
0.11	0.778	1.806	2.135	2.932	3.908	4.952	6.030	7.103	8.168	9.225
0.12	0.744	1.772	2.065	2.804	3.756	4.794	5.875	6.954	8.026	9.090
0.13	0.710	1.737	2.004	2.683	3.606	4.633	5.714	6.798	7.876	8.948
0.14	0.676	1.701	1.950	2.569	3.459	4.472	5.551	6.637	7.721	8.799
0.15	0.641	1.663	1.904	2.463	3.316	4.311	5.385	6.472	7.560	8.643
0.16	0.608	1.624	1.863	2.365	3.179	4.153	5.218	6.304	7.395	8.483
0.17	0.574	1.584	1.828	2.277	3.048	3.998	5.051	6.134	7.226	8.318
0.18	0.542	1.543	1.796	2.197	2.924	3.847	4.886	5.964	7.055	8.150
0.19	0.511	1.502	1.768	2.125	2.808	3.701	4.723	5.793	6.883	7.978
0.20	0.481	1.460	1.742	2.060	2.699	3.560	4.563	5.623	6.709	7.805
0.22	0.424	1.377	1.693	1.951	2.503	3.297	4.254	5.289	6.362	7.454
0.24	0.373	1.295	1.648	1.864	2.336	3.058	3.963	4.965	6.020	7.102
0.25	0.350	1.254	1.626	1.828	2.263	2.949	3.825	4.808	5.851	6.928
0.26	0.328	1.214	1.604	1.795	2.195	2.846	3.693	4.655	5.685	6.754
0.28	0.287	1.136	1.559	1.739	2.077	2.658	3.445	4.363	5.363	6.412
0.30	0.251	1.060	1.513	1.692	1.979	2.494	3.219	4.089	5.054	6.079
0.32	0.220	0.988	1.465	1.652	1.897	2.351	3.014	3.834	4.761	5.758
0.34	0.193	0.920	1.417	1.616	1.829	2.227	2.831	3.599	4.484	5.451
0.35	0.180	0.887	1.393	1.600	1.799	2.171	2.747	3.489	4.353	5.302
0.36	0.169	0.856	1.369	1.583	1.771	2.120	2.667	3.383	4.225	5.158
0.38	0.148	0.795	1.320	1.551	1.723	2.028	2.522	3.186	3.983	4.880
0.40	0.130	0.738	1.270	1.520	1.681	1.948	2.393	3.006	3.759	4.617
0.42	0.115	0.686	1.221	1.489	1.644	1.880	2.278	2.844	3.551	4.370
0.44	0.101	0.636	1.173	1.458	1.611	1.821	2.178	2.697	3.360	4.139
0.45	0.095	0.613	1.149	1.443	1.596	1.794	2.132	2.629	3.270	4.029
0.46	0.090	0.591	1.125	1.427	1.581	1.770	2.089	2.564	3.183	3.923
0.48	0.079	0.548	1.078	1.395	1.553	1.725	2.011	2.445	3.022	3.722
0.50	0.071	0.509	1.033	1.362	1.526	1.685	1.942	2.338	2.874	3.535
0.55	0.053	0.423	0.924	1.279	1.463	1.603	1.802	2.115	2.559	3.126
0.60	0.040	0.353	0.823	1.195	1.402	1.537	1.697	1.946	2.309	2.517
0.65	0.031	0.295	0.732	1.112	1.339	1.479	1.616	1.816	2.112	2.517
0.70	0.024	0.248	0.650	1.030	1.276	1.426	1.551	1.714	1.956	2.296
0.80	0.015	0.177	0.512	0.876	1.147	1.322	1.445	1.568	1.735	1.971
0.90	0.010	0.129	0.404	0.740	1.020	1.219	1.353	1.463	1.588	1.757
1.00	0.007	0.095	0.320	0.622	0.900	1.114	1.265	1.377	1.482	1.609
1.10	0.005	0.072	0.255	0.522	0.790	1.012	1.172	1.298	1.398	1.502
1.20	0.003	0.055	0.205	0.439	0.690	0.914	1.090	1.221	1.324	1.418
1.30	0.003	0.042	0.165	0.369	0.602	0.822	1.004	1.145	1.254	1.346
1.40	0.002	0.033	0.134	0.311	0.524	0.736	0.921	1.070	1.186	1.280
1.50	0.001	0.026	0.110	0.263	0.457	0.659	0.843	0.997	1.120	1.218
1.60		0.021	0.091	0.223	0.398	0.588	0.769	0.926	1.055	1.158
1.70		0.017	0.075	0.190	0.347	0.525	0.700	0.857	0.990	1.099
1.80		0.014	0.063	0.163	0.304	0.468	0.636	0.792	0.928	1.041
1.90		0.011	0.053	0.139	0.266	0.418	0.578	0.731	0.868	0.984
2.00		0.010	0.044	0.120	0.233	0.373	0.525	0.674	0.810	0.929
2.50		0.004	0.021	0.060	0.126	0.216	0.324	0.443	0.564	0.680
3.00		0.002	0.011	0.033	0.072	0.130	0.204	0.292	0.389	0.489
3.50		0.001	0.006	0.019	0.043	0.081	0.132	0.196	0.270	0.331
4.00		0.001	0.004	0.012	0.027	0.053	0.088	0.134	0.190	0.254
5.00			0.002	0.005	0.012	0.025	0.043	0.067	0.099	0.137
6.00			0.001	0.003	0.006	0.013	0.023	0.037	0.055	0.079

Table 6.1.1.3. *Mean atomic scattering factors in electrons for chemically significant ions*

Methods: C: correlated; HF: non-relativistic Hartree–Fock; RHF: relativistic Hartree–Fock; *DS: modified Dirac–Slater.

Element	H^{1-}	Li^{1+}	Be^{2+}	C_{val}	O^{1-}	F^{1-}	Na^{1+}	Mg^{2+}	Al^{3+}	Si_{val}
Z	1	3	4	6	8	9	11	12	13	14
Method	C	C	C	HF	HF	HF	RHF	RHF	HF	HF
$(\sin\theta)/\lambda$ (Å^{-1})										
0.00	2.000	2.000	2.000	6.000	9.000	10.000	10.000	10.000	10.000	14.000
0.01	1.983	1.999	1.999	5.989	8.986	9.988	9.995	9.997	9.997	13.973
0.02	1.933	1.997	1.999	5.956	8.945	9.953	9.981	9.986	9.989	13.894
0.03	1.857	1.994	1.997	5.903	8.878	9.895	9.958	9.969	9.976	13.766
0.04	1.763	1.990	1.995	5.829	8.785	9.816	9.925	9.945	9.957	13.593
0.05	1.659	1.984	1.992	5.738	8.670	9.716	9.883	9.914	9.933	13.381
0.06	1.550	1.977	1.988	5.629	8.534	9.597	9.833	9.876	9.904	13.138
0.07	1.442	1.968	1.983	5.507	8.381	9.461	9.773	9.832	9.870	12.870
0.08	1.338	1.959	1.978	5.372	8.211	9.309	9.705	9.782	9.831	12.586
0.09	1.238	1.948	1.973	5.227	8.029	9.144	9.630	9.725	9.787	12.293
0.10	1.145	1.936	1.966	5.074	7.836	8.967	9.546	9.662	9.738	11.995
0.11	1.058	1.923	1.959	4.916	7.635	8.781	9.455	9.594	9.684	11.700
0.12	0.978	1.909	1.952	4.754	7.429	8.586	9.357	9.519	9.625	11.410
0.13	0.904	1.894	1.944	4.591	7.218	8.386	9.253	9.440	9.563	11.130
0.14	0.836	1.877	1.935	4.428	7.005	8.181	9.142	9.355	9.495	10.862
0.15	0.773	1.860	1.925	4.267	6.792	7.973	9.026	9.265	9.424	10.608
0.16	0.715	1.842	1.915	4.109	6.579	7.762	8.904	9.171	9.349	10.368
0.17	0.661	1.823	1.905	3.954	6.368	7.551	8.777	9.072	9.270	10.143
0.18	0.612	1.804	1.894	3.805	6.160	7.341	8.647	8.969	9.187	9.933
0.19	0.567	1.783	1.882	3.661	5.956	7.131	8.512	8.862	9.101	9.737
0.20	0.526	1.762	1.870	3.523	5.756	6.924	8.374	8.751	9.011	9.553
0.22	0.452	1.718	1.845	3.266	5.371	6.517	8.089	8.521	8.823	9.222
0.24	0.390	1.671	1.817	3.035	5.008	6.126	7.795	8.280	8.623	8.931
0.25	0.362	1.647	1.803	2.930	4.836	5.937	7.646	8.156	8.520	8.798
0.26	0.337	1.623	1.788	2.831	4.670	5.753	7.496	8.030	8.414	8.671
0.28	0.291	1.573	1.758	2.651	4.357	5.399	7.195	7.774	8.198	8.435
0.30	0.253	1.523	1.726	2.495	4.068	5.067	6.894	7.513	7.975	8.214
0.32	0.220	1.471	1.692	2.358	3.804	4.756	6.597	7.251	7.747	8.005
0.34	0.192	1.419	1.658	2.241	3.564	4.467	6.304	6.987	7.515	7.803
0.35	0.179	1.394	1.641	2.188	3.452	4.330	6.160	6.856	7.399	7.704
0.36	0.168	1.368	1.623	2.139	3.345	4.199	6.018	6.725	7.282	7.606
0.38	0.147	1.316	1.587	2.050	3.147	3.951	5.739	6.465	7.047	7.410
0.40	0.129	1.265	1.551	1.974	2.969	3.724	5.471	6.210	6.813	7.215
0.42	0.113	1.215	1.514	1.907	2.808	3.514	5.212	5.959	6.581	7.021
0.44	0.100	1.165	1.476	1.849	2.663	3.322	4.964	5.715	6.350	6.826
0.45	0.094	1.141	1.458	1.822	2.597	3.233	4.845	5.595	6.237	6.729
0.46	0.089	1.117	1.439	1.798	2.533	3.147	4.728	5.477	6.124	6.632
0.48	0.079	1.069	1.401	1.752	2.417	2.987	4.503	5.247	5.901	6.437
0.50	0.070	1.023	1.364	1.711	2.313	2.841	4.290	5.025	5.683	6.244
0.55	0.0526	0.914	1.270	1.624	2.097	2.531	3.808	4.508	5.162	5.766
0.60	0.0401	0.814	1.179	1.552	1.934	2.288	3.395	4.046	4.681	5.303
0.65	0.0311	0.724	1.091	1.488	1.808	2.096	3.046	3.641	4.243	4.865
0.70	0.0243	0.643	1.007	1.428	1.710	1.945	2.753	3.288	3.851	4.455
0.80	0.0155	0.507	0.852	1.315	1.567	1.729	2.305	2.724	3.195	3.734
0.90	0.0102	0.400	0.717	1.204	1.463	1.585	1.997	2.315	2.693	3.150
1.00	0.0070	0.317	0.602	1.096	1.376	1.481	1.785	2.023	2.319	2.691
1.10	0.0049	0.253	0.505	0.992	1.296	1.397	1.635	1.813	2.041	2.338
1.20	0.0036	0.203	0.424	0.894	1.219	1.322	1.524	1.662	1.837	2.069
1.30	0.0026	0.164	0.357	0.802	1.143	1.252	1.438	1.548	1.685	1.867
1.40	0.0020	0.133	0.301	0.718	1.067	1.184	1.367	1.460	1.570	1.713
1.50	0.0015	0.109	0.255	0.642	0.994	1.117	1.304	1.388	1.479	1.595
1.60	0.0012	0.090	0.216				1.246	1.326		
1.70	0.0009	0.075	0.184				1.191	1.270		
1.80	0.0008	0.062	0.157				1.137	1.218		
1.90	0.0006	0.053	0.135				1.084	1.168		
2.00	0.0005	0.044	0.116				1.032	1.119		

6.2. Trigonometric intensity factors

By H. Lipson, J. I. Langford and H.-C. Hu

6.2.1. Expressions for intensity of diffraction

The expressions for the intensity of diffraction of X-rays contain several trigonometrical factors. The earlier series of *International Tables* (Kasper & Lonsdale, 1959, 1972) gave extensive tables of these functions, but such tables are now unnecessary, as the functions are easily computed. In fact, many crystallographers can ignore the trigonometric factors entirely, as they are built into 'black-box' data-processing programs. The formulae for single-crystal reflections (*b*) and (*c*) of Table 6.2.1.1 in the previous edition (Lipson & Langford, 1998) list only the integrated reflection power ratio (*i.e.* integrated reflection) under the strong absorption case. The revised formulae given here include both the reflection power ratio and the integrated reflection power ratio for a crystal slab of finite thickness with any values of the ratio of the absorption to the diffraction cross sections and under all possible kinds of diffraction geometry.

A conspectus of the expressions for the intensity of diffraction as recorded by various techniques, including the fundamental constants as well as the trigonometric factors, is given in Table 6.2.1.1. Details of the techniques are given elsewhere in this volume (Chapters 2.1–2.3) and in textbooks, such as those of Arndt & Willis (1966) for single-crystal diffractometry and Klug & Alexander (1974) for powder techniques. Notes on individual factors follow.

6.2.2. The polarization factor

X-rays are an electromagnetic radiation, and the amplitude with which they are scattered is proportional to the sine of the angle between the direction of the electric vector of the incident radiation and the direction of scattering. Synchrotron radiation is practically plane-polarized, with the electric vector in the plane of the ring, but the radiation from an ordinary X-ray tube is unpolarized, and it may thus be regarded as consisting of two equal parts, half with the electric vector in the plane of scattering, and half with the electric vector perpendicular to this plane. For the latter, the relevant angle is $\pi/2$, and for the former it is $(\pi/2) - 2\theta$. The intensity is proportional to the square of the amplitude, so that the polarization factor – really the non-polarization factor – is

$$\begin{aligned}&\{\sin^2(\pi/2) + \sin^2[(\pi/2) - 2\theta)]\}/2\\ &\quad = (1 + \cos^2 2\theta)/2. \qquad (6.2.2.1)\end{aligned}$$

If the radiation has been 'monochromatized' by reflection from a crystal, it will be partially polarized, and the two parts of the beam will be of unequal intensity. The intensity of reflection then depends on the angular relations between the original, the reflected, and the scattered beams, but in the commonest arrangements all three are coplanar. The polarization factor then becomes

$$(1 + A\cos^2 2\theta)/(1 + A), \qquad (6.2.2.2)$$

where

$$A = \cos^2 2\theta_M \qquad (6.2.2.3)$$

and θ_M is the Bragg angle of the monochromator crystal. The expression (6.2.2.2) may be substituted for (6.2.2.1) in Table 6.2.1.1 whenever appropriate.

6.2.3. The angular-velocity factor

In experiments where the crystal is rotated or oscillated, reflection of X-rays takes place as a reciprocal-lattice point moves through the surface of the sphere of reflection. The intensity is thus proportional to the time required for the transit of the point through the surface, and so is inversely proportional to the component of the velocity perpendicular to the surface. In most experimental arrangements – the precession camera (Buerger, 1944) is an exception – the crystals move with a constant angular velocity, and the perpendicular component of the velocity varies in an easily calculable way with the 'latitude' of the reciprocal-lattice point referred to the axis of rotation. If the reciprocal-lattice point lies in the equatorial plane and the radiation is monochromatic – the most important case in practice – the angular-velocity factor is

$$\operatorname{cosec} 2\theta. \qquad (6.2.3.1)$$

If the latitude of the reciprocal-lattice point is φ, a somewhat more complex calculation shows that the factor becomes

$$\operatorname{cosec} \theta(\cos^2 \varphi - \sin^2 \theta)^{1/2}. \qquad (6.2.3.2)$$

For $\varphi = 0$, the expression (6.2.3.2) reduces to (6.2.3.1). In some texts, φ is used for the co-latitude; this and various trigonometric identities can give superficially very different appearances to (6.2.3.2).

6.2.4. The Lorentz factor

There has been some argument over the meaning to be attached to the term *Lorentz factor*, probably because Lorentz did not publish his results in the ordinary way; they appear in a note added in proof to a paper on temperature effects by Debye (1914). Ordinarily, *Lorentz factor* is used for the trigonometric part of the angular-velocity factor, or its equivalent, if the sample is stationary. (See below).

6.2.5. Special factors in the powder method

In the powder method, all rays diffracted through an angle 2θ lie on the surface of a cone, and in the absence of preferred orientation the diffracted intensity is uniformly distributed over the circumference of the cone. The amount effective in blackening film, or intercepted by the receiving slit of a diffractometer, is thus inversely proportional to the circumference of the cone, and directly proportional to the fraction of the crystallites in a position to reflect. When allowance is made for these geometrical factors, it is found that for the Debye–Scherrer and diffractometer arrangements the intensity is proportional to

$$p'' \operatorname{cosec} \theta, \qquad (6.2.5.1)$$

where p'' is the multiplicity factor (the number of permutations of *hkl* leading to the same value of θ). For the flat-plate front-reflection arrangement, the variation becomes

$$p'' \cos 2\theta \operatorname{cosec} \theta. \qquad (6.2.5.2)$$

Combining the polarization, angular-velocity, and special factors gives a trigonometric variation of

$$p''(1 + \cos^2 2\theta) \sec \theta \operatorname{cosec}^2 \theta \qquad (6.2.5.3)$$

$$W(\Delta) = \frac{1}{\eta\sqrt{2\pi}} \exp\left(-\frac{\Delta^2}{2\eta^2}\right), \qquad (6.4.8.2)$$

where Δ is the angular deviation of the block from the mean orientation of all blocks in the crystal, and η is the standard deviation of the distribution. (The assumption of a Gaussian distribution is not critical to the argument that follows.)

Let the crystal be a cube of side L, and let α be the probability that a ray reflected by the first block is reflected again by a subsequent block. The effective size of the crystal for Bragg scattering of a single incident ray is then

$$\langle L \rangle = \ell + (L - \ell)\alpha, \qquad (6.4.8.3)$$

while the size of the crystal for all other attenuation processes is L, since, for them, the Bragg condition does not apply. The probability of re-scattering, α, can readily be expressed in terms of crystallographic quantities. The full width at half-maximum intensity of the Darwin reflection curve is given, after conversion to the glancing-angle (θ) scale, by Zachariasen (1945) as

$$\Delta\theta = \frac{3\lambda^2 N_c F}{\pi\sqrt{2}\sin 2\theta} \text{ (radians)}. \qquad (6.4.8.4)$$

The full width at half-maximum (FWHM) of the mosaic-block distribution (6.4.8.2) is derived in the usual way, and the parameter g $(= 1/2\eta\sqrt{\pi})$ is introduced to clear (to 1%) numerical constants. Then α, which is equal to the ratio of the widths, is given by

$$\alpha = \frac{g N_c \lambda^2 F}{\sin 2\theta}. \qquad (6.4.8.5)$$

Insertion of $\langle L \rangle$ [equation (6.4.8.3)] in place of ℓ in equation (6.4.8.1) for x leads to

$$x = [N_c \lambda F \ell + g Q_\theta (L - \ell)]^2, \qquad (6.4.8.6)$$

where $Q_\theta = N_0^2 \lambda^3 F^2 / \sin 2\theta$.

6.4.9. Secondary extinction

A separate treatment of secondary extinction is required only in the uncorrelated block model, and the method given by Hamilton (1957) is used in this work. The coupling constant in the H–D equations is given by $\sigma(\Delta\theta) = Q_\theta E_p W(\Delta\theta)$, where $Q_\theta = N_c^2 \lambda^3 F^2 / \sin 2\theta$ for equatorial reflections in the neutron case, E_p is the correction for primary extinction evaluated at the angle θ, and $W(\Delta\theta)$ is the distribution function for the tilts between mosaic blocks. The choice of this function has a significant influence on the final result (Sabine, 1985), and a rectangular or triangular form is suggested.

In the following equations for the secondary-extinction factor,

$$x = E_p Q_\theta G D, \qquad (6.4.9.1)$$

and A and B are given by equations (6.4.5.6) and (6.4.5.7). The average path length through the crystal for the reflection under consideration is D and G is the integral breadth of the angular distribution of mosaic blocks. It is important to note that A should be set equal to one if the data have been corrected for absorption, and B should be set equal to one if absorption-weighted values of D are used. If D for each reflection is not known, the average dimension of the crystal may be used for all reflections.

For a rectangular function, $W(\Delta\theta) = G$, for $|\Delta\theta| \leq 1/2G$, $W(\Delta\theta) = 0$ otherwise, and the secondary-extinction factor becomes

$$E_L = \frac{\exp(-\mu D)}{2x}[1 - \exp(-2x)], \qquad (6.4.9.2)$$

$$E_B = \frac{A}{1 + Bx}. \qquad (6.4.9.3)$$

For a triangular function, $W(\Delta\theta) = G(1 - |\Delta\theta|G)$, for $|\Delta\theta| \leq 1/G$, $W(\Delta\theta) = 0$ otherwise, and the secondary-extinction factor becomes

$$E_L = \frac{\exp(-\mu D)}{x}\left\{1 - \frac{1}{2x}[1 - \exp(-2x)]\right\}, \qquad (6.4.9.4)$$

$$E_B = \frac{2A}{(Bx)^2}[Bx - \ln|1 + Bx|]. \qquad (6.4.9.5)$$

6.4.10. The extinction factor

6.4.10.1. *The correlated block model*

For this model of the real crystal, the variable x is given by equation (6.4.8.6), with ℓ and g the refinable variables. Extinction factors are then calculated from equations (6.4.5.3), (6.4.5.4), and (6.4.5.5). For a reflection at a scattering angle of 2θ from a reasonably equiaxial crystal, the appropriate extinction factor is given by (6.4.7.1) as $E(2\theta) = E_L \cos^2 2\theta + E_B \sin^2 2\theta$.

It is a meaningful procedure to refine both primary and secondary extinction in this model. The reason for the high correlation between ℓ and g that is found when other theories are applied, for example that of Becker & Coppens (1974), lies in the structure of the quantity x. In the theory presented here, x is proportional to F^2 for pure primary extinction and to Q_θ^2 for pure secondary extinction.

6.4.10.2. *The uncorrelated block model*

When this model is used, two values of x are required. These are designated x_p for primary extinction and x_s for secondary extinction. Equation (6.4.8.1) is used to obtain a value for x_p. The primary-extinction factors are then calculated from (6.4.5.3), (6.4.5.4) and (6.4.5.5), and $E_p(2\theta)$ is given by equation (6.4.7.1). In the second step, x_s is obtained from equation (6.4.9.1), and the secondary-extinction factors are calculated from either (6.4.9.2) and (6.4.9.3) or (6.4.9.4) and (6.4.9.5). The result of these calculations is then used in equation (6.4.7.1) to give $E_s(2\theta)$. It is emphasised that x_s includes the primary-extinction factor. Finally, $E(2\theta) = E_p(2\theta) E_s[E_p(2\theta), 2\theta]$.

Application of both models to the analysis of neutron diffraction data has been carried out by Kampermann, Sabine, Craven & McMullen (1995).

6.4.11. Polarization

The expressions for the extinction factor have been given, by default, for the σ-polarization state, in which the electric field vector of the incident radiation is perpendicular to the plane defined by the incident and diffracted beams. For this state, the polarization factor is unity. For the π-polarization state, in which the electric vector lies in the diffraction plane, the factor is $\cos 2\theta$. The appropriate values for the extinction factors for this state are given by multiplying F by $\cos 2\theta$ wherever F occurs.

For neutrons, which are matter waves, the polarization factor is always unity.

For an unpolarized beam from an X-ray tube, the observed integrated intensity is given by $I^{\text{obs}} = \frac{1}{2} I_\theta^{\text{kin}} (E_\sigma + E_\pi \cos^2 2\theta)$. In the kinematic limit, $E_\sigma = E_\pi = 1$, and the power to which $\cos 2\theta$

Table 7.3.2.1. *Neutron capture reactions used in neutron detection*

n = neutron, $p = H^+$ = proton, $t = {}^3H^-$ = triton, $\alpha = {}^4H^+$ = alpha, e^- = electron

Capture reaction	Cross section at 1 Å (barns)	Secondary-particle energies (MeV)
${}^3He + n \rightarrow t + p$	3000	t 0.20 p 0.57
${}^6Li + n \rightarrow t + \alpha$	520	t 3.74 α 2.05
${}^{10}B + n \rightarrow {}^7Li^* + \alpha$ (93%) $\hookrightarrow {}^7Li + \gamma$ $\rightarrow {}^7Li + \alpha$ (7%)	2100	α 1.47 ${}^7Li$ 0.83 γ 0.48 α 1.78 ${}^7Li$ 1.01
${}^{157}Gd + n \rightarrow Gd^*$ $\hookrightarrow \gamma$ + conversion electrons	74000 (${}^{nat}Gd$: 17000)	e^- spectrum 0.07 to 0.182 γ spectrum up to 8
${}^{235}U + n \rightarrow$ fission fragments	320	Fission fragments up to 80

There are two modes of operation.

In the case of *direct collection of charges*, the 25 000 electrons corresponding to one neutron capture (*primary electrons*) are collected by the anode in about 100–500 ns, and generate an input pulse in the charge preamplifier (see Section 7.3.4).

If the electrical field created by the high voltage applied to the anode exceeds a critical value, the electrons will be accelerated sufficiently to produce a cascade of ionizing collisions with the neutral molecules they encounter, the new electrons liberated in the process being called *secondary electrons*. This phenomenon, *gas multiplication*, occurs in the vicinity of the thin wire anode, since the field varies as $1/r$. The avalanche stops when all the free electrons have been collected at the anode. With proper design, the number of secondary electrons is proportional to the number of primary electrons. For cylindrical geometries, the multiplication coefficient M can be calculated (Wolf, 1974). This type of detection mode is called the proportional mode. It is very commonly used because it gives a better signal-to-noise ratio (see Section 7.3.4).

A few critical remarks about gas detectors:

(i) Some gases have a tendency to form negative ions by the attachment of a free electron to a neutral gas molecule, giving a loss of detector current. This effect is negligible for ${}^3He$ but it limits the use of ${}^{10}BF_3$ to about 2 atmospheres pressure, although traces of gases such as O_2 or H_2O (*e.g.* detector materials and wall outgasing) are often the reason for loss by attachment.

(ii) Pure ${}^3He$ and ${}^{10}BF_3$ gas detectors are practically insensitive to γ radiation. This is no longer the case when additional gases, which are necessary for ${}^3He$, are used, although the polyatomic additives C_3H_8 and CF_4 are much better than the rare gases Kr, Xe, and Ar (Fischer, Radeka & Boie, 1983).

(iii) For various reasons (the price of ${}^3He$ and ${}^{10}BF_3$ and the toxicity of BF_3), neutron gas detectors are closed chambers, which must be leak-proof and insensitive to BF_3 corrosion. The wall thickness must be adapted to the inside pressure, which sometimes implies a rather thick front aluminium window (*e.g.* a 10 mm window for a 16 bar ${}^3He$ gas position-sensitive detector; aluminium is chosen for its very good transmission of neutrons, about 90% for 10 mm thickness).

7.3.3.2. *Detection via solid converter and gas ionization: the foil detector*

This mode of detection is generally used for monitors. In a typical design, a ${}^{10}B$ deposit of controlled thickness, for example $t = 0.04\,\mu m$ giving a capture efficiency of 10^{-3} at $\lambda = 1$ Å, is made on a thin aluminium plate (see Fig. 7.3.3.2). One of the two particles (α, Li) produced in the solid by the capture reaction is absorbed by the plate; the other escapes and ionizes the gas. The electrons produced are collected by the aluminium plate, itself acting as the anode, or by a separate anode wire, allowing the use of the proportional mode. The detection efficiency is proportional to the deposit thickness t, but t must be kept less than the average range r of the secondary particles in the deposit (for ${}^{10}B$, $r_\alpha = 3.8\,\mu m$ and $r_{Li} = 1.7\,\mu m$), which limits the efficiency to a maximum value of 3–4% for $\lambda = 1$ Å. The fraction of the secondary particle energy that is lost in the deposit reduces the detector current, *i.e.* the signal-to-noise ratio, and worsens the amplitude spectrum (see Section 7.3.4).

7.3.3.3. *Detection via scintillation*

In the detection process *via* scintillation (see Table 7.3.3.1), the secondary particles produced by the neutron capture ionize and excite a number of valence-band electrons of the solid scintillator to high-energy states, from which they tend to decay with the emission of a light flash of photons detected by a photomultiplier [see Fig. 7.3.3.3(*a*)]. A number of conditions must be satisfied:

(i) The scintillation must be immediate after the neutron-capture triggering event.

(ii) The scintillation decay time must be short. It depends on materials, and is around 50–100 ns for lithium silicate glasses.

(iii) A large fraction of the energy must be converted into light (rather than heat).

(iv) The material must be transparent to its own radiation.

Most thermal neutron scintillation detectors are currently based on inorganic salt crystals or glasses doped with traces of an activating element (Eu, Ce, Ag, *etc.*) (extrinsic scintillators). (A plastic scintillator might be considered to be a solid organic solution with a neutron converter.)

The use of extrinsic scintillators (Convert & Forsyth, 1983), although less efficient energetically, permits better decoupling of the energy of the photon-emitting transition (occurring now in the activator centres) from that of the valence-band electron excitation or ionization energy. The crystal or glass is then transparent to its own emission, and the light emitted is shifted to a wavelength better adapted to the following optical treatment.

$$\tau = T/t, \quad (7.5.3.7)$$

where t is the time devoted to the measurement, and the variance of the counting rate is

$$\sigma^2(\tau) = T/t^2 = \tau/t. \quad (7.5.3.8)$$

Similar expressions apply for the background, with B for the count, b for the time, and β for the counting rate. For the reflection count, the corresponding expressions are

$$\rho = T/t - B/b, \quad (7.5.3.9)$$

$$\sigma^2(\rho) = \tau/t + \beta/b. \quad (7.5.3.10)$$

To avoid confusion, upper-case italic letters are used for *numbers* of counts, lower-case italic for counting *times*, and the corresponding lower-case Greek letters for the corresponding counting *rates*. In accordance with common practice, however, I_j will be used for the intensity of the jth reflection, the context making it clear whether I is a number of counts or a counting rate.

7.5.4. Fixed-count timing

The probability of a time t being required to accumulate N counts when the true counting rate is ν is given by a Γ distribution (Abramowitz & Stegun, 1964, p. 255):

$$p(t)\,\mathrm{d}t = [(N-1)!]^{-1}(\nu t)^{N-1}\exp(-\nu t)\,\mathrm{d}(\nu t). \quad (7.5.4.1)$$

The ratio N/t is a slightly biased estimate of the counting rate ν; the unbiased estimate is $(N-1)/t$. The variance of this estimate is $\nu^2/(N-2)$, or, nearly enough for most purposes, $(N-1)^2/(N-2)t^2$. The differences introduced by the corrections -1 and -2 are generally negligible, but would not be so for counts as low as those proposed by Killean (1967). If such corrections are important, it should be noticed that there is an ambiguity concerning N, depending on how the timing is triggered. It may be triggered by a count that is counted, or by a count that is not counted, or may simply be begun, independently of the incidence of a count. Equation (7.5.4.1) assumes the first of these.

Equation (7.5.4.1) may be inverted to give the probability distribution of the observed counting rate ν_o instead of the probability distribution of the time t:

$$p(\nu_o)\,\mathrm{d}\nu_o = [(N-1)!]^{-1}[\nu(N-1)/\nu_o]^{N-1} \times \exp\{-(N-1)\nu/\nu_o\}\,\mathrm{d}[\nu_o/(N-1)\nu]. \quad (7.5.4.2)$$

There does not seem to be any special name for the distribution (7.5.4.2). Only its first $(N-1)$ moments exist, and the integral expressing the probability distribution of the difference of the reflection and the background rates is intractable (Wilson, 1980).

7.5.5. Complicating phenomena

7.5.5.1. *Dead time*

After a count is recorded, the detector and the counting circuits are 'dead' for a short interval, and any ionizing event occurring during that interval is not detected. This is important if the dead time is not negligible in comparison with the reciprocal of the counting rate, and corrections have to be made; these are large for Geiger counters, and may sometimes be necessary for counters of other types. The need for the correction can be eliminated by suitable monitoring (Eastabrook & Hughes, 1953); other advantages of monitoring are described in Chapter 2.3.

7.5.5.2. *Voltage fluctuations*

Mains-voltage fluctuations, unless compensated, and unsmoothed high-tension supplies may affect the sensitivity of detectors and counting circuits, and in any case cause the probability distribution of the arrival of counts to be non-Poissonian. Backlash in the diffractometer drives may be even more important in altering the observed counting rates. As de Boer (1982) says, the ideal distributions represent a Utopia that experimenters can approach but never reach. He observed erratic fluctuations in counting rates, up to ten times as big as the expected statistical fluctuations. When care is taken, the instabilities observed in practice are much less than those of the extreme cases described by de Boer. Stabilizing an X-ray source and testing its stability are discussed in Subsection 2.3.5.1.

7.5.6. Treatment of measured-as-negative (and other weak) intensities

It has been customary in crystallographic computations, but without theoretical justification, to omit all reflections with intensities less than two or three times their standard uncertainties. Hirshfeld & Rabinovich (1973) asserted that the failure to use all reflections, even those for which the subtraction of background has resulted in a negative net intensity, at their measured values will lead to a bias in the parameters resulting from a least-squares refinement. This is, however, inconsistent with the Gauss–Markov theorem (see Section 8.1.2), which shows that least-squares estimates are unbiased, independent of the weights used, if the observations are unbiased estimates of quantities predicted by a model. Giving some observations zero weight therefore cannot introduce bias. Provided the set of included observations is sufficient to give a nonsingular normal equations matrix, parameter estimates will be unbiased, but inclusion of as many well determined observations as possible will yield the most precise estimates. Requiring that the net intensity be greater than 2σ assures that the value of $|F|$ will be well determined. Furthermore, Prince & Nicholson (1985) showed that, if the net intensity, I, or $|F|^2$ is used as the observed quantity, weak reflections have very little leverage (see Section 8.4.4), and therefore omitting them cannot have a significant effect on the precision of parameter estimates.

The use of negative values of I or $|F|^2$ is also inconsistent with Bayes's theorem, which implies that a negative value cannot be an unbiased estimate of an inherently non-negative quantity. There are statistical methods for estimating the positive value of $|F|$ that led to a negative value of I. The best known approach is the Bayesian method of French & Wilson (1978), who observe that ''Instead of thanking the data for the information that certain structure factor moduli are small, we accuse them of assuming 'impossible' negative values. What we should do is combine our knowledge of the non-negativity of the true intensities with the information concerning their magnitudes contained in the data.''

7.5.7. Optimization of counting times

There have been many papers on optimizing counting times for achieving different purposes, and all optimization procedures require some knowledge of the distributions of counts or counting rates; often only the mean and variance of the distribution are required. It is also necessary to know the functional relationship between the quantity of interest and the counts (counting rates, intensities) entering into its measurement. Typically, the object is to minimize the variance of some

might seem to have the effect of making the weights dependent on the calculated values, so that the right-hand side of (8.2.2.6) is no longer zero, but this applies only if the weights are changed during the refinement. There is thus no conflict with the result in (8.1.2.9). In practice, in any case, many other sources of uncertainty are much more important than any possible bias that could be introduced by this effect.

8.2.3. Entropy maximization

8.2.3.1. *Introduction*

Entropy maximization, like least squares, is of interest primarily as a framework within which to find or adjust parameters of a model. Rationalization of the name 'entropy maximization' by analogy to thermodynamics is controversial, but there is formal proof (Shore & Johnson, 1980) supporting entropy maximization as the unique method of inference that satisfies basic consistency requirements (Livesey & Skilling, 1985). The proof consists of discovering the consequences of four consistency axioms, which may be stated informally as follows:

(1) the result of the inference should be unique;
(2) the result of the inference should be invariant to any transformations of coordinate system;
(3) it should not matter whether independent information is accounted for independently or jointly;
(4) it should not matter whether independent subsystems are treated separately in conditional problems or collected and treated jointly.

The term 'entropy' is used in this chapter as a name only, the name for variation functions that include the form $\varphi \ln \varphi$, where φ may represent probability or, more generally, a positive proportion. Any positive measure, either observed or derived, of the relative apportionment of a characteristic quantity among observations can serve as the proportion.

The method of entropy maximization may be formulated as follows: given a set of n observations, y_i, that are measurements of quantities that can be described by model functions, $M_i(\mathbf{x})$, where $\mathbf{x}$ is a vector of parameters, find the prior, positive proportions, $\mu_i = f(y_i)$, and the values of the parameters for which the positive proportions $\varphi = f[M_i(\mathbf{x})]$ make the sum

$$S = -\sum_{i=1}^{n} \varphi_i' \ln(\varphi_i'/\mu_i'), \qquad (8.2.3.1)$$

where $\varphi_i' = \varphi_i / \sum \varphi_j$ and $\mu_i' = \mu_i / \sum \mu_j$, a maximum. S is called the *Shannon–Jaynes entropy*. For some applications (Collins, 1982), it is desirable to include in the variation function additional terms or restraints that give S the form

$$S = -\sum_{i=1}^{n} \varphi_i' \ln(\varphi_i'/\mu_i') + \lambda_1 \xi_1(\mathbf{x}, \mathbf{y}) + \lambda_2 \xi_2(\mathbf{x}, \mathbf{y}) + \ldots, \quad (8.2.3.2)$$

where the λs are undetermined multipliers, but we shall discuss here only applications where $\lambda_i = 0$ for all i, and an unrestrained entropy is maximized. A necessary condition for S to be a maximum is for the gradient to vanish. Using

$$\frac{\partial S}{\partial x_j} = \sum_{i=1}^{n} \left(\frac{\partial S}{\partial \varphi_i}\right)\left(\frac{\partial \varphi_i}{\partial x_j}\right) \qquad (8.2.3.3)$$

and

$$\frac{\partial S}{\partial \varphi_i} = \sum_{k=1}^{n} \left(\frac{\partial S}{\partial \varphi_k'}\right)\left(\frac{\partial \varphi_k'}{\partial \varphi_i}\right), \qquad (8.2.3.4)$$

straightforward algebraic manipulation gives equations of the form

$$\sum_{i=1}^{n} \left\{ \frac{\partial \varphi_i}{\partial x_j} - \varphi_i' \left(\sum_{k=1}^{n} \frac{\partial \varphi_k}{\partial x_j} \right) \right\} \ln\left(\frac{\varphi_i'}{\mu_i'}\right) = 0. \qquad (8.2.3.5)$$

It should be noted that, although the entropy function should, in principle, have a unique stationary point corresponding to the global maximum, there are occasional circumstances, particularly with restrained problems where the undetermined multipliers are not all zero, where it may be necessary to verify that a stationary solution actually maximizes entropy.

8.2.3.2. *Some examples*

For an example of the application of the maximum-entropy method, consider (Collins, 1984) a collection of diffraction intensities in which various subsets have been measured under different conditions, such as on different films or with different crystals. All systematic corrections have been made, but it is necessary to put the different subsets onto a common scale. Assume that every subset has measurements in common with some other subset, and that no collection of subsets is isolated from the others. Let the measurement of intensity I_h in subset i be J_{hi}, and let the scale factor that puts intensity I_h on the scale of subset i be k_i. Equation (8.2.3.1) becomes

$$S = -\sum_{h=1}^{n} \sum_{i=1}^{m} (k_i I_h)' \ln\left[\frac{(k_i I_h)'}{J_{hi}'}\right], \qquad (8.2.3.6)$$

where the term is zero if I_h does not appear in subset i. Because k_i and I_h are parameters of the model, equations (8.2.3.5) become

$$\sum_{i=1}^{m} k_i \ln\left[\frac{(k_i I_h)'}{J_{hi}'}\right] - \sum_{h=1}^{n} \sum_{i=1}^{m} (k_i I_h)' \left(\sum_{l=1}^{m} k_l\right) \ln\left[\frac{(k_i I_h)'}{J_{hi}'}\right] = 0, \qquad (8.2.3.7a)$$

and

$$\sum_{h=1}^{n} I_h \ln\left[\frac{(k_i I_h)'}{J_{hi}'}\right] - \sum_{h=1}^{n} \sum_{i=1}^{m} (k_i I_h)' \left(\sum_{l=1}^{n} I_l\right) \ln\left[\frac{(k_i I_h)'}{J_{hi}'}\right] = 0. \qquad (8.2.3.7b)$$

These simplify to

$$\ln I_h = Q - \sum_{i=1}^{m} k_i' \ln(k_i/J_{hi}) \qquad (8.2.3.8a)$$

and

$$\ln k_i = Q - \sum_{h=1}^{n} I_h' \ln(I_h/J_{hi}), \qquad (8.2.3.8b)$$

where

$$Q = \sum_{h=1}^{n} \sum_{i=1}^{m} (k_i I_h)' \ln[(k_i I_h)/J_{hi}]. \qquad (8.2.3.8c)$$

Equations (8.2.3.8) may be solved iteratively, starting with the approximations $k_i = \sum_{h=1}^{n} J_{hi}$ and $Q = 0$.

The standard uncertainties of scale factors and intensities are not used in the solution of equations (8.2.3.8), and must be computed separately. They may be estimated on a fractional basis from the variances of estimated population means $\langle J_{hi}/I_h \rangle$ for a scale factor and $\langle J_{hi}/k_i \rangle$ for an intensity, respectively. The maximum-entropy scale factors and scaled intensities are relative, and either set may be multiplied by an arbitrary, positive constant without affecting the solution.

Profile R factor:

$$R_P = \frac{\sum_i |y_i(\text{obs.}) - y_i(\text{calc.})|}{\sum_i y_i(\text{obs.})}.$$

Weighted profile R factor:

$$R_{wP} = \left[\frac{\sum_i w_i |y_i(\text{obs.}) - y_i(\text{calc.})|^2}{\sum_i w_i y_i^2(\text{obs.})}\right]^{1/2}.$$

Bragg R factor:

$$R_I = \frac{\sum_k |I_k(\text{obs.}) - I_k(\text{calc.})|}{\sum_k I_k(\text{obs.})}.$$

Expected R factor:

$$R_E = \left[\frac{\mathcal{N} - P}{\sum_i w_i y_i^2(\text{obs.})}\right]^{1/2}.$$

I_k is the integrated intensity of the kth reflection, $\mathcal{N}$ is the number of independent observations, and P is the number of refined parameters. The most important indicators are R_{wP} and R_E. The ratio R_{wP}/R_E is the so-called 'goodness-of-fit', χ^2: in a successful refinement χ^2 should approach unity. The Bragg R factor is useful, since it depends on the fit of the structural parameters and not on the profile parameters.

8.6.2. Problems with the Rietveld method

One should be aware of certain problems that may give rise to failure in a Rietveld refinement.

8.6.2.1. *Indexing*

The first step in refinement is the indexing of the pattern. As the Rietveld method is often applied to the refinement of data for which the unit-cell parameters and space group are already known, there is then little difficulty in indexing the pattern, provided that there are a few well resolved lines. Without this knowledge, the indexing requires, as a starting point, the measurement of the d values of low-angle diffraction lines to high accuracy. According to Shirley (1980): 'Powder indexing works beautifully on good data, but with poor data it usually will not work at all'. The indexing of powder patterns and associated problems are discussed by Shirley (1980), Pawley (1981), Cheetham (1993) and Werner (2002).

8.6.2.2. *Peak-shape function (PSF)*

The appropriate function to use varies with the nature of the experimental technique. In addition to the Gaussian PSF in (8.6.1.3), functions commonly used for angle-dispersive data are (Young & Wiles, 1982):

$$G_{ik} = \frac{2}{\pi H_k}\left[1 + 4\left(\frac{\Delta 2\theta_{ik}}{H_k}\right)^2\right]^{-1} \quad \text{(Lorentzian)}$$

$$G_{ik} = \frac{2\eta}{\pi H_k}\left[1 + 4\left(\frac{\Delta 2\theta_{ik}}{H_k}\right)^2\right]^{-1} + (1-\eta)\frac{2\sqrt{\ln 2}}{\sqrt{\pi}H_k}\exp\left[-4\ln 2\left(\frac{\Delta 2\theta_{ik}}{H_k}\right)^2\right] \quad \text{(pseudo-Voigt)}$$

$$G_{ik} = \frac{2\Gamma(n)(2^{1/n}-1)}{\pi H_k \Gamma(n-\frac{1}{2})}\left[1 + 4(2^{1/n}-1)\left(\frac{\Delta 2\theta_{ik}}{H_k}\right)^2\right]^{-n} \quad \text{(Pearson VII)}$$

where $\Delta 2\theta_{ik} = 2\theta_i - 2\theta_k$. η is a parameter that defines the fraction of Lorentzian character in the pseudo-Voigt profile. $\Gamma(n)$ is the gamma function: when $n = 1$, Pearson VII becomes a Lorentzian, and when $n = \infty$, it becomes a Gaussian.

The tails of a Gaussian distribution fall off too rapidly to account for particle size broadening. The peak shape is then better described by a convolution of Gaussian and Lorentzian functions [*i.e.* Voigt function: see Ahtee, Nurmela & Suortti (1984) and David & Matthewman (1985)]. A pulsed neutron source gives an asymmetrical line shape arising from the fast rise and slow decay of the neutron pulse: this shape can be approximated by a pair of exponential functions convoluted with a Gaussian (Albinati & Willis, 1982; Von Dreele, Jorgensen & Windsor, 1982).

The pattern from an X-ray powder diffractometer gives peak shapes that cannot be fitted by a simple analytical function. Will, Parrish & Huang (1983) use the sum of several Lorentzians to express the shape of each diffraction peak, while Hepp & Baerlocher (1988) describe a numerical method of determining the PSF. Pearson VII functions have also been successfully used for X-ray data (Immirzi, 1980). A modified Lorentzian function has been employed for interpreting data from a Guinier focusing camera (Malmros & Thomas, 1977). PSFs for instruments employing X-ray synchrotron radiation can be represented by a Gaussian (Parrish & Huang, 1980) or a pseudo-Voigt function (Hastings, Thomlinson & Cox, 1984).

8.6.2.3. *Background*

The background may be determined by measuring regions of the pattern that are free from Bragg peaks. This procedure assumes that the background varies smoothly with $\sin\theta/\lambda$, whereas this is not the case in the presence of disorder or thermal diffuse scattering (TDS), which rises to a maximum at the Bragg positions. An alternative approach is to include a background function in the refinement model (Richardson, 1993). If the background is not accounted for satisfactorily, the temperature factors may be incorrect or even negative. The various procedures for estimating the background for X-ray, synchrotron, constant-wavelength and TOF neutron powder patterns are reviewed by McCusker *et al.* (1999).

In neutron diffraction, the main contribution to the background from hydrogen-containing samples is due to incoherent scattering. Deuterating the sample is essential in order to substantially reduce this background.

Two other types of homogeneous sphere packings (15 and 16) with contact number $k = 10$ also refer to densest layers of spheres. In these cases, each sphere has three contacts to one neighbouring layer and one contact to the other layer that is stacked directly above or below the original layer.

Cubic closest packings may also be regarded as built up from square layers 4^4 stacked in such a way that each sphere has four neighbouring spheres in the same layer and four neighbours each from the layers above and below (*cf.* Fig. 9.1.1.3). If square layers are stacked such that each sphere has contact to four spheres of one neighbouring layer and to two spheres of the other layer (*cf.* Fig. 9.1.1.4), sphere packings with contact number 10 result. In total, two types of homogeneous packings (17 and 18) with this kind of stacking exist. Sphere packings of type 9 may also be decomposed into 4^4 layers parallel to (101) or (011) in a five-layer sequence. These nets are made up from parallel rhombi and stacked such that each sphere has contact with three other spheres from the layer above and from the layer below. If such layers are stacked in a two-layer sequence, sphere packings of type 13 with symmetry *Cmcm* result (O'Keeffe, 1998). Sphere packings of type 14 are also build up from 4^4 layers, but here the rhombi occur in two different orientations (O'Keeffe, 1998). Sphere packings with high contact numbers may also be derived by stacking of other layers. Type 20, for example, refers to 3^46 layers where each sphere is in contact with three spheres of one neighbouring net and two spheres of the other one (Sowa & Koch, 1999). Such a sphere packing may alternatively be derived from the cubic closest packing by omitting systematically 1/7 of the spheres in each of the 3^6 nets.

Sphere packings of types 8 and 19 (*cf.* Figs. 9.1.1.5 and 9.1.1.6) cannot be built up from plane layers of spheres in contact although their contact numbers are also high.

Table 9.1.1.2 contains complete information on homogeneous sphere packings with $k = 10$, 11, and 12 and with cubic or tetragonal symmetry.

The least dense (most open) homogeneous sphere packings known so far have already been described by Heesch & Laves (1933). Sphere packings of that type (24) cannot be stable because their contact number is 3 (*cf.* Fig. 9.1.1.7). As discussed

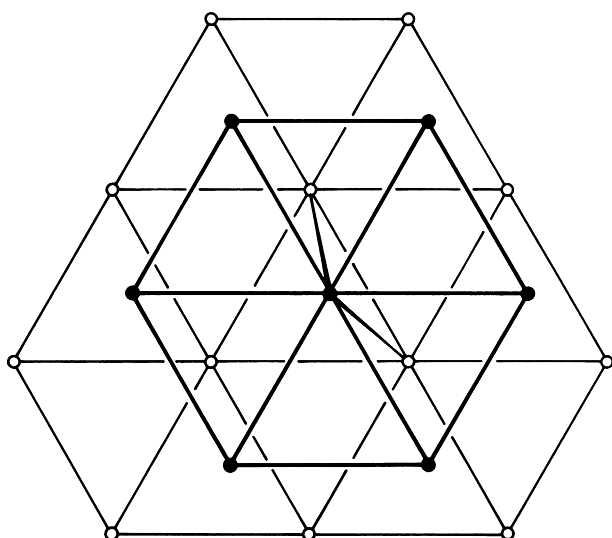

Fig. 9.1.1.2. Two triangular nets representing two densest packed layers of spheres. The layers are stacked in such a way that each sphere is in contact with two spheres of the other layer.

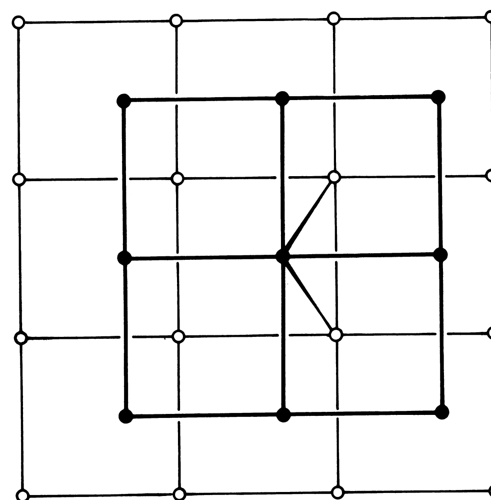

Fig. 9.1.1.4. Two square nets representing two layers of spheres stacked in such a way that each sphere is in contact with two spheres of the other layer.

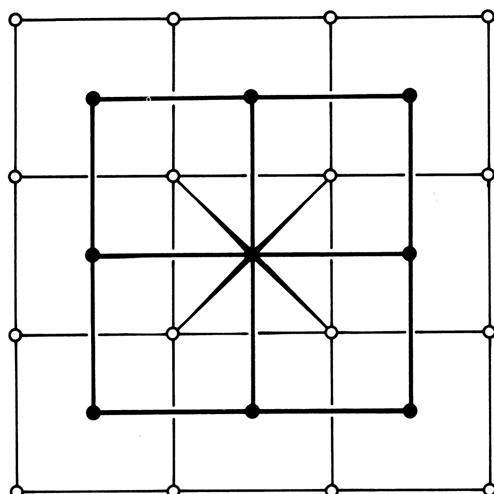

Fig. 9.1.1.3. Two square nets representing two layers of spheres stacked in such a way that each sphere is in contact with four spheres of the other layer.

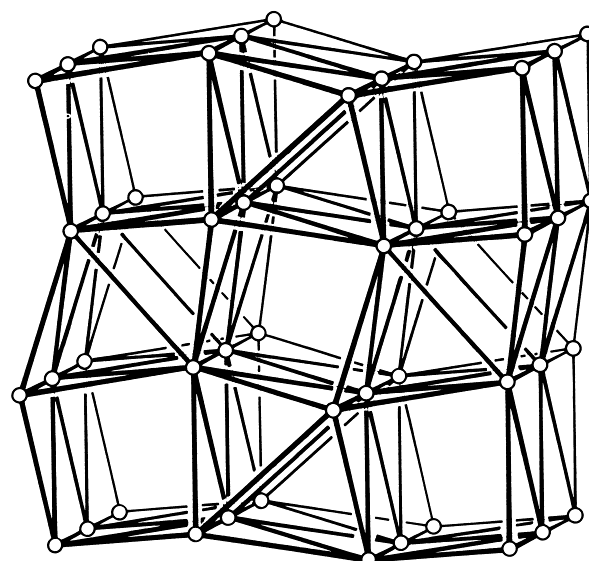

Fig. 9.1.1.5. Sphere packing of type 8 (Table 9.1.1.2) represented by a graph: $k = 11$, $P4_2/mnm$, $4(f)$, $xx0$.

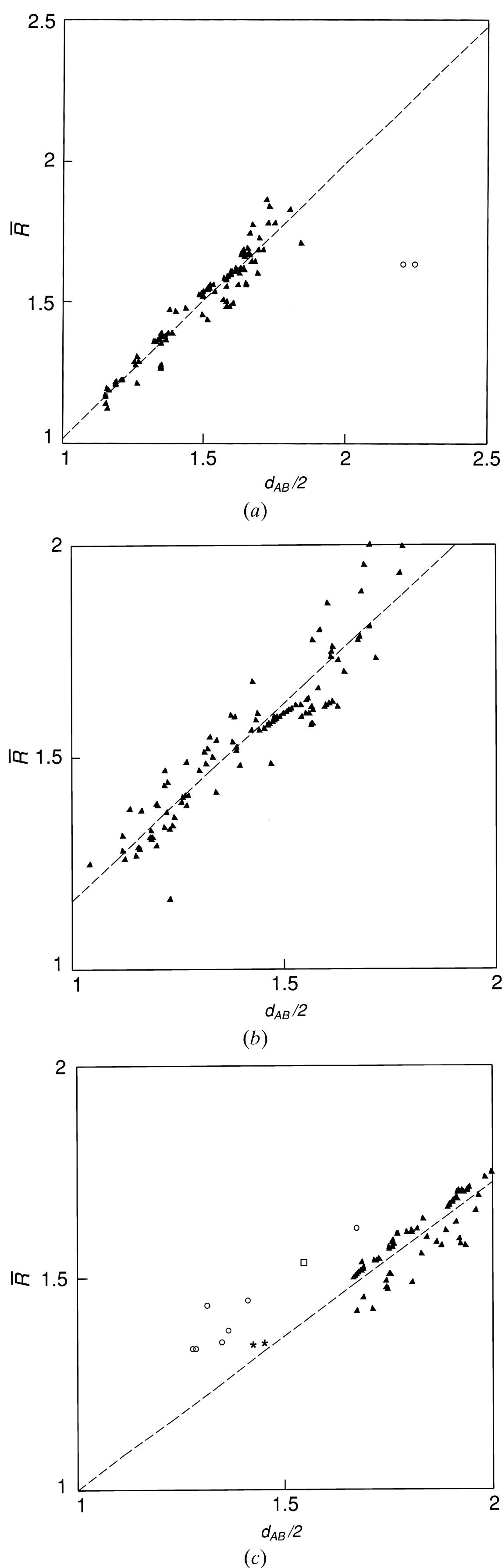

Fig. 9.3.2. (*a*) Plot of d_{AB} *versus* $\overline{R}$ for the binary compounds crystallizing in *hP*3 AlB_2. (*b*) Plot of d_{AB} *versus* $\overline{R}$ for the binary compounds crystallizing in *oP*12 Co_2Sb. (*c*) Plot of d_{AB} *versus* $\overline{R}$ for the binary compounds crystallizing in *tP*6 Cu_2Sb.

bond radius, and $n = V/12$, with V being the elemental valence, to adjust the radii to coordination numbers other than 12. The adjustment of the radii to the coordination numbers of the structure type of concern is a first approximation adjustment to the structure type. The broken lines in Figs. 9.3.2(*a*)–(*c*) are the results of a least-squares analysis.

Much more information about the short-range atomic arrangement, and a deeper insight into the geometry within a structure type, is obtained by looking at the coordination polyhedra (atomic environments AE) instead of looking only at the interatomic distances. These coordination polyhedra or AE not only give geometrical information about an atom and its neighbours but also give the correct coordination number. An AE is determined by using Brunner & Schwarzenbach's (1971) method, in which all interatomic distances between an atom and its neighbours are plotted in a next-neighbour histogram (NNH), as shown in Fig. 9.3.3(*a*). In most cases, a clear maximum gap is revealed. All atoms to the left of the maximum gap belong to the AE of the central atom; the coordination polyhedron constructed with these atoms is depicted in Fig. 9.3.3(*b*).

In cases where no maximum gap is found, Daams, Villars & van Vucht (1992) used the maximum convex rule. The maximum convex volume is defined as the maximum volume around only one central atom enclosed by convex faces with all the coordinating atoms lying at the intersection of at least three faces. Systematic studies of all intermetallic structure types

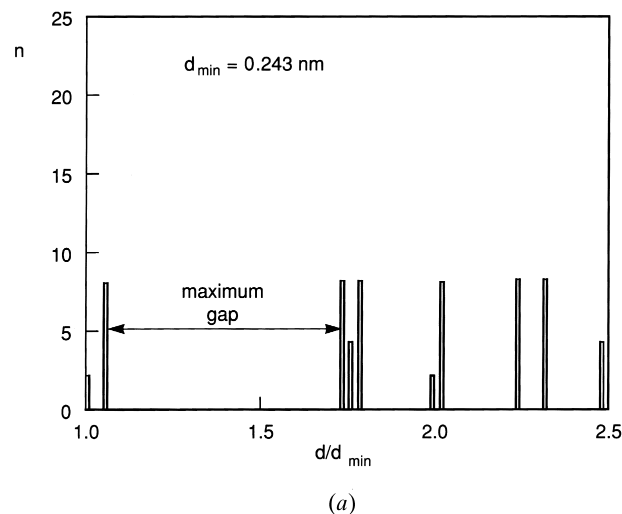

(*a*)

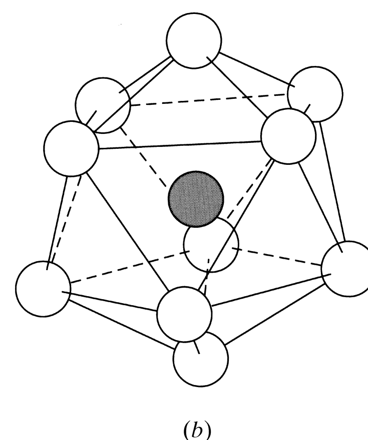

(*b*)

Fig. 9.3.3. (*a*) A typical example of a next-neighbour histogram (NNH) and (*b*) the atomic environment (AE) coordination polyhedron belonging to this NNH.

Table 9.5.1.1. *Average lengths (cont.)*

Bond	Substructure	d	m	σ	q_l	q_u	n	Note
B(4)—I	see TMPBTI (2.220, 2.253)							
B(4)—N(3)	X_3—**B**—**N**(=C)(X)	1.611	1.617	0.013	1.601	1.625	8	
	in pyrazaboles	1.549	1.552	0.015	1.536	1.560	10	
B(3)—N(3)	X_2—**B**—**N**—C_2: all coplanar	1.404	1.404	0.014	1.389	1.408	40	*2*
	for τ(BN) > 30° see BOGSUL, BUSHAY, CILRUK (1.434–1.530)							
	S_2—**B**—**N**—X_2	1.447	1.443	0.013	1.435	1.470	14	
B(4)—O	**B**—**O** in BO_4^-	1.468	1.468	0.022	1.453	1.479	24	
	for neutral **B**—**O** see Note 3							*3*
B(3)—O(2)	X_2—**B**—**O**—X	1.367	1.367	0.024	1.349	1.382	35	
B(n)—P	n = 4: **B**—**P**	1.922	1.927	0.027	1.900	1.954	10	
	n = 3: see BUPSIB10 (1.892, 1.893)							
B(4)—S	**B**(4)—**S**(3)	1.930	1.927	0.009	1.925	1.934	10	
	B(4)—**S**(2)	1.896	1.896	0.004	1.893	1.899	6	
B(3)—S	N—**B**—$\mathbf{S_2}$	1.806	1.806	0.010	1.799	1.816	28	
	(=X—)(N—)**B**—**S**	1.851	1.854	0.013	1.842	1.859	10	
Br—Br	see BEPZEB, TPASTB	2.542	2.548	0.015	2.526	2.551	4	
Br—C	**Br**—**C***	1.966	1.967	0.029	1.951	1.983	100	*4*
	Br—**C**sp^3 (cyclopropane)	1.910	1.910	0.010	1.900	1.914	8	
	Br—**C**sp^2	1.883	1.881	0.015	1.874	1.894	31	*4*
	Br—$\mathbf{C_{ar}}$ (mono-Br + m,p-Br_2)	1.899	1.899	0.012	1.892	1.906	119	*4*
	Br—$\mathbf{C_{ar}}$ (o-Br_2)	1.875	1.872	0.011	1.864	1.884	8	*4*
$^-$Br(2)—Cl	see TEACBR (2.362–2.402)							†
Br—I	see DTHIBR10 (2.646), TPHOSI (2.695)							
Br—N	see NBBZAM (1.843)							
Br—O	see CIYFOF	1.581	1.581	0.007	1.574	1.587	4	
Br—P	see CISTED (2.366)							
Br—S(2)	see BEMLIO (2.206)							†
Br—S(3)	see CIWYIQ (2.435, 2.453)							†
Br—S(3)$^+$	see THINBR (2.321)							†
Br—Se	see CIFZUM (2.508, 2.619)							
Br—Si	see BIZJAV (2.284)							
Br—Te	In $\mathbf{Br_6Te}^{2-}$ see CUGBAH (2.692–2.716)							
	Br—**Te**(4) see BETUTE10 (3.079, 3.015)							
	Br—**Te**(3) see BTUPTE (2.835)							
Csp^3—Csp^3	$C^{\#}$—$\mathbf{CH_2}$—$\mathbf{CH_3}$	1.513	1.514	0.014	1.507	1.523	192	
	$(C^{\#})_2$—**CH**—$\mathbf{CH_3}$	1.524	1.526	0.015	1.518	1.534	226	
	$(C^{\#})_3$—**C**—$\mathbf{CH_3}$	1.534	1.534	0.011	1.527	1.541	825	
	$C^{\#}$—$\mathbf{CH_2}$—$\mathbf{CH_2}$—$C^{\#}$	1.524	1.524	0.014	1.516	1.532	2459	
	$(C^{\#})_2$—**CH**—$\mathbf{CH_2}$—$C^{\#}$	1.531	1.531	0.012	1.524	1.538	1217	
	$(C^{\#})_3$—**C**—$\mathbf{CH_2}$—$C^{\#}$	1.538	1.539	0.010	1.533	1.544	330	
	$(C^{\#})_2$—**CH**—**CH**—$(C^{\#})_2$	1.542	1.542	0.011	1.536	1.549	321	
	$(C^{\#})_3$—**C**—**CH**—$(C^{\#})_2$	1.556	1.556	0.011	1.549	1.562	215	
	$(C^{\#})_3$—**C**—**C**—$(C^{\#})_3$	1.588	1.580	0.025	1.566	1.610	21	
	C*—**C*** (overall)	1.530	1.530	0.015	1.521	1.539	5777	*5, 6*

Table 9.8.3.5. (3 + 1)-*Dimensional superspace groups*

The number labelling the superspace group is denoted by *n.m*, where *n* is the number attached to the three-dimensional basic space group and *m* numbers the various superspace groups having the same basic space group. The symbol of the basic space group, the symbol for the four-dimensional point group K_s, the number of the four-dimensional Bravais class to which the superspace group belongs (Table 9.8.3.2*a*), and the superspace-group symbol are also given. The superspace-group symbol is indicated in the short notation, *i.e.* for the basic group one uses the short symbol from *International Tables for Crystallography*, Volume A, and then the values of τ are given for each of the generators in this symbol, unless all these values are zero. Then, instead of writing a number of zeros, one omits them all. Finally, the special reflection conditions due to non-primitive translations are given, for *hklm* if $\mathbf{q}^r = 0$ and for *HKLm* otherwise. Recall the *HKLm* are the indices with respect to a conventional basis $\mathbf{a}_c^*, \mathbf{b}_c^*, \mathbf{c}_c^*, \mathbf{q}^i$ as in Table 9.8.3.2(*a*). The reflection conditions due to centring translations are given in Table 9.8.3.6.

No.	Basic space group	Point group K_s	Bravais class No.	Group symbol	Special reflection conditions
1.1	$P1$	$(1, 1)$	1	$P1(\alpha\beta\gamma)$	
2.1	$P\bar{1}$	$(\bar{1}, \bar{1})$	1	$P\bar{1}(\alpha\beta\gamma)$	
3.1	$P2$	$(2, \bar{1})$	2	$P2(\alpha\beta0)$	
3.2		$(2, \bar{1})$	3	$P2(\alpha\beta\tfrac{1}{2})$	
3.3		$(2, 1)$	5	$P2(00\gamma)$	
3.4		$(2, 1)$	5	$P2(00\gamma)s$	$00lm$: $m = 2n$
3.5		$(2, 1)$	6	$P2(\tfrac{1}{2}0\gamma)$	
4.1	$P2_1$	$(2, \bar{1})$	2	$P2_1(\alpha\beta0)$	$00l0$: $l = 2n$
4.2		$(2, 1)$	5	$P2_1(00\gamma)$	$00lm$: $l = 2n$
4.3		$(2, 1)$	6	$P2_1(\tfrac{1}{2}0\gamma)$	$00Lm$: $L = 2n$
5.1	$B2$	$(2, \bar{1})$	4	$B2(\alpha\beta0)$	
5.2		$(2, 1)$	7	$B2(00\gamma)$	
5.3		$(2, 1)$	7	$B2(00\gamma)s$	$00lm$: $m = 2n$
5.4		$(2, 1)$	8	$B2(0\tfrac{1}{2}\gamma)$	
6.1	Pm	$(m, 1)$	2	$Pm(\alpha\beta0)$	
6.2		$(m, 1)$	2	$Pm(\alpha\beta0)s$	$hk0m$: $m = 2n$
6.3		$(m, 1)$	3	$Pm(\alpha\beta\tfrac{1}{2})$	
6.4		$(m, \bar{1})$	5	$Pm(00\gamma)$	
6.5		$(m, \bar{1})$	6	$Pm(\tfrac{1}{2}0\gamma)$	
7.1	Pb	$(m, 1)$	2	$Pb(\alpha\beta0)$	$hk0m$: $k = 2n$
7.2		$(m, 1)$	3	$Pb(\alpha\beta\tfrac{1}{2})$	$HK0m$: $K = 2n$
7.3		$(m, \bar{1})$	5	$Pb(00\gamma)$	$hk00$: $k = 2n$
7.4		$(m, \bar{1})$	6	$Pb(\tfrac{1}{2}0\gamma)$	$HK00$: $K = 2n$
8.1	Bm	$(m, 1)$	4	$Bm(\alpha\beta0)$	
8.2		$(m, 1)$	4	$Bm(\alpha\beta0)s$	$hk0m$: $m = 2n$
8.3		$(m, \bar{1})$	7	$Bm(00\gamma)$	
8.4		$(m, \bar{1})$	8	$Bm(0\tfrac{1}{2}\gamma)$	
9.1	Bb	$(m, 1)$	4	$Bb(\alpha\beta0)$	$hk0m$: $k = 2n$
9.2		$(m, \bar{1})$	7	$Bb(00\gamma)$	$hk00$: $k = 2n$
10.1	$P2/m$	$(2/m, \bar{1}1)$	2	$P2/m(\alpha\beta0)$	
10.2		$(2/m, \bar{1}1)$	2	$P2/m(\alpha\beta0)0s$	$hk0m$: $m = 2n$
10.3		$(2/m, \bar{1}1)$	3	$P2/m(\alpha\beta\tfrac{1}{2})$	
10.4		$(2/m, 1\bar{1})$	5	$P2/m(00\gamma)$	
10.5		$(2/m, 1\bar{1})$	5	$P2/m(00\gamma)s0$	$00lm$: $m = 2n$
10.6		$(2/m, 1\bar{1})$	6	$P2/m(\tfrac{1}{2}0\gamma)$	
11.1	$P2_1/m$	$(2/m, \bar{1}1)$	2	$P2_1/m(\alpha\beta0)$	$00l0$: $l = 2n$
11.2		$(2/m, \bar{1}1)$	2	$P2_1/m(\alpha\beta0)0s$	$00l0$: $l = 2n$; $hk0m$: $m = 2n$
11.3		$(2/m, 1\bar{1})$	5	$P2_1/m(00\gamma)$	$00lm$: $l = 2n$
11.4		$(2/m, 1\bar{1})$	6	$P2_1/m(\tfrac{1}{2}0\gamma)$	$00Lm$: $L = 2n$
12.1	$B2/m$	$(2/m, \bar{1}1)$	4	$B2/m(\alpha\beta0)$	
12.2		$(2/m, \bar{1}1)$	4	$B2/m(\alpha\beta0)0s$	$hk0m$: $m = 2n$
12.3		$(2/m, 1\bar{1})$	7	$B2/m(00\gamma)$	
12.4		$(2/m, 1\bar{1})$	7	$B2/m(00\gamma)s0$	$00lm$: $m = 2n$
12.5		$(2/m, 1\bar{1})$	8	$B2/m(\tfrac{1}{2}0\gamma)$	
13.1	$P2/b$	$(2/m, \bar{1}1)$	2	$P2/b(\alpha\beta0)$	$hk0m$: $k = 2n$
13.2		$(2/m, \bar{1}1)$	3	$P2/b(\alpha\beta\tfrac{1}{2})$	$HK0m$: $m = 2n$
13.3		$(2/m, 1\bar{1})$	5	$P2/b(00\gamma)$	$hk00$: $k = 2n$
13.4		$(2/m, 1\bar{1})$	5	$P2/b(00\gamma)s0$	$00lm$: $m = 2n$; $hk00$: $k = 2n$
13.5		$(2/m, 1\bar{1})$	6	$P2/b(\tfrac{1}{2}0\gamma)$	$HK00$: $K = 2n$
14.1	$P2_1/b$	$(2/m, \bar{1}1)$	2	$P2_1/b(\alpha\beta0)$	$00l0$: $l = 2n$; $hk0m$: $k = 2n$
14.2		$(2/m, 1\bar{1})$	5	$P2_1/b(00\gamma)$	$00lm$: $l = 2n$; $hk00$: $k = 2n$
14.3		$(2/m, 1\bar{1})$	6	$P2_1/b(\tfrac{1}{2}0\gamma)$	$00Lm$: $L = 2n$; $HK00$: $K = 2n$
15.1	$B2/b$	$(2/m, \bar{1}1)$	4	$B2/b(\alpha\beta0)$	$hk0m$: $k = 2n$
15.2		$(2/m, 1\bar{1})$	7	$B2/b(00\gamma)$	$hk00$: $k = 2n$
15.3		$(2/m, 1\bar{1})$	7	$B2/b(00\gamma)s0$	$00lm$: $m = 2n$; $hk00$: $k = 2n$